PRACTICALITY AND USABILITY OF HIGH-DENSITY SURFACE ELECTROMYOGRAPHY FOR LOWER LIMB PROSTHESIS CONTROL

by

Fred Wallace Christensen

A thesis submitted in partial fulfillment
of the requirements for the degree

of

Master of Science

in

Mechanical and Industrial Engineering

MONTANA STATE UNIVERSITY
Bozeman, Montana

December 2022

ACKNOWLEDGEMENTS

Special thanks to Matthew Robinett for help with data collection and filter design, Kendall Larson for help with data collection and anatomical knowledge, Krishna Tiwadi and Suzanne Loviska for help with data collection, everyone who participated, and everyone who gave feedback on this project. Thank you for helping this come to be.

TABLE OF CONTENTS

TABLE OF CONTENTS CONTINUED

LIST OF TABLES

LIST OF FIGURES

LIST OF FIGURES CONTINUED

LIST OF FIGURES CONTINUED

LIST OF FIGURES CONTINUED

NOMENCLATURE

Transtibial amputation - lower limb removed between the ankle joint and the knee joint, leading to the loss of foot, ankle, and portion of shank.

Transfemoral amputation - lower limb removed between the knee joint and the hip joint, leading to the loss of foot, ankle, shank, knee, and portion of thigh

Intent Detection – Using data to predict what motions a patient will perform

Electromyography (EMG) - measurement of electrical signals in muscles caused by action potential and activity.

Surface Electromyography (sEMG) – obtaining EMG information by placing an electrode on the skin.

High Density Surface Electromyography (HDsEMG) – surface electromyography sensors arranged in a close grid on a small area, recording at once.

Crosstalk – interference in EMG signals from nearby muscles operating in similar frequency spectra

Traditional sEMG – sEMG collection system gathering data from a single electrode channel.

Best Signal – single signal selected from the available HDsEMG signal channels due to lack of noise content

Composite Signal – signal created by combining HDsEMG channels to form a single signal. This experiment uses a time series mean

Threshold Signal – Subset of Composite Signal that selects for HDsEMG signals with low noise content

ABSTRACT

Surface electromyography (sEMG) presents a pathway for prosthesis control but is prone to excess noise and signal corruption due to displacement. High Density Surface Electromyography (HDsEMG), which covers the same area as Traditional sEMG with multiple electrode channels as opposed to one channel, presents a way to overcome these challenges. Seven healthy participants were recruited and performed several activities of daily living with both Traditional sEMG and HDsEMG sensors on their Rectus Femoris, Biceps Femoris, Vastus Lateralis, and Semitendinosus muscles. These sensors were placed in both optimal locations over the muscle belly and in a location 1 cm distally from that optimal placement to simulate sensor displacement with use. From the data collected, four signals were created: a Traditional sEMG signal, the single HDsEMG signal with the highest signal-to-noise ratio (SNR) (Best Signal), a time mean of all HDsEMG signals (Composite Signal), and a time mean of all HDsEMG signals with SNR values greater than 2 dB (Threshold Signal). All signals' values for SNR, root-mean-squared means (RMS), DP ratio, and Ω ratio were compared in both optimal and displaced conditions. Phase lag and power domain similarity were used to assess response to displacement. Threshold mean and straight mean signals were identical in most values. The best signal displayed highest SNR, with the composite signal displaying second highest, and sEMG displaying lowest. These differences were more pronounced in extensor muscles in activities that involved large amounts of knee movements. sEMG signals displayed higher relative RMS values, as well as higher DP values. sEMG displayed statistically higher, but numerically similar Ω values. sEMG displayed a greater agreement between optimal and displaced signals in the frequency domain. Similarity was more dependent on activity type than signal type. Phase lag was determined to not be relevant. HDsEMG was proved to have potential for improved prosthesis control.

INTRODUCTION

Amputation and its Effects

Amputation presents a serious medical problem. At least 100,000 extremity amputation procedures are performed in the United States each year[1]. Amputation is a permanent procedure; the number of people missing at least one limb is increasing over time. Reasons for amputation include trauma[2], cancer[3], and vascular problems[4], of which diabetes is the main cause.

Prostheses as a Response to Amputation

A method to help amputees regain mobility is to replace the missing limb with a prosthesis. Prostheses are replicas of body parts meant to replace a lost body part for cosmetic or functional purposes. The first known functional prosthesis was a replica big toe found in ancient Egypt[5], which was able to return natural walking to the wearer. Prosthesis technology started with crude wood and metal replacements[6], with lower limb replacements being little more than an attached crutch which sometimes had a hinge. More naturally controlled prosthetics were created by the French doctor Pare in the 16th century[7], who developed a mechanical hand controlled with springs and a leg that could kneel with an artificial joint. Further prosthesis development occurred in the Victorian era[8], due to factory accidents increasing demand. In this situation, legs such as the Clapper Leg and the Cork Leg were created (Figure 1, left), which involved using artificial catgut tendons to link the motion of the knee and ankle joints. Over time, developing technology was added to prostheses, culminating in a concerted technological advancement during World War 2[9]. This led to the creation of suction attachments and lightweight aluminum devices. The main change would be the involvement of government-

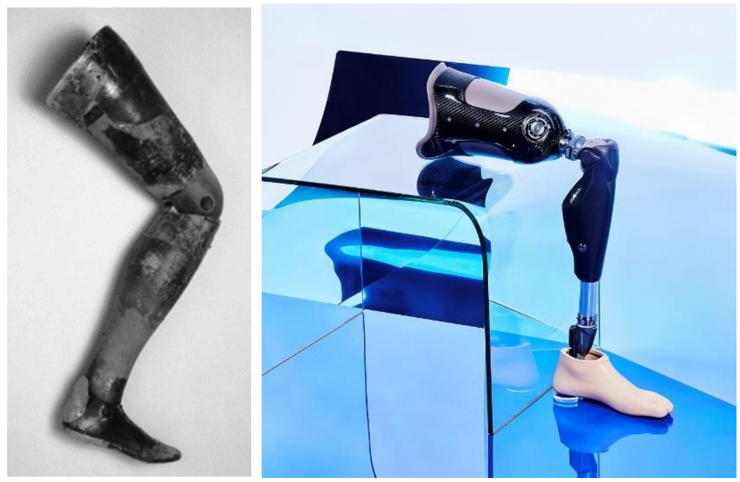

Figure 1: The Anglesey, or Clapper, Leg, designed in the 1800s. Artificial tendons made the ankle joint move when the knee joint moved[7].(left) and the modern C-Leg (Right) containing controlled knee and ankle joints[10].

sponsored research in prostheses, opening the way for more advanced devices to be developed and forming the research model that is used to this day.

Modern-day prostheses present a wide range of available options (Figures 2-4). The simplest ones are passive prostheses, which have no powered or controlled components. These kinds change knee and ankle angles based on gravity and internal components, and those that have bands of elastic to return energy and assist the user are known as passive-elastic prostheses. Others feature microprocessor-controlled joints. The most common of these is the

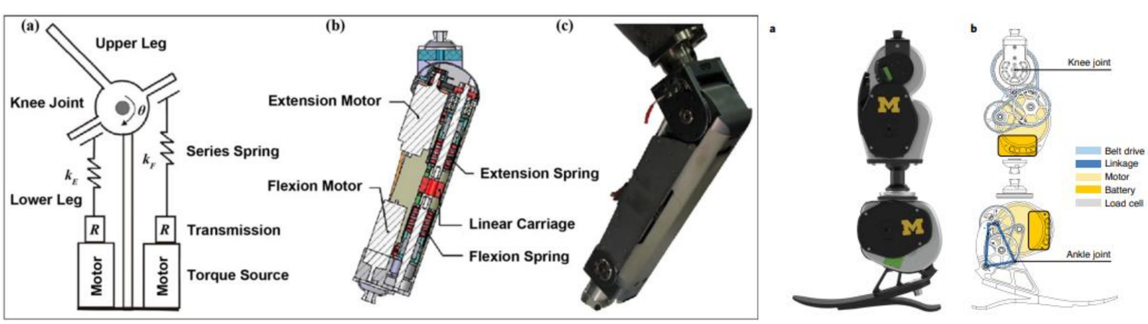

Figure 2: A two motor leg[14] (left) and the Open Source Leg (OSL, right)[15], demonstrating two models of joint mechanics. Due to the absence of actual muscles, alternate methods of motion are necessary.

microprocessor-controlled knee[11] (MPK), which uses a microprocessor to control the knee angle of the device. MPKs have been shown to increase amputee mobility and perceived safety with use. Ankle devices can include microprocessor control, and the control state of one joint does not determine the control state of the other. An ankle could be passive while the knee is microprocessor controlled, or both could be microprocessor controlled. The most advanced prosthesis technology is powered prostheses. These devices have an onboard battery continuously feeding power to the joints, leading to smoother, more accurate control. This power also allows for more opportunities, such as altering prosthesis stiffness while turning[12] or returning energy while walking to simulate the elasticity of the Achilles tendon[13].

Prosthesis Control

A prosthesis needs to be able to respond to the patient's movements in a manner that returns mobility and decreases fall risk. To accomplish this, a control system is needed to ensure that the user's intended motions are replicated adequately and at the correct time. However, activities of daily living are highly complex and variable, such as walking, sitting, running, and turning. These activities occur at various speeds and on various surfaces. A prosthesis control system needs to account for these variables. At the most basic, a control system will take inputs and turn them into useful outputs[16]. For prosthesis control, these outputs are the joint angles and segment location of the device. The process to achieve this involves taking signals collected from the body and device and determining the actions of the patient, known as intent detection. The ability to recognize the desired movements compared to others is known as classification accuracy[17, 18], and the higher the accuracy the better the control scheme. Once the control system decides, the device responds as informed. The time taken to process the data and produce an output is important, as well as the accuracy of that output. The number of parameters that the device can alter is known as its degrees of freedom. A higher number of degrees of freedom requires a more complex control scheme[19]. Prosthesis control is an important, yet complex topic, and improving control schemes can improve patient mobility.

Inputs for Control

The inputs chosen for prosthesis control are important since incorrect inputs lead to incorrect outputs. Inputs that are well-chosen and represent the correct motions for intent detection lead to an accurately controlled prosthesis. The input signal is analyzed for specific cues and items which relate to specific motions or needed responses, known as feature extraction[16]. Extra noise in a signal can cover up necessary features or add in false features, while incorrectly chosen inputs can present seemingly relevant features at the wrong time or present features that do not matter. The more inputs that can be placed into the control system, the more accurate a picture it can form of the patient's movement and make more accurate predictions, yet the larger the computation load and the longer the time needed to reach a decision.

Different types of inputs have been considered for prosthesis control. The earliest, most basic passive prostheses used motion and gravity as a control input, with the leg weighted such that the shank would always point downwards, with artificial tendons altering the ankle angle to match the resulting knee angle.[8] A more advanced input uses real-time data collection devices Inertial Motion Units (IMUs)[20]. These devices contain an accelerometer and a gyroscope, containing information about the direction, orientation, and speed of the device. From this, it can extrapolate which actions need to be performed next. Simple versions of this control place IMUs on the prosthesis itself, while more advanced versions place IMUs on the patient's sound leg and torso, resulting in a full body control system capable of achieving 100% accuracy in treadmill walking (Figure 3). Electroencephalography, or EEG, which measures the electrical activity in the brain, has been used as well[21]. This has been successful, with a simple knee lock/unlock mechanism having between 50 and 100 percent accuracy during walking between parallel bars[22]. EEG does not work as well to control more passive activities that do not require direct thought. Another form of control includes distance sensors such as infrared imaging or radar to give the prosthesis a view of the area around it to avoid hitting objects and predict activities such as stair walking[22].

Thermal imaging has been tested for monitoring muscle movements directly[23], but the technology is too bulky for practical use. These sensors are an integral part of a prosthesis control system, and their functionality directly affects the system’s performance.

Electromyography

One input method that has potential for prosthesis control is electromyography (EMG).

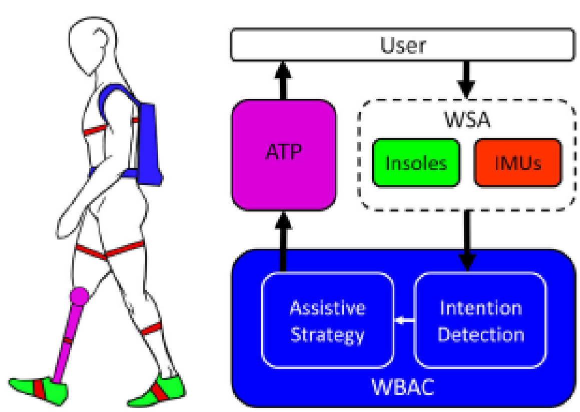

Figure 3: Model of full body awareness control, featuring IMUs placed on legs and torso, pressure sensitive insoles, and the control device in a backpack[20].

EMG works by measuring the electrical signals that occur in muscles due to contractions and action potentials[24]. The activity levels of relevant muscles can be measured as they occur. Three main kinds of electromyography exist: needle EMG (nEMG), implantable myoelectric sensors (IMES EMG), and surface EMG (sEMG) (Figure 4). nEMG works by inserting an electrode on a needle directly into the muscle of interest[25]. Direct insertion produces a clearer signal, as the electrode is in direct contact with the area to be measured. Needle placement can occur with high degrees of accuracy. However, nEMG is an invasive technique, requiring the needles to be inserted every time or leaving the sensors inside the patient, making it impractical for prosthesis control. IMES EMG solves this issue by designing the EMG electrodes to be permanently implanted at the muscle site[26-28]. This preserves the signal quality without the need for continual insertion. Several examples of arm and hand prostheses use IMES EMG as control inputs[25,30,31]. However, the immune system can form scar tissue around the sensor over time, leading to a loss in signal quality.

sEMG works by placing an electrode on the surface of the skin. Due to the sensitivity of the electrode, muscular impulses can be read through the skin. This layer of skin between the

Figure 4: nEMG electrode (left[32], Traditional sEMG electrode (center, picture by researcher), and IMES electrode (right)[29] Each type has advantages and disadvantages that must be considered before use

muscle and the sensor increases the amount of impedance, leading to noise in the signal. This noise can be reduced through cleaning of the skin before sensor placement but cannot be completely eliminated[31]. Due to the non-invasive nature of sEMG, it is more useful for situations where sensor placement is temporary or where surgery is to be avoided. sEMG has been used to control exoskeletons[33] (Figure 5) and prostheses[34] of both the upper and lower limb. Upper limb sEMG control devices are more common than sEMG lower limb devices. Control using EMG techniques uses signals from relevant muscles for intent detection purposes, either through passive monitoring of nearby muscles during activities or by having the patient flex their phantom limb in predetermined ways[35]. Saving the affected muscles, instead of removal during initial surgery helps this process, as the patient can flex the relevant muscle for control. Due to inherent variability in an individual's muscular function and activity and the patient's need to learn a new control scheme, there is usually a training period with these devices[35]. Traditional sEMG techniques do have inherent challenges to overcome. sEMG data is very sensitive to the location and size of the electrode[36], meaning that an electrode that is misplaced during initial donning of a device can affect its reliability. Electrodes can drift due to device movement during daily activities, known as pistoning[37]. Displacement increases the chance for the electrical

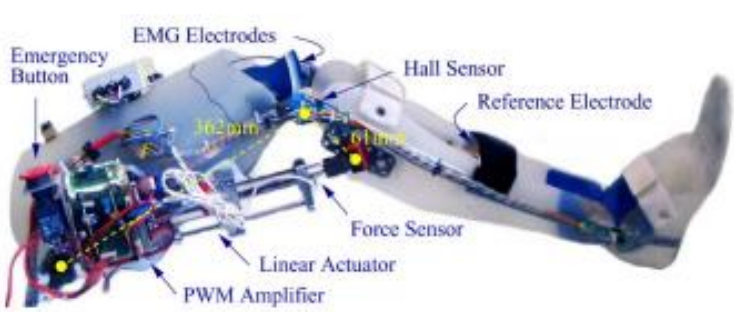

Figure 5: Exoskeleton controlled by EMG electrodes on model leg[23] demonstrating that sEMG control can benefit non-amputee populations

activity of other, nearby muscles to be picked up by the sensor. This interference is known as crosstalk. The potential for crosstalk is increased by most commercial sEMG sensors using single channel electrode arrays. If this one channel starts putting out data corrupted by noise or crosstalk, then the control system will not be as accurate.

High Density Surface Electromyography

One recent advance in traditional sEMG technology is the development of High Density Surface Electromyography (HDsEMG) (figure 6, bottom right). In HDsEMG sensors with multiple electrodes are placed over a muscle or area of interest. Each electrode channel records independent EMG signals. Early use of HDsEMG successfully identified individual motor units[38] and innervation zones[37]. HDsEMG has detected individual motions in small muscles, such as finger extensors[40], and was able to estimate finger movements. It has been proven to reduce crosstalk[41] and characterize muscles that are hard to measure with traditional sEMG

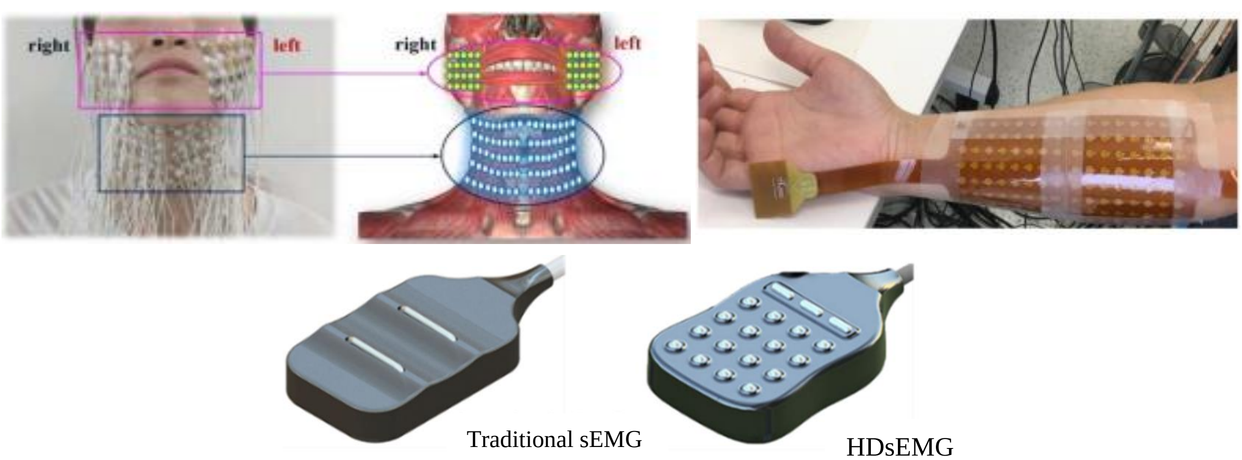

Figure 6: HDsEMG grid attached to face[44] (left, top) and forearm muscles[45] (right, top). These were the two main methods used before the creation of commercial HDsEMG sensors (right, bottom), which feature 16 sensors compared to the single channel seen in the single channel on a traditional sEMG sensor (left, bottom)

techniques, such as laryngeal muscles[42] and facial muscles[43]. It has demonstrated usefulness in machine learning applications, as a speech recognition experiment[44] showed that an array placed on the cheeks and the throat could distinguish between two languages spoken by a participant.

Previous HDsEMG devices were made in the labs using them for the specific task at hand. These were made from individual electrodes placed in a tight planned cluster (Figure 6, top left), or a flat sheet electrode array that is wrapped on the area of interest (Figure 6, top right). While this allowed data to be collected, there was no specific way to compare a standardized array to an existing sEMG sensor. However, Delsys recently released the first commercial HDsEMG sensor, the Delsys Maize. This device is the same size as their standard sEMG sensors (Delsys Avanti), with an extra grounding segment, and fits 16 electrodes in the same area that their traditional sEMG system fits one (Figure 6, bottom). Most work with HDsEMG has been comparing the activation levels in individual electrodes. Little work has been done to use a combination of signals from HDsEMG sensors to characterize the activation of an individual muscle with greater accuracy.

Purpose and Hypotheses

With these advantages, HDsEMG presents an advance that could make sEMG technology more useful for prosthesis control. Due to the multiple electrode channels analyzing the same area, more muscle activation data can be measured from the same surface area as traditional sEMG, allowing for higher definition control inputs for those with less surface area left after amputation. This study seeks to compare signal quality and responses to displacement and crosstalk in HDsEMG sensors to Traditional sEMG sensors to determine which would be more useful for lower limb prosthesis control. We also seek to determine ways to characterize the performance of the HDsEMG sensor, both on a channel-by-channel basis and as a whole unit, for future use in evaluating the quality of collected HDsEMG data. Therefore, this project has three main aims:

Aim 1

Quantify signal quality differences between HDsEMG and Traditional sEMG

HDsEMG provides a greater density of data for an individual muscle and has shown promise of producing high quality information about the state of muscle activation. We hypothesized that HDsEMG signals will result in higher signal quality than Traditional sEMG for prosthesis control.

Aim 2

Quantify signal variations during non-optimal placement for HDsEMG and traditional sEMG

Both surface-level sensor displacement and subcutaneous muscle displacement have been shown to affect EMG data. sEMG sensors used within a prosthesis socket are subject to cyclical motion and daily donning and doffing that can move the sensors away from their optimal placement. However, HDsEMG has a broader coverage over the muscle and may have the ability to compensate for small dislocations. We hypothesized that HDsEMG signals will accommodate displacement (retain higher signal quality) than Traditional sEMG sensors when displaced from optimal positions.

Aim 3

Identify effective processing methods when using HDsEMG signals for prosthesis control.

The HDsEMG sensors have multiple electrodes in an array creating a multitude of opportunities to select optimal signals individually or as combinations of several sensors in the group. We hypothesized that signals combining multiple sensors in the array to reject noise and improve quality will allow HDsEMG to produce higher quality signals as compared to traditional sEMG.

METHODS

Recruitment and Screening

To evaluate the hypotheses an experimental study was performed to generate a data pool of Traditional sEMG and HDsEMG data on a collection of activities of daily living while calculating basic quality comparison metrics to determine if further work is warranted. Recruitment occurred through advertisements in the local student newsletters, paper advertisements placed on billboards in public places, and awareness speeches made in relevant classes. Possible participants were encouraged to email Dr. Pew. Procedures were explained to the participants and ability to perform the activities was determined. Participants were asked if they had any musculoskeletal injuries or surgery in the last year or if they were displaying symptoms of COVID-19. No compensation was offered for participation. Seven healthy participants with no musculoskeletal injuries or surgery in the last year were recruited (4 male, 19-41 years old). Once a participant expressed interest and was deemed eligible, an appointment was made to meet in the lab On the day of the appointment, participants had the experiment explained to them while filling out a consent form and completed a leg dominance test (Waterloo Footedness Test)[46] and a physical activity level questionnaire (IPAQ short)[47]. The Waterloo Test determined which leg the sensors were placed on, while the IPAQ short was saved to investigate the role of fitness in a potential later study. After completing the paperwork, participants changed into provided shorts modified to attach motion capture markers to the skin.

Equipment and Setup

The locations for the EMG sensors of four muscles of knee movement on the dominant limb, Rectus Femoris (RF), Vastus Lateralis (VL), Semitendinosus (ST), and Biceps Femoris (BF), were determined using palpation techniques[48] (Figure 7, left). The VL and RF were chosen to represent knee extensors, and ST and BF were chosen to represent knee flexors. These muscles were chosen due to prominence and closeness to the surface. Once optimal placement sites were found, an sEMG sensor was placed on the location, and a partial outline was made using a surgical marker. A tape measure was used to measure 1 cm distally perpendicular to the bottom of the sensor, and the sensor was moved. A second partial outline was drawn based on the new location (Figure 7, right). This created the displaced data used for the analysis of aim 2. Medial/lateral displacement was not considered to limit variables. Displaced sensors were attached as normal. While this does not directly represent any loss of contact or sensor loosening due to displacement, it was more consistent in application and procedure. Previous work on torso

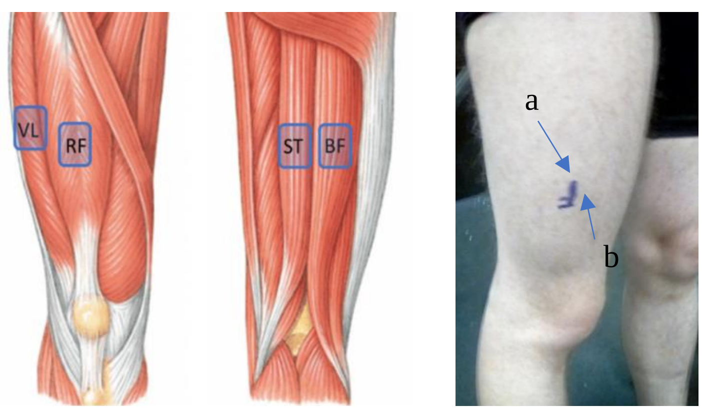

Figure 7: Anatomical locations of muscles (left) and exterior markings after palpation (right). VL - Vastus Lateralis, RF - Rectus Femoris, ST - Semitendinosus, BF - Biceps Femoris. Extensor muscles are on the left (anterior), while flexors are on the right (posterior). Upper marking (a) is optimal location. Lower marking (b) is displaced location. Right leg Vastus Lateralis used as an example.

muscles has found that displacement in the medial-lateral plane has less effect on the signal than displacement in other planes, leading to the distal displacement used here[49]. The outline was used to ensure sensors were placed in the same location during condition changes. 59 motion capture tracking markers were attached to the participant in a full-body modified Plug-in Gait pattern. Modifications included the addition of markers to the anterior thighs and calves, first and fifth metatarsal heads, medial aspects of ankle and knee joints, fibular trochanters, and iliac crests of both sides[50] (see Appendix I). Thickness measurements were taken of the ankles, knees, hands, wrists, elbows, and shoulders, as well as leg length, for future modeling from motion capture data. The participant then stood on a force plate array (AMTI, Watertown MA) and completed a lab standard calibration process with the motion capture software (Motion Analysis Corp). This process involved holding a static pose, walking around the capture area, and completing a range of motion test involving waving arms, swinging hips, and squatting[51]. EMG sensors were attached after motion capture markers and calibration to preserve battery life. All four muscles had a sensor attached, with one flexor and one extensor having an HDsEMG sensor and one flexor and one extensor having a standard sEMG sensor. This was due to limited amounts of HDsEMG sensors. After completing all activities of daily living, sensor type was swapped for each muscle (Figure 8). Sensors were placed in either the optimal placement or the 1 cm distal displaced placement. All sensors in a condition were in the same placement.

This resulted in four sensor conditions (Table 1). Sensor order was randomized for each subject to minimize fatigue effects on data collected. Transition occurred between each set of activities of daily living, and care was taken to ensure that sensors were placed in the same locations each time. Ground sensors for the HDsEMG sensors were placed in the IT band if possible and placed on an area with fewer muscles below the glutes if not possible for flexor muscles.

Location	Muscles with HD sensors	Muscles with Trad sensors
Optimal	Rectus Femoris, Biceps Femoris	Vastus Lateralis, Semitendinosus
Optimal	Vastus Lateralis, Semitendinosus	Rectus Femoris, Biceps Femoris
Displaced	Rectus Femoris, Biceps Femoris	Vastus Lateralis, Semitendinosus
Displaced	Vastus Lateralis, Semitendinosus	Rectus Femoris, Biceps Femoris

Table 1: Sensor conditions used. Traditional sEMG (Trad), HDsEMG (HD) sensors, optimal is on muscle belly, and displaced is 1 cm distal from muscle belly

Activity	Recording Method	Extra Equipment	Trial Criteria
Walking	Individual	Timing gates	Foot contact on force plate, speed within 10% of precalculated average
Internal Turning	Continuous	Stool placed as visual aid for turning	Foot contact on force plate, turning on dominant foot
External Turning	Continuous	Stool placed as visual aid for turning	Foot contact on force plate, turning on dominant foot
Ramp Walking	Individual	10 degree ramp with landing at top	Foot contact on force plate
Stair Climbing	Individual	Staircase	Foot contact on force plate
Squats	Continuous	N/A	N/A
Sit-to-stand	Continuous	Plastic chair	N/A

Table 2: Activities of daily living. Individual recording method refers to recording each trial as a singular run, while continuous refers to chaining all trials together without breaks

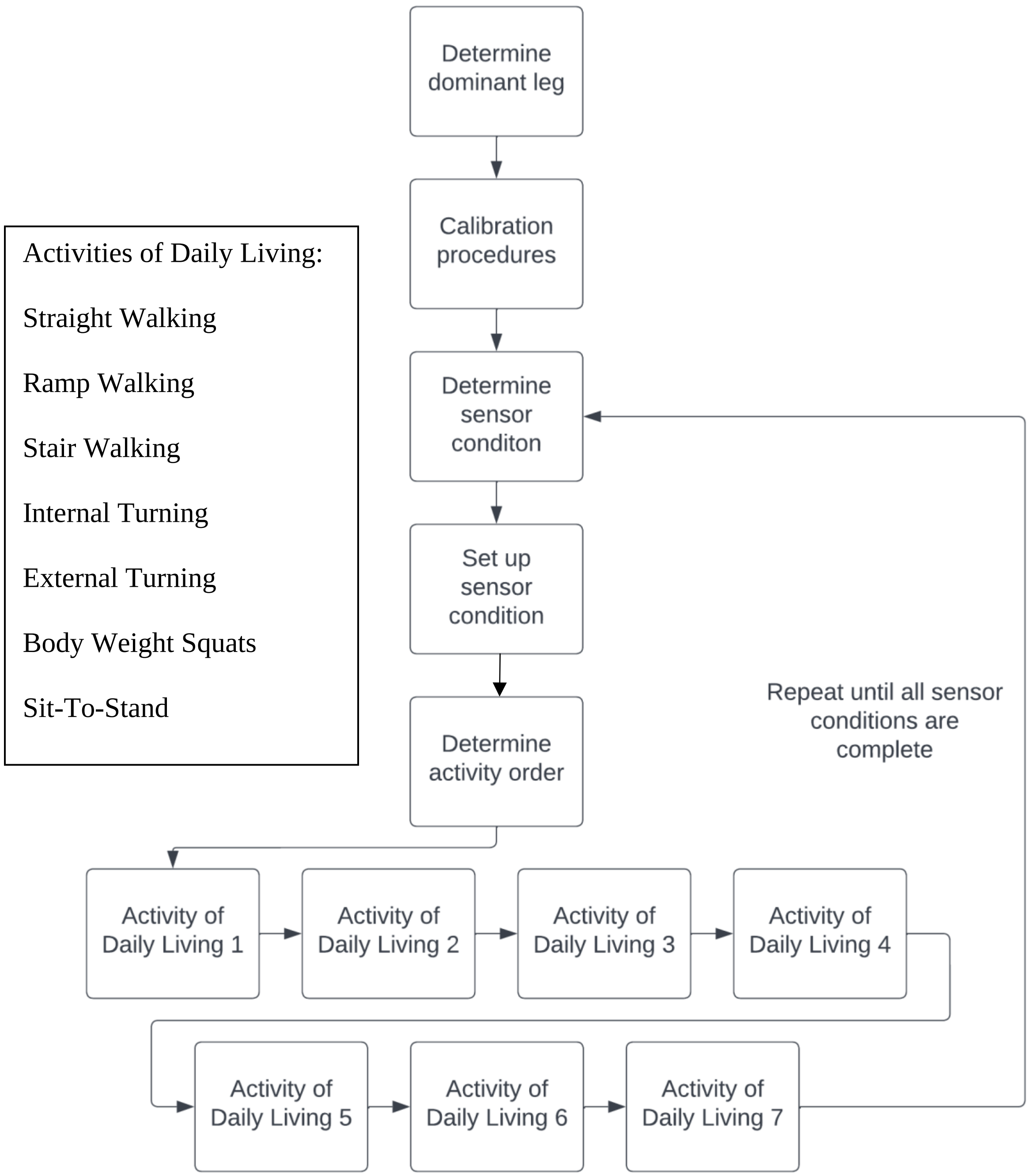

Figure 8: Flowchart of experimental protocol. Conditions were chosen from Table 1 in a randomized order, and activities of daily living were chosen from Table 2 in a randomized order

Activities of Daily Living

For each sensor condition, participants completed several different activities of daily living. These activities were selected to simulate basic activities that a person would complete throughout a normal day and included straight walking[52], stair walking[53], ramp walking[54], internal turns, external turns[55], body weight squats, and sitting and standing[56]. The activities were performed until three trials meeting the criteria in the detailed list and Table 2 were collected. Motion capture and EMG started recording simultaneously using a trigger module. Data recording started when the participant was given a verbal cue to begin. Movements were described and demonstrated during the participant's first sensor condition, and a short overview was given for each subsequent sensor condition. Observers ensured that correct trial criteria were met. The participant was not informed about the criteria to maintain normal biomechanics. Criteria included the dominant foot fully touching a force plate without interference from the

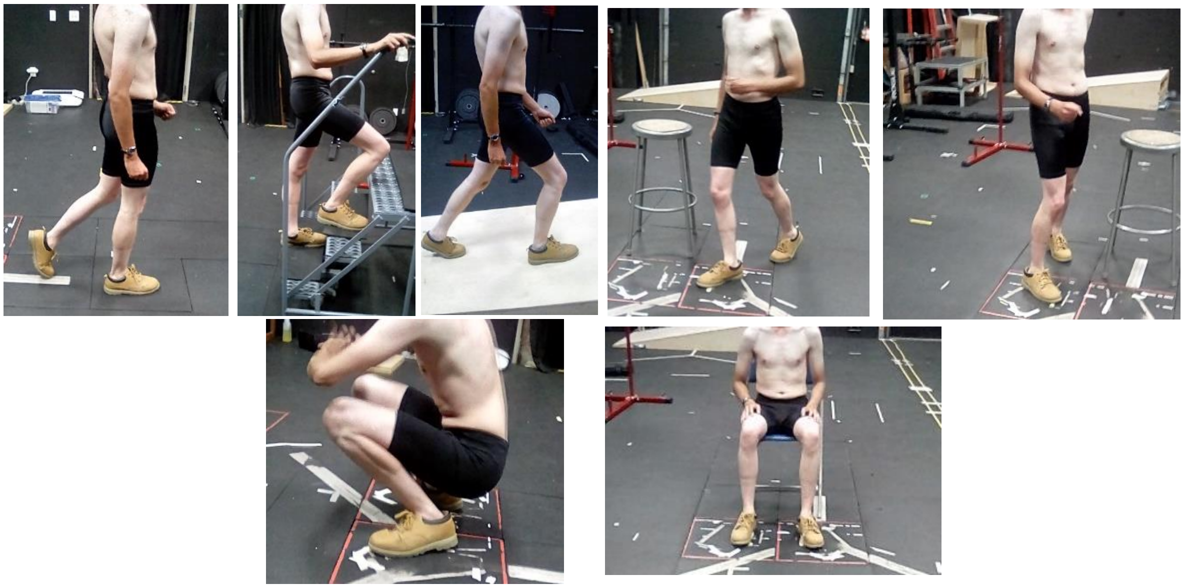

Figure 9: Activities of daily living, in order left to right, top to bottom: Straight Walking, Stair Walking, Ramp Walking, Internal Turn, External Turn, Squats, Sit to Stand

other foot, correctly performing the action, and in the case of the walking trial, maintaining walking speed within 10% of a previously calculated mean speed. Participants completed the following activities (Table 2).

Straight Walking: participant walked forward over the force plate array from a marked starting line. Timing was maintained using a split gate timing system (FITLIGHT Trainer, FITLIGHT Corp, Miami, FL), and three representative walking trials were completed before calibration to obtain a mean walking time. Individual walking trials were cued. The trial was considered completed once the participant had left the force plate array. The trial was analyzed from toe off of dominant leg before contact with force plate to toe off from force plate. See Figure 9.

Stair Walking: participant walked forward over the force plate array and up a set of stairs placed at the end of the array. At the top, they turned around and walked back across the force plate array to the starting point. The trial was considered completed after leaving the force plate array after finishing the stair task. Individual stair walking trials were cued. The trial was analyzed from toe off before stair contact to heel strike after last stair contact. See Figure 9.

Ramp Walking: participant walked forward over the force plate array and up a 10-degree ramp[56,57] placed at the end of the array. At a landing placed level with the top of the ramp, the participant turned around and walked back down and across the force plate array to the starting point. The trial was considered completed after leaving the force plate array after finishing the ramp task. Individual ramp trials were cued. Effort was made to make stair and ramp walking as similar as possible, leaving the surface walked on as the only variable. The trial was analyzed from toe off before ramp contact to heel strike after last ramp contact. See Figure 9.

Internal Turn: participant walked forward over the force plate array and made a turn with their dominant leg being the pivot point and closest to the direction turned in. For most participants, this was a right turn. The turning point was visually cued by a stool placed before the turning location for the participant to turn around. Difference between internal and external turns was demonstrated to the participant. Performing an external turn with their non-dominant foot was considered reason to reject a trial. All internal turning trials were executed in sequence with no breaks. The trial was considered complete after completing the turn and moving forwards past the stool. The trial was analyzed from toe off before initial turn start to heel strike after moving past stool. See Figure 9.

External Turn: participant walked forward over the force plate array and made a turn with their dominant leg being the pivot point and furthest from the direction turned in. For most participants, this was a left turn. The turning point was visually cued by a stool placed before the turning location for the participant to turn around. Difference between internal and external turns was demonstrated to the participant. Performing an internal turn with their non-dominant foot was considered reason to reject a trial. All external turning trials were executed in sequence with no breaks. The trial was considered complete after completing the turn and moving forwards past the stool. Care was taken to make internal and external turning trials as similar as possible so that the direction turned was the main variable. The trial was analyzed from toe off before initial turn start to heel strike after moving past stool. See Figure 9.

Squatting: participant stood with one foot each on a force plate and completed three body-weight squats in sequence. Participants were instructed to squat to a comfortable depth that they could repeat and to pause for 1-2 seconds when they reached the bottom of the squat and when they returned to standing. The trial was considered complete when the participant returned to the standing pose. The trial was analyzed from initial bending of knees to begin squat to straightening of legs after completion of the squat. See Figure 9.

Sit to stand: participant started from a comfortable sitting position with each foot on a force plate and the chair on the force plate array. They then stood up at a comfortable pace and then sat back down three times in succession. They were instructed to pause for 1-2 seconds after fully standing up, and when they returned to the sitting position. The trial was considered complete when the participant returned to sitting position. The trial was analyzed from initial torso movement to begin standing to end of torso movement after sitting. See Figure 9.

Signal Processing and Generation

All 16 HDsEMG signals and Traditional sEMG signals were processed together. Signals were rectified and normalized to the subject's highest EMG value for sensor and muscle across all activities and displacement types (Appendix 3). Signals were mean corrected and 4th order Butterworth filtered between 20 and 350 Hz[59,60]. Initial signal-to-noise ratio (SNR) and root-mean-squared level (RMS) and power spectrum calculations were performed on the filtered signals. Traditional sEMG signal was complete after this point.

For this experiment, three signals were created from data taken from HDsEMG electrodes (collectively known as HDsEMG signals). The first is the Best Signal, created to represent a control system that works from one out of the 16 channels exclusively. This was determined by choosing the one channel out of the 16 that had the highest SNR values. The second signal was the Composite Signal, meant to represent a simple and quick method of combining all 16 channels. This was initially decided to be a time series mean of all 16 channels, with more intensive combination methods saved for further research. The third and last HD-derived signal was the Threshold Composite Signal, or the Threshold Signal. This was created by a time series mean of all HDsEMG channels that had a calculated SNR of greater than 2 dB. This value was chosen as the level at which a signal is unusable due to excess noise[61]. All 16 SNR values were calculated, and the channel displaying the highest was saved as the Best Signal. This process was carried out for each individual trial, without accounting for previously determined Best Signals in similar trials, though the physical location of each channel was saved for later analysis. The Composite Signal was created through a time mean of all 16 HDsEMG channels throughout the entire area of interest. The last signal to be created was the Threshold Signal using all channels with SNR greater than 2 dB. Both Composite and Threshold Signals were formed from unfiltered data, which was processed after signal creation. There are more advanced ways of combining signals, especially post-collection, prosthesis control occurs in real-time and requires a faster processing time and lower computing needs to make sure outputs are synced with the necessary patient motions.

Signal Quality and Symmetry Measures

Aim 1

Quality measurements were calculated from the four created signals to fulfill Aim 1 and create a comparison for Aim 2. For Normal, Best, Composite, and Threshold signals, a single value for each measure for Traditional sEMG, and HDsEMG values for each of the 16 channels were calculated. Channel number and physical location for the maximum and minimum values were recorded, along with the overall mean for all 16 channels. The quality measures were:

Signal-to-Noise Ratio[61,62]: a measure of the level of the desired signal in the data to the level of noise in the data. A higher value denotes a signal greater than the noise present, and thus large values indicate a better signal. As the value gets larger, the signal is less distorted by noise. Values above 10 dB can be considered free from most noise distortion for sEMG signals. Signal was defined as the filtered version, and noise was isolated by subtracting the filtered signal from the raw signal.

Root-Mean-Squared[62]: an altered method of finding the average value of signal amplitude. Higher values denote a signal with a higher amplitude, and thus a stronger signal. Due to an amplification factor present for several sEMG sensors, these values had to be computed based on data normalized to the highest value seen in a given sensor and muscle (Appendix III). These values were calculated on the processed data.

DP Ratio[62]: this method determines whether the peak of the power density, where the signal should be, is sufficiently larger than the areas of low power density, where noise is. This is obtained by dividing the highest mean power density by the lowest mean power density. A sufficiently large value indicates the presence of a strong signal, and a lower value indicates a weak signal or no signal. This differs from determining signal strength through RMS methods, as RMS is based in the time domain and DP is based in the power domain. Therefore, having both gives a full characterization of signal strength. A value above 30 dB denotes a good signal.

Ω Ratio[62]: the Ω ratio is used to find changes in symmetry around the central frequency and extra sources of noise that might not be found in the SM ratio. It is found by manipulating the spectral moments using the equation

$$(1)\ \Omega = (M_2/M_0)^{1/2}/(M_1/M_0)$$

where M represents spectral moments calculated during initial signal processing. These values were calculated on the processed data. Values for diaphragm EMG, which was used for the initial source of this measurement, are recommended to be below 1.4. Little work has been done for Ω for lower limb sEMG.

Aim 2

Because traditional sEMG systems only gather data from a singular channel, they are susceptible to effects of crosstalk and excess noise when displaced. HDsEMG sensors have extra electrodes, so if some are displaced from optimal placement, the others have the potential to still be collecting data. The decline in quality will be measured by comparing the previously mentioned quality measurements taken in an optimally placed sensor to quality measurements taken from the same sensors in an intentionally displaced location. Crosstalk was analyzed by determining the similarity between the optimal and displaced signals. Similarity in the time domain was measured using cross correlation and cross covariance, which measure offset and lag between two signals. The lower the cross correlation or covariance values, the less lag is present. The two methods will act as checks against each other. Similarity in the frequency domain was analyzed using mean squared correlation, which returns a value between 0 and 1 for each part of the frequency band, with values closer to 1 meaning that the power in the frequency is closer for the two signals. If high signal quality was found, but low similarity, this means that that sensor is susceptible to cross talk, while high similarity and quality mean that the signal is good despite being displaced. The signal similarity measures were:

Cross Correlation[63]: measures how similar two time domain series are when one is shifted to detect any time offset or phase lag. This could be useful for detecting lag due to displacement or crosstalk from offset muscles. A lower value, denoting a lower amount of lag separating the two signals, denotes a more similar signal. The desired output is 0. Optimal placement was used as the base signal, with the displaced signal being compared. These values were calculated on the processed data.

Cross Covariance[64]: measures how similar two time domain series are when one is shifted to detect any time offset. Due to using a different mathematical method, this works as a check for the cross correlation measure, with agreement between the two meaning both measures are reliable, and disagreement denoting the necessity for further signal analysis. Like cross coherence, a lower value denotes lower phase lag, meaning the signals are more similar. A signal with low cross coherence and cross covariance is very similar in the time domain. Therefore, the desired value would be 0. These values were calculated on the processed data.

Magnitude Squared Coherence[65]: measures how similar the magnitude of each frequency component is across the frequency spectrum, with a higher value denoting greater similarity. Due to MATLAB requiring vectors of the same size to carry out this function, signals with fewer

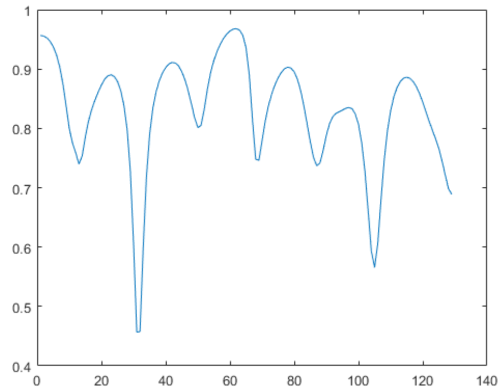

Figure 10: Full magnitude squared coherence graph across all relevant frequencies. Coherence mean is the mean of all values and Coherence Deviation is the standard deviation for all values. A higher mean and lower deviation denotes greater signal similarity.

values were up-sampled to meet the same length as the signal with the greater amount of values. Since this characterizes similarity in the frequency domain, it works well with the time domain analysis mentioned earlier, with signals displaying close similarity in both domains being considered very similar and less affected by crosstalk. Since magnitude squared coherence returns a value for each frequency (Figure 10), consistently high values denote greater similarities. This does make it harder to analyze in bulk, so further measures are needed for simplification.

Mean Coherence: the mean of all values across the frequency spectrum from magnitude squared coherence. A higher mean coherence value denotes higher magnitude squared coherence values across the entire spectrum, making a higher mean coherence denote a more similar signal. However, this measure is sensitive to individual outlier values, which can skew the mean coherence positive or negative. These values were calculated on the processed data.

Coherence Deviation: the standard deviation of magnitude squared coherence values across the frequency spectrum. This measures how closely grouped the coherence values are, with more similar values across the frequency spectrum resulting in a lower deviation value. Combined with a higher mean coherence, this provides the case for the two signals being overall similar throughout the entire frequency spectrum. However, it does not contain much information about individual outliers in the frequency spectrum. These values were calculated on the processed data.

If two signals are uncontaminated by crosstalk, they will display lower cross correlation and cross covariance values, a high mean coherence, and low coherence range and coherence deviation values. Similarity measures were calculated for each of the 16 HDsEMG channels, and the highest, lowest, mean, and sensor channels for highest and lowest determined to characterize the HDsEMG sensor. A signal type that displays both high quality measures and high similarity measures can be considered both free of noise and unaffected by crosstalk when displaced, making it useful for prosthesis control. Due to comparison between two different trials, some level of variation is expected, and not a perfect coherence value of 1 with a negligible standard deviation.

Statistical Analysis

Statistical analysis and modeling were accomplished with the help of Mark Greenwood, a member of the Montana State University campus statistics faculty. Because the Composite and Threshold signals had the potential to generate the same values Pearson correlation between the two signals with regards to several quality measures was calculated. Pearson correlation measures the similarity between the series of numbers, with values closer to a one-to-one line representing more similar outputs.

The signal quality output variables were analyzed by a multilevel random effects model in R, which considered multiple layers of variability including signal type, muscle, activity, specific trial, and individual subject as well as accounting for repeated measures[66,67]. Model layers were removed if they were found to be irrelevant, simplifying the model. Individual subjects and individual trials were found to be irrelevant, meaning no group of outliers was linked to a specific subject. All collected data values were used in the model, with no in-subject averaging. Due to the spread of certain data values, a log10 transformation was used to reduce variance to levels needed for accurate statistical analysis. Significance was determined to be at $p<0.05$.

RESULTS

Similarity between Composite and Threshold Signals

Pearson analysis showed a 1-1 correlation between the Composite and Threshold signals. Due to this similarity, the results would be the same for both signals. Thus, only the Composite Signal was considered for statistical analysis.

Signal to Noise Ratio

Signal to Noise Ratio (SNR) is measured in decibels (dB). Statistical modeling showed that there were significant differences tied to muscle, signal, and activity ($p<0.01$), as well as two-way interactions occurring between muscles and signals, location and signals, and muscles and activities ($p<0.01$), and three-way interactions occurring between muscles, locations, and signals ($p<0.01$) and muscles, signals, and activities ($p=0.033$). All signals showed similar trends of having the highest SNR values for Best signals, with Composite signals having lower, but similar levels, and sEMG signals displaying smaller SNR values (Figures 11-18). This held true for all activities, muscles, and sensor locations. Displaced sensors generally displayed similar or slightly lower SNR values than optimal values, but there were a few instances where displaced sensors showed larger SNR values. A few specific activities and muscles displayed an increase in SNR when displaced for Traditional sEMG signals only. The differences in SNR between the two HD-derived signals and the Traditional sEMG signal differed between activities and muscles. The highest difference in mean between signal types was seen in the Vastus Lateralis and Rectus Femoris. Specific trials impacted were stair walking, sit-to-stand, and squat trials.

Effects analysis determined that 57% of variability was due to fixed effects and 95% of variability was due to a combination of fixed and random effects.

Activity	Muscle	Best - Opt	Best - Disp	Comp - Opt	Comp - Disp	sEMG - Opt	sEM - Disp
Internal Turn	Vastus Lateralis	11.99 +/- 0.96	11.59 +/- 0.96	9.7 +/- 0.96	8.51 +/- 0.96	4.32 +/- 0.96	3.61 +/- 0.96
	Rectus Femoris	10.3 +/- 0.96	9.41 +/- 0.96	8.74 +/- 0.96	7.77 +/- 0.96	2.43 +/- 0.96	2.27 +/- 0.96
	Biceps Femoris	12.74 +/- 0.96	11.79 +/- 0.96	10.55 +/- 0.96	9.12 +/- 0.96	6.96 +/- 0.96	5.67 +/- 0.96
	Semitendinosus	10.62 +/- 0.96	9.87 +/- 0.96	8.28 +/- 0.96	6.60 +/- 0.96	6.40 +/- 0.96	6.60 +/- 0.96
External Turn	Vastus Lateralis	12.79 +/- 0.99	11.55 +/- 0.96	10.54 +/- 0.96	8.49 +/- 0.99	4.07 +/- 0.96	3.96 +/- 0.99
	Rectus Femoris	10.56 +/- 0.96	8.79 +/- 0.99	8.73 +/- 0.96	7.53 +/- 0.99	2.71 +/- 0.99	2.46 +/- 0.96
	Biceps Femoris	12.23 +/- 0.96	10.81 +/- 0.99	10.43 +/- 0.96	8.7 +/- 0.99	6.61 +/- 0.99	6.28 +/- 0.96
	Semitendinosus	10.38 +/- 0.99	10.38 +/- 0.96	7.67 +/- 0.96	7.4 +/- 0.96	4.9 +/- 0.96	4.97 +/- 0.99
Walking	Vastus Lateralis	12.36 +/- 1.00	10.59 +/- 1.01	9.37 +/- 1.00	8.31 +/- 1.01	4.19 +/- 0.96	4.76 +/- 0.96
	Rectus Femoris	9.32 +/- 0.96	8.98 +/- 0.96	7.68 +/- 0.96	7.88 +/- 0.96	1.19 +/- 1.00	1.97 +/- 1.01
	Biceps Femoris	10.25 +/- 0.96	10.39 +/- 0.96	7.7 +/- 0.96	8.29 +/- 0.96	5.65 +/- 1.00	6.85 +/- 1.01
	Semitendinosus	9.3 +/- 1.00	8.66 +/- 1.01	7.36 +/- 1.00	6.07 +/- 1.01	5.05 +/- 0.96	4.99 +/- 0.96
Stair Walking	Vastus Lateralis	15.62 +/- 0.98	15.8 +/- 0.96	12.32 +/- 0.98	14.02 +/- 0.96	7.58 +/- 0.97	7.56 +/- 0.96
	Rectus Femoris	12.82 +/- 0.97	13.59 +/- 0.96	10.99 +/- 0.97	11.79 +/- 0.96	4.08 +/- 0.98	4.54 +/- 0.96
	Biceps Femoris	12.4 +/- 0.97	12.52 +/- 0.96	10.42 +/- 0.97	10.86 +/- 0.96	5.53 +/- 0.98	7.1 +/- 0.96
	Semitendinosus	12.2 +/- 0.98	11.45 +/- 0.96	9.93 +/- 0.98	9.12 +/- 0.96	7.24 +/- 0.97	7.32 +/- 0.96
Ramp Walking	Vastus Lateralis	13.6 +/- 0.97	12.15 +/- 1.01	11.29 +/- 0.97	9.57 +/- 1.01	6.08 +/- 0.97	4.77 +/- 1.01
	Rectus Femoris	11.63 +/- 0.96	10.48 +/- 0.96	9.36 +/- 0.96	8.98 +/- 0.96	2.29 +/- 0.97	2.85 +/- 1.01
	Biceps Femoris	11.29 +/- 0.96	9.6 +/- 0.97	9.51 +/- 0.97	7.66 +/- 0.97	5.12 +/- 0.97	6.33 +/- 1.01
	Semitendinosus	11.55 +/- 0.97	11.1 +/- 1.01	9.07 +/- 0.97	8.19 +/- 1.01	5.67 +/- 0.96	5.42 +/- 0.96
Sit to Stand	Vastus Lateralis	18.74 +/- 1.04	17.95 +/- 0.96	17.75 +/- 1.04	15.61 +/- 0.96	7.24 +/- 0.96	8.26 +/- 0.96
	Rectus Femoris	15.13 +/- 0.96	16.01 +/- 0.96	13.21 +/- 0.96	13.51 +/- 0.96	2.34 +/- 1.04	4.16 +/- 0.96
	Biceps Femoris	12.1 +/- 0.96	10.22 +/- 0.96	8.87 +/- 0.96	7.47 +/- 0.96	2.36 +/- 1.04	3.87 +/- 0.96
	Semitendinosus	12.29 +/- 1.04	9.93 +/- 0.96	9.51 +/- 1.04	6.95 +/- 0.96	3.89 +/- 0.96	3.87 +/- 0.96
Squats	Vastus Lateralis	18.77 +/- 0.96	19.82 +/- 1.11	15.91 +/- 0.96	16.67 +/- 1.11	9.6 +/- 0.96	9.9 +/- 1.11
	Rectus Femoris	17.91 +/- 0.96	17.18 +/- 0.99	15.28 +/- 0.96	15.06 +/- 0.99	7.51 +/- 0.96	7.84 +/- 1.11
	Biceps Femoris	11.16 +/- 0.96	8.95 +/- 0.99	7.96 +/- 0.96	6.59 +/- 0.99	4.94 +/- 0.96	4.42 +/- 1.11
	Semitendinosus	13.21 +/- 0.96	10.8 +/- 1.11	9.98 +/- 0.96	7.35 +/- 1.11	4.39 +/- 0.96	4.55 +/- 0.99

Table 3: Signal to Noise Ratio means (dB) with standard error. Best – best selected signal, Comp – composite signal, sEMG – traditional sEMG, Opt – optimally placed over muscle belly, Disp - displaced 1 cm distal from muscle belly

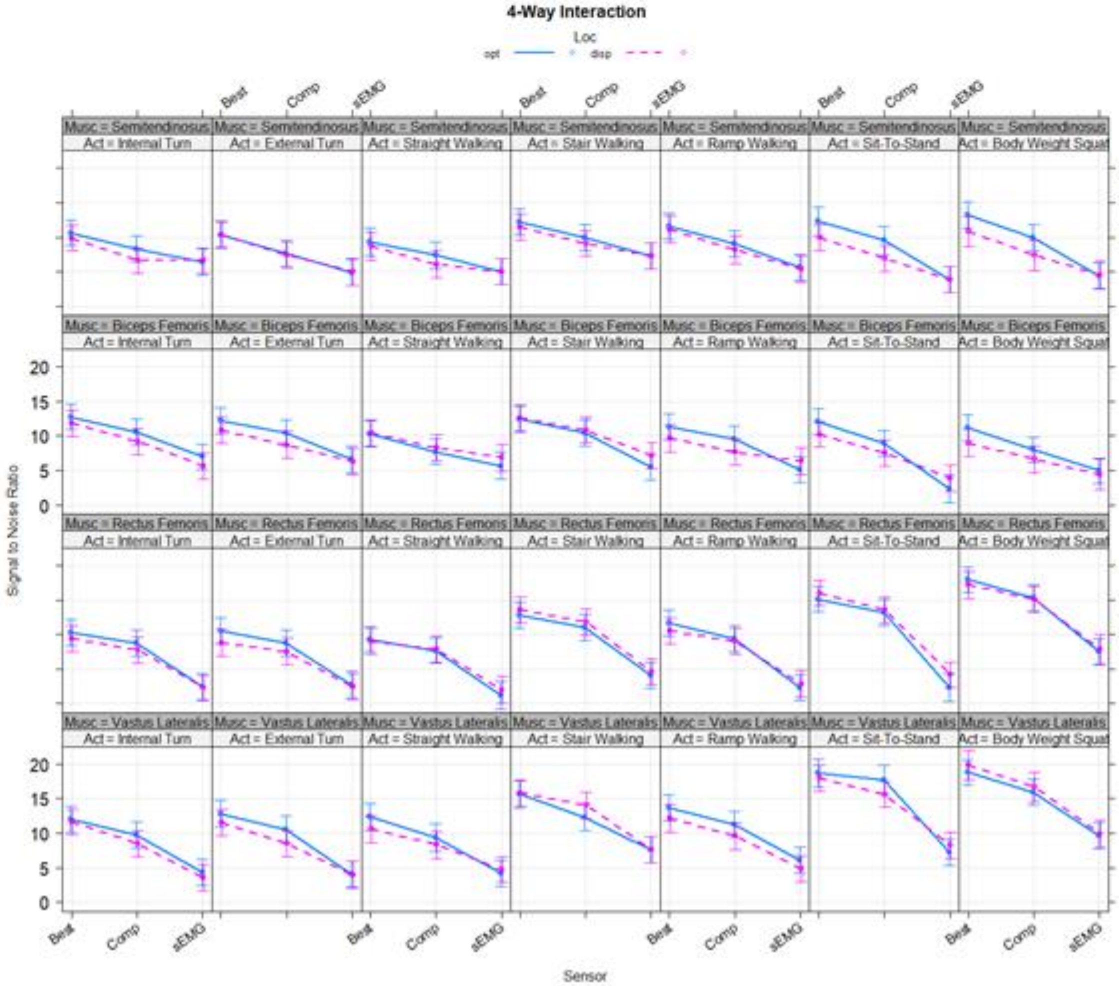

Figure 11: Effects plot of signal to noise ratio. Solid blue is optimal placement, dashed pink is displaced. Best is Best Signal, Comp is Composite Signal, sEMG is Traditional sEMG. Note the higher means for Best and Comp for all trials, in particular for Rectus Femoris and Vastus Lateralis. Displaced displayed lower mean values for several activity types while following general signal type based trends.

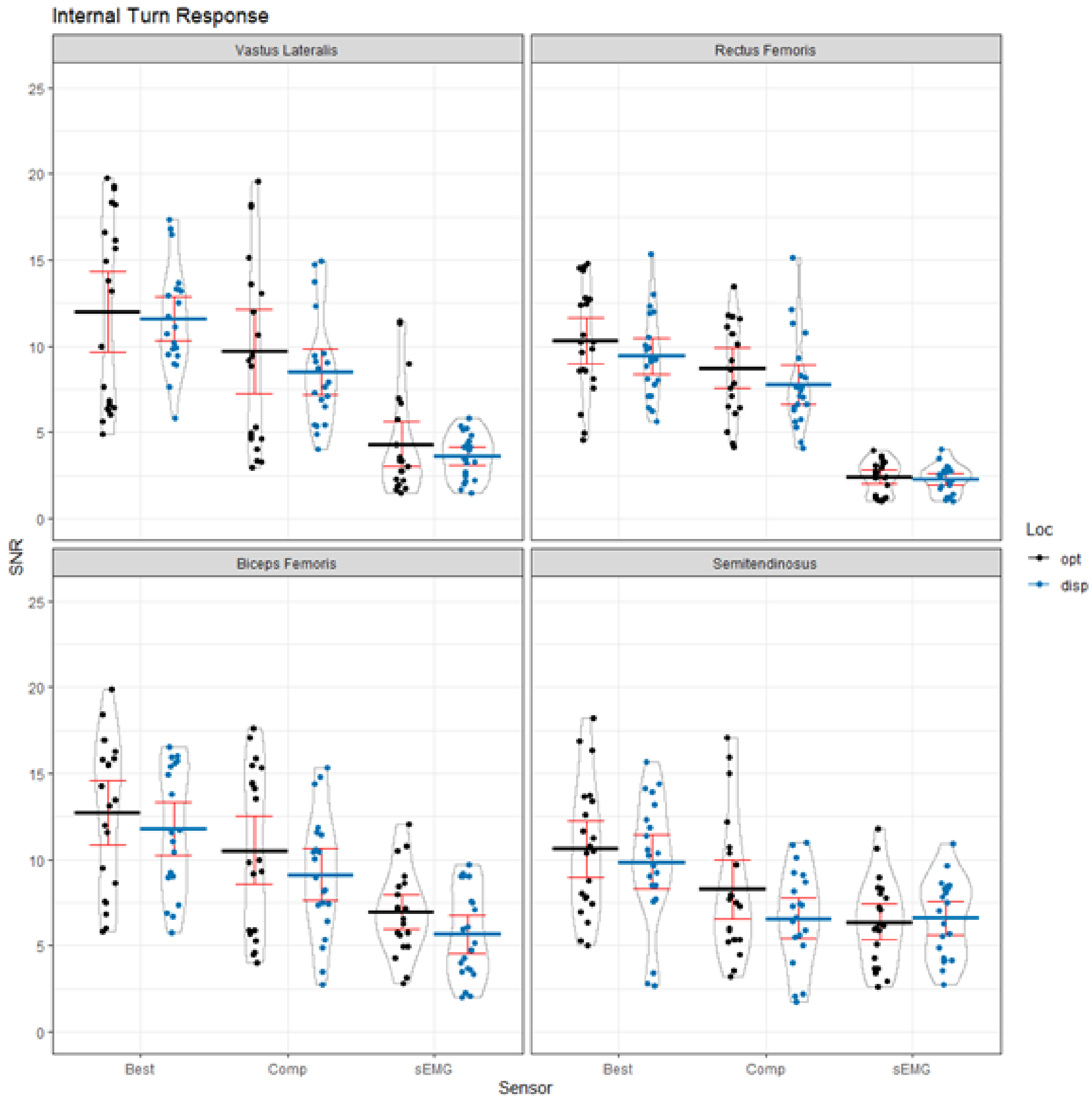

Figure 12: Violin plot of SNR (Signal to Noise Ratio) for Internal Turn. Opt denotes optimal placement while disp denotes displacement. Best is Best Signal, Comp is Composite Signal, sEMG is Traditional sEMG. Note the larger difference between means for Rectus Femoris (top right).

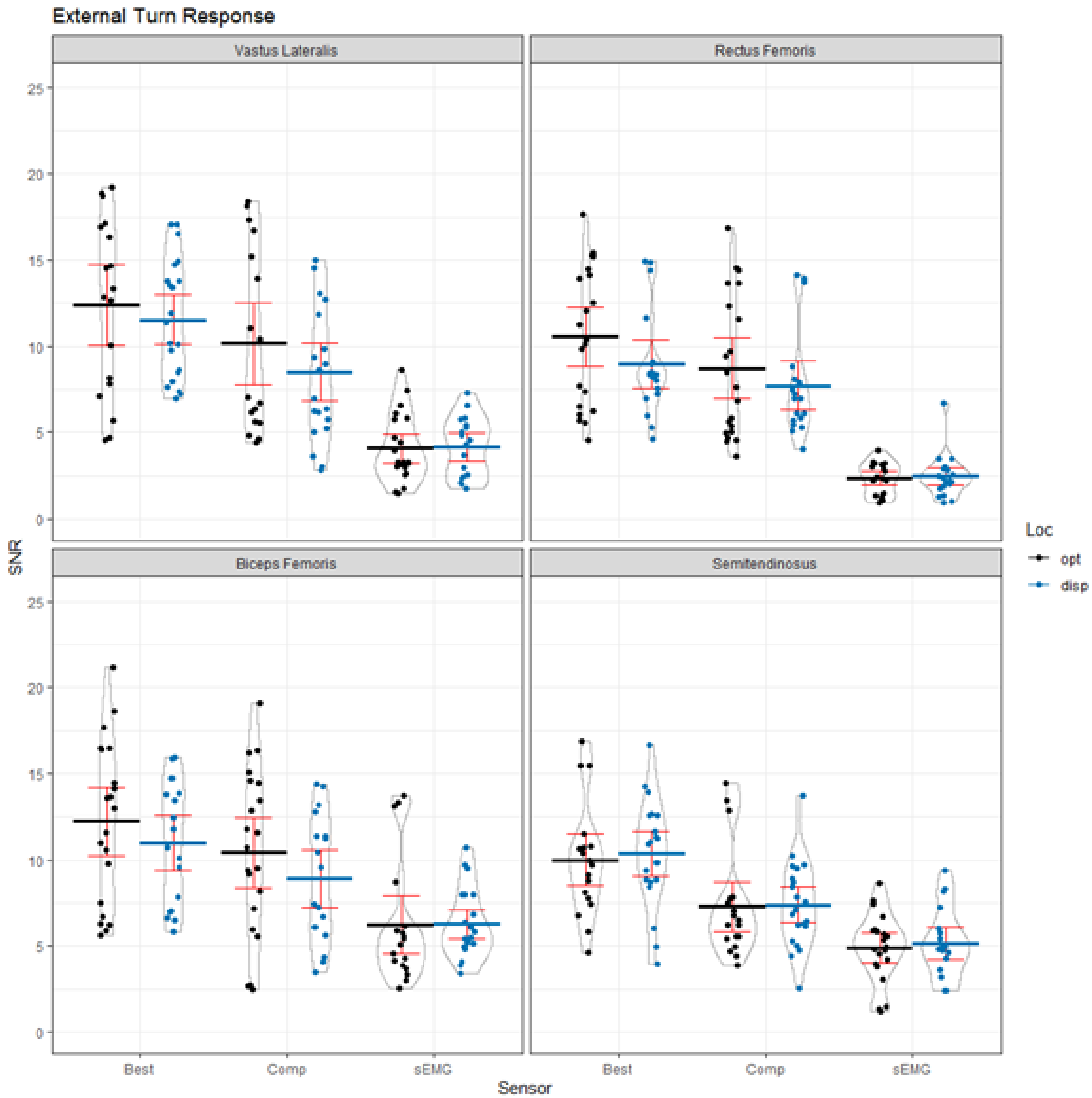

Figure 13: Violin plot of SNR (Signal to Noise Ratio) for Internal Turn. Opt denotes optimal placement while disp denotes displacement. Best is Best Signal, Comp is Composite Signal, sEMG is Traditional sEMG. Note the larger difference between means for Rectus Femoris (top right).

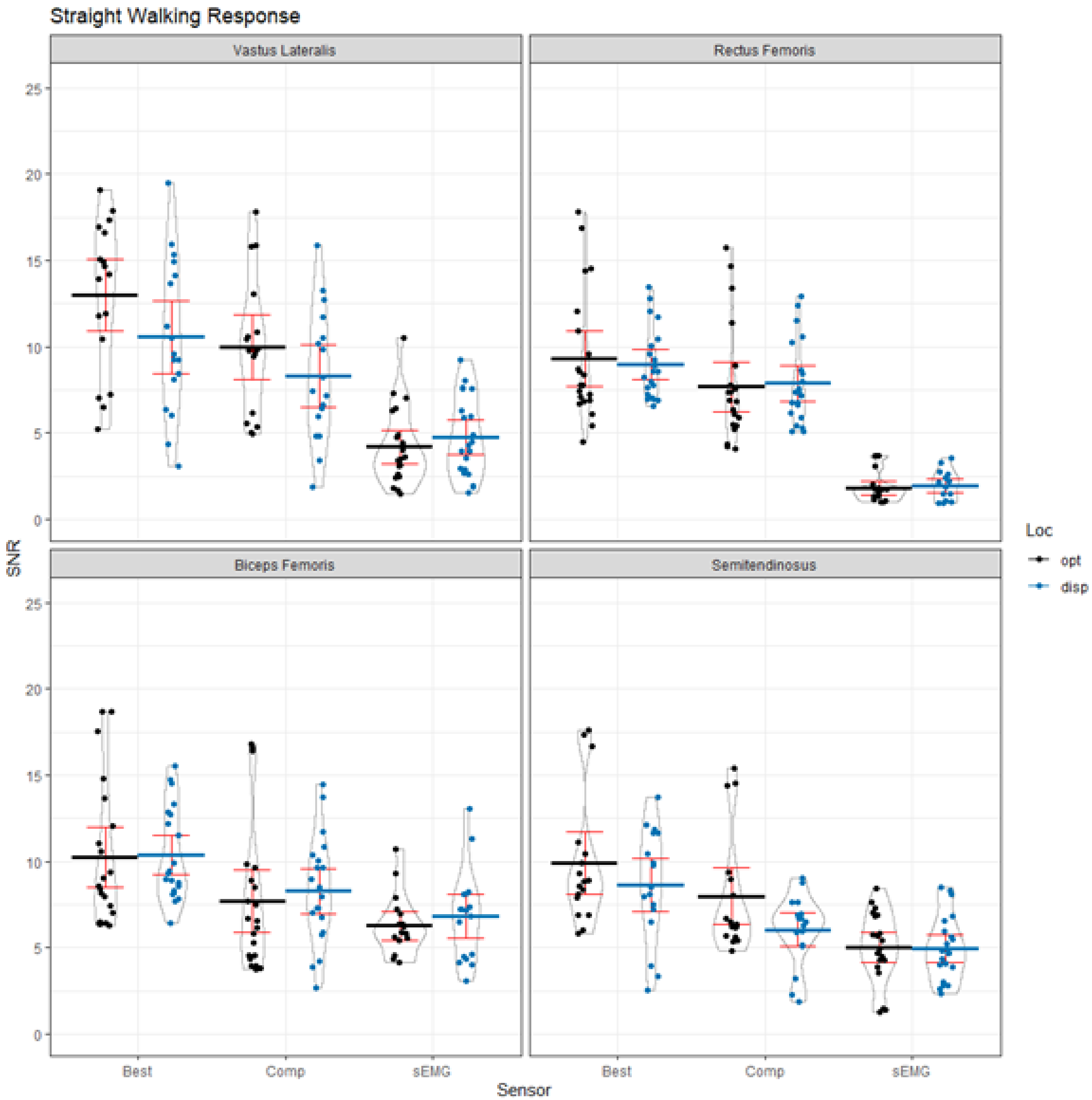

Figure 14: Violin plot of SNR (Signal to Noise Ratio) for Internal Turn. Opt denotes optimal placement while disp denotes displacement. Best is Best Signal, Comp is Composite Signal, sEMG is Traditional sEMG. Note the larger difference between means for Rectus Femoris (top right).

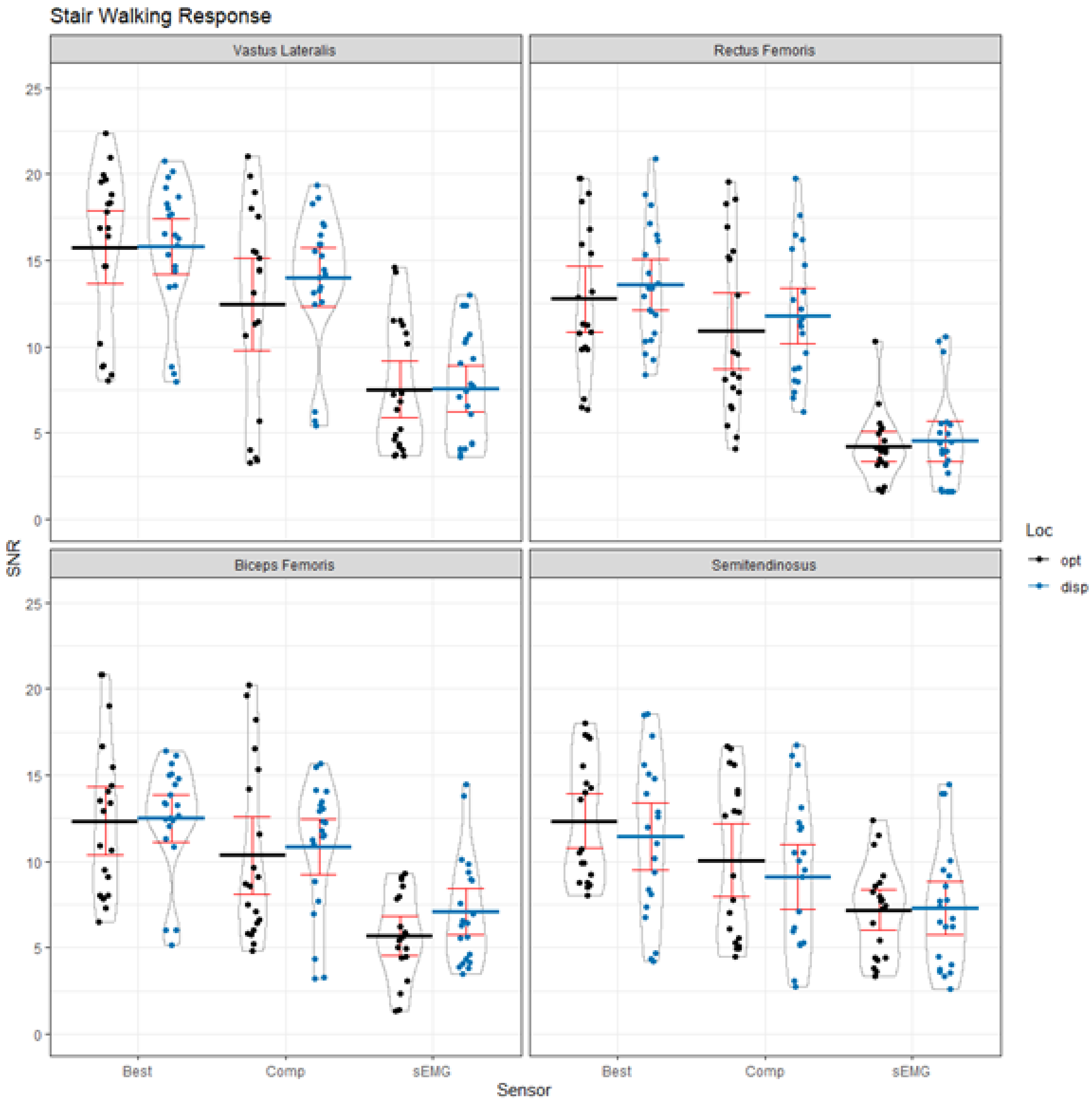

Figure 15: Violin plot of SNR (Signal to Noise Ratio) for Internal Turn. Opt denotes optimal placement while disp denotes displacement. Best is Best Signal, Comp is Composite Signal, sEMG is Traditional sEMG. Note the larger difference between means for Rectus Femoris (top right) and Vastus Lateralis (top left).

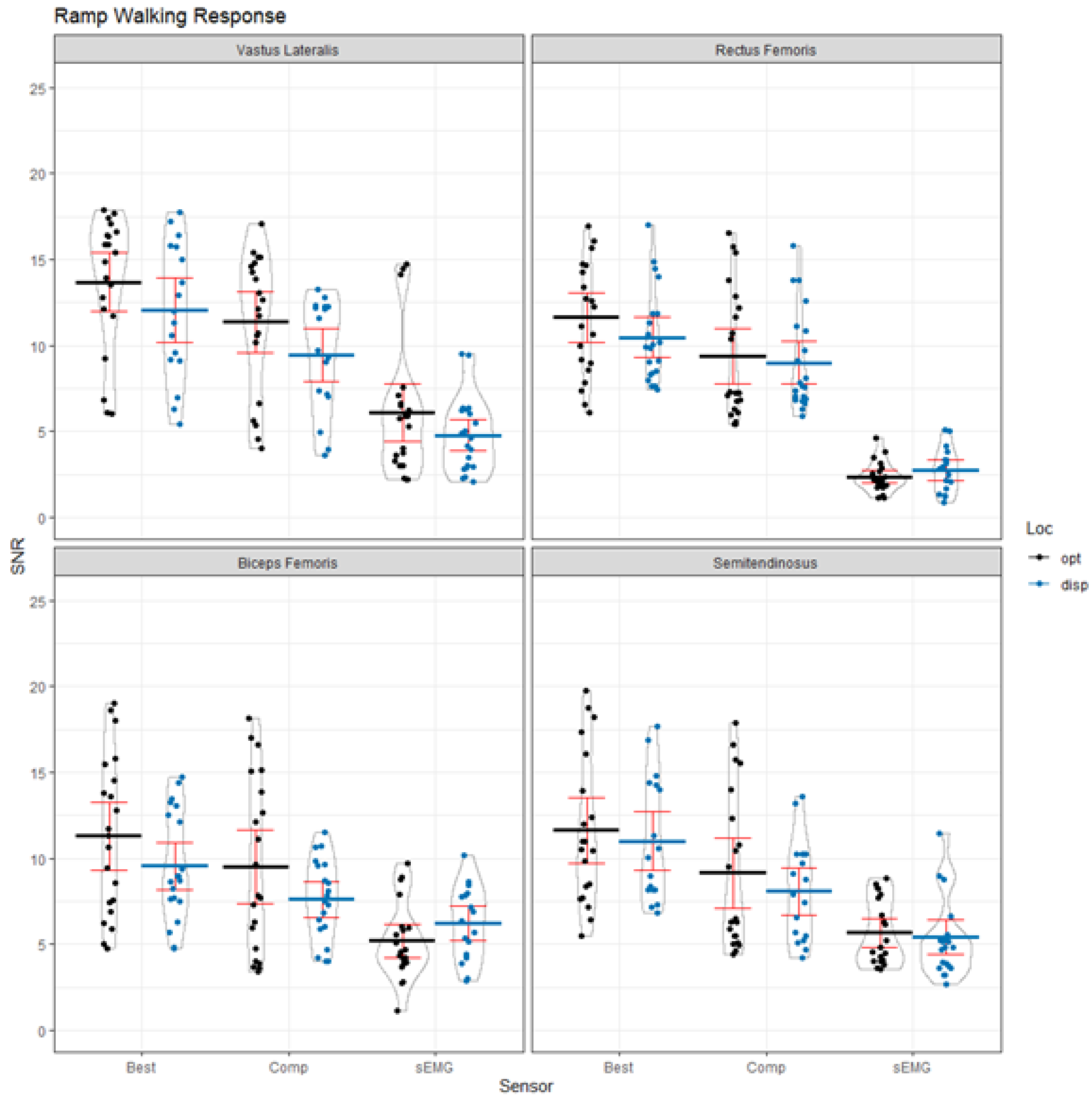

Figure 16: Violin plot of SNR (Signal to Noise Ratio) for Internal Turn. Opt denotes optimal placement while disp denotes displacement. Best is Best Signal, Comp is Composite Signal, sEMG is Traditional sEMG. Note the larger difference between means for Rectus Femoris (top right).

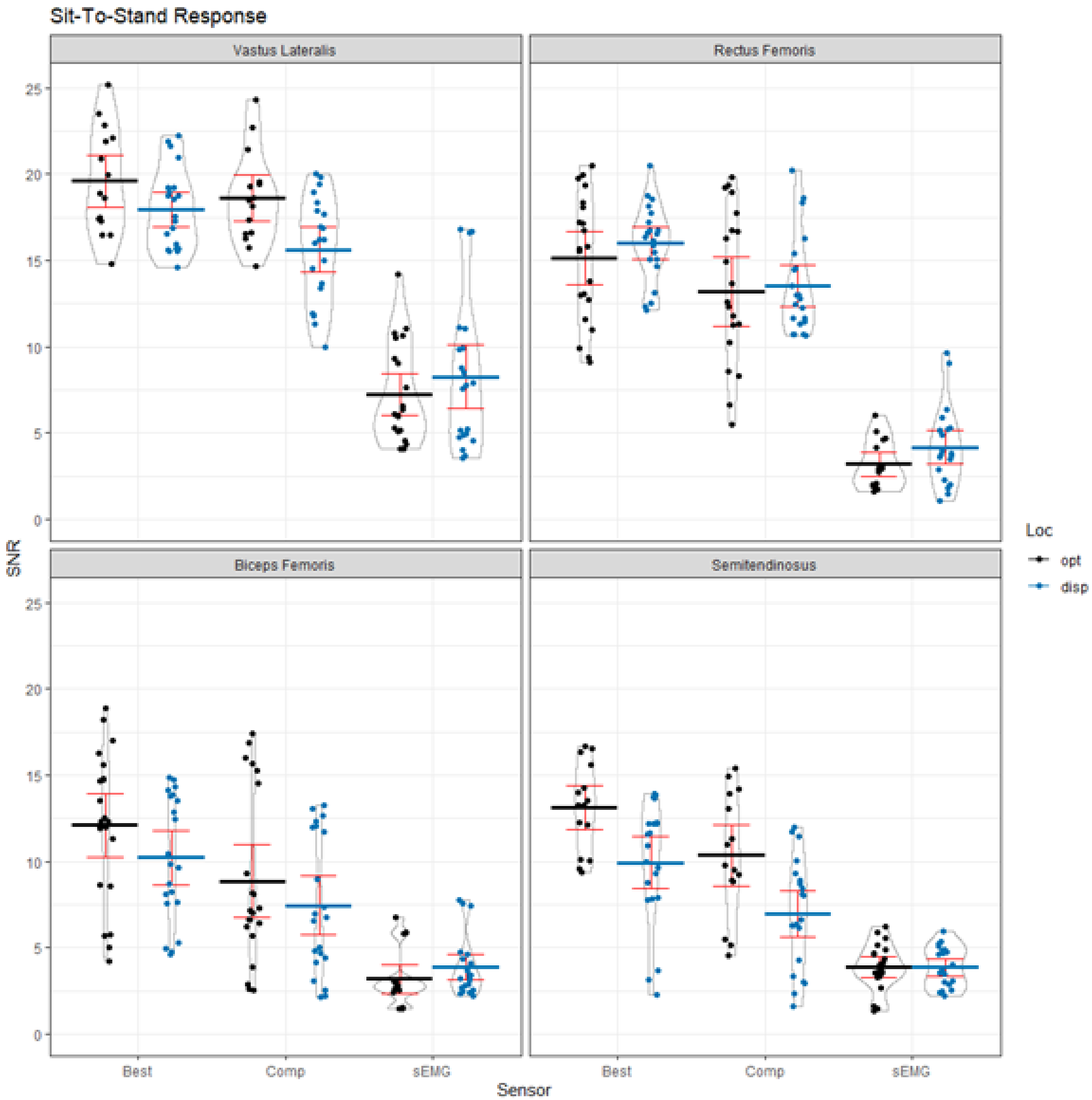

Figure 17: Violin plot of SNR (Signal to Noise Ratio) for Internal Turn. Opt denotes optimal placement while disp denotes displacement. Best is Best Signal, Comp is Composite Signal, sEMG is Traditional sEMG. Note the larger difference between means for Rectus Femoris (top right) and Vastus Lateralis (top left).

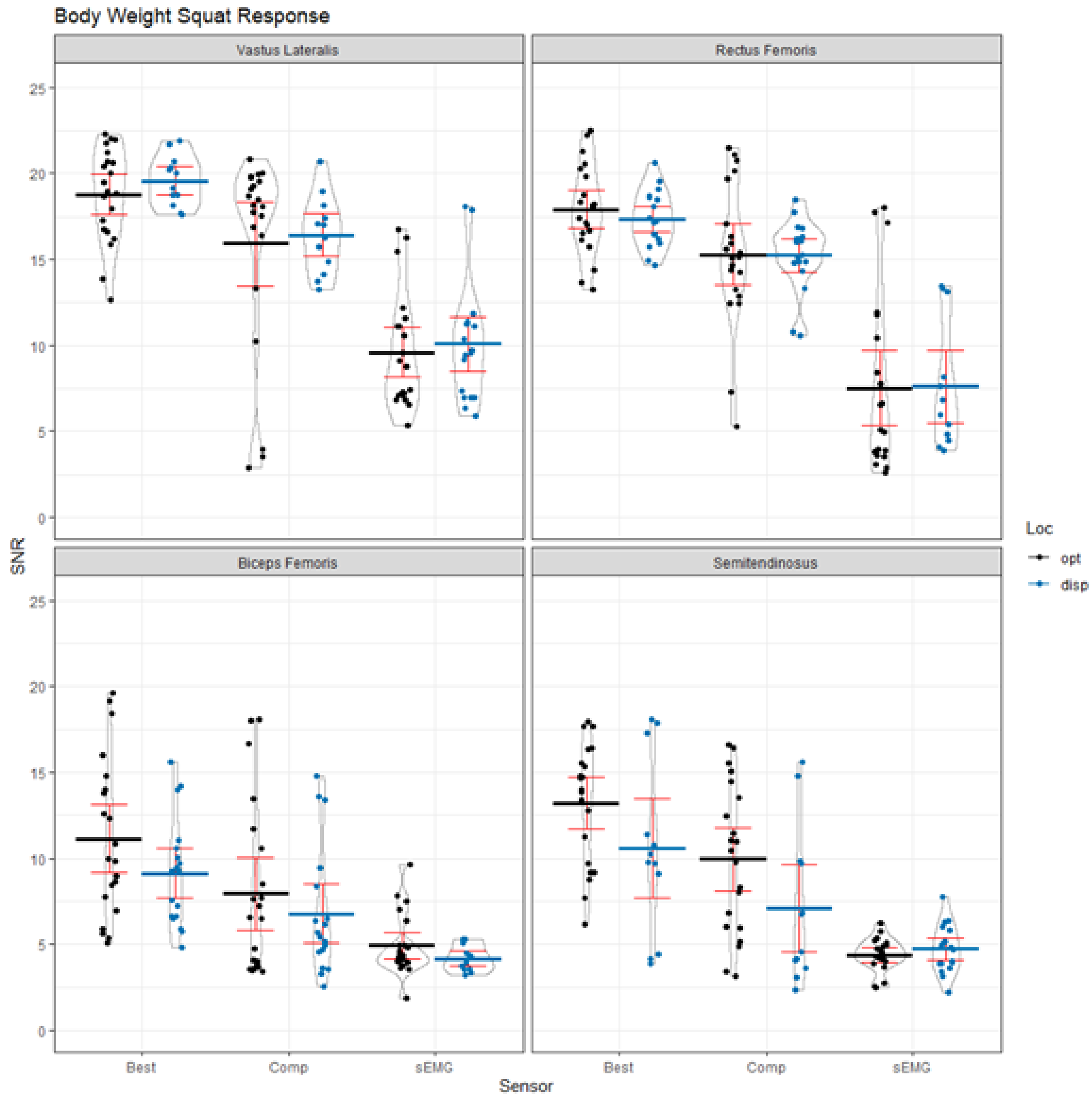

Figure 18: Violin plot of SNR (Signal to Noise Ratio) for Internal Turn. Opt denotes optimal placement while disp denotes displacement. Best is Best Signal, Comp is Composite Signal, sEMG is Traditional sEMG. Note the larger difference between means for Rectus Femoris (top right) and Vastus Lateralis (top left).

Root Mean Squared

Root mean squared values were calculated from normalized data. Due to the internal comparative nature of this measurement, the values have no units. Due to differences in variance, RMS values were modeled and analyzed using a log10 scale instead of raw values (see Appendix 2). Single-level interactions were seen for muscles, signals, and activities ($p<0.01$), as well as two-level interactions between muscle and location, muscle and signal, location and signal, and muscle and activity ($p<0.01$). A three-way interaction was seen between muscle, location, and signal ($p<0.01$), and a four-way interaction between muscle, location, signal, and activity ($p=0.019$). Traditional sEMG sensors displayed greater relative RMS values than Best Signals or Composite Signals (Figures 19-26). Effects analysis determined that 19% of variability was due to fixed effects and 79% of variability was due to a combination of fixed and random effects.

Activity	Muscle	Best - Opt	Best - Disp	Comp - Opt	Comp - Disp	sEMG - Opt	sEMG - Disp
Internal Turn	Vastus Lateralis	0.012 +/- 0.009	0.019 +/- 0.009	0.044 +/- 0.009	0.013 +/- 0.009	0.030 +/- 0.009	0.022 +/- 0.009
	Rectus Femoris	0.011 +/- 0.009	0.010 +/- 0.009	0.019 +/- 0.009	0.011 +/- 0.009	0.017 +/- 0.009	0.041 +/- 0.009
	Biceps Femoris	0.018 +/- 0.009	0.042 +/- 0.009	0.015 +/- 0.009	0.031 +/- 0.009	0.045 +/- 0.009	0.040 +/- 0.009
	Semitendinosus	0.026 +/- 0.009	0.033 +/- 0.009	0.030 +/- 0.009	0.044 +/- 0.009	0.040 +/- 0.009	0.044 +/- 0.009
External Turn	Vastus Lateralis	0.015 +/- 0.009	0.012 +/- 0.009	0.016 +/- 0.009	0.019 +/- 0.009	0.030 +/- 0.009	0.022 +/- 0.009
	Rectus Femoris	0.011 +/- 0.009	0.013 +/- 0.009	0.016 +/- 0.009	0.011 +/- 0.009	0.053 +/- 0.009	0.032 +/- 0.009
	Biceps Femoris	0.013 +/- 0.009	0.057 +/- 0.009	0.010 +/- 0.009	0.045 +/- 0.009	0.032 +/- 0.009	0.038 +/- 0.009
	Semitendinosus	0.010 +/- 0.009	0.010 +/- 0.009	0.011 +/- 0.009	0.019 +/- 0.009	0.028 +/- 0.009	0.039 +/- 0.009
Walking	Vastus Lateralis	0.017 +/- 0.010	0.022 +/- 0.010	0.017 +/- 0.010	0.021 +/- 0.010	0.029 +/- 0.009	0.030 +/- 0.009
	Rectus Femoris	0.011 +/- 0.009	0.010 +/- 0.009	0.011 +/- 0.009	0.011 +/- 0.009	0.017 +/- 0.010	0.052 +/- 0.010
	Biceps Femoris	0.013 +/- 0.009	0.035 +/- 0.009	0.010 +/- 0.009	0.030 +/- 0.009	0.035 +/- 0.010	0.033 +/- 0.010
	Semitendinosus	0.012 +/- 0.010	0.057 +/- 0.010	0.013 +/- 0.010	0.082 +/- 0.010	0.030 +/- 0.009	0.038 +/- 0.009
Stair Walking	Vastus Lateralis	0.035 +/- 0.009	0.033 +/- 0.009	0.061 +/- 0.009	0.026 +/- 0.009	0.059 +/- 0.009	0.054 +/- 0.009
	Rectus Femoris	0.030 +/- 0.009	0.029 +/- 0.009	0.029 +/- 0.009	0.027 +/- 0.009	0.041 +/- 0.009	0.039 +/- 0.009
	Biceps Femoris	0.016 +/- 0.009	0.038 +/- 0.009	0.015 +/- 0.009	0.035 +/- 0.009	0.039 +/- 0.009	0.038 +/- 0.009
	Semitendinosus	0.017 +/- 0.009	0.039 +/- 0.009	0.020 +/- 0.009	0.037 +/- 0.009	0.043 +/- 0.009	0.052 +/- 0.009
Ramp Walking	Vastus Lateralis	0.021 +/- 0.009	0.019 +/- 0.010	0.019 +/- 0.009	0.021 +/- 0.010	0.043 +/- 0.009	0.028 +/- 0.009
	Rectus Femoris	0.012 +/- 0.009	0.012 +/- 0.009	0.013 +/- 0.009	0.011 +/- 0.009	0.043 +/- 0.009	0.034 +/- 0.010
	Biceps Femoris	0.015 +/- 0.009	0.010 +/- 0.009	0.010 +/- 0.009	0.012 +/- 0.009	0.032 +/- 0.009	0.030 +/- 0.010
	Semitendinosus	0.010 +/- 0.009	0.023 +/- 0.010	0.011 +/- 0.009	0.018 +/- 0.010	0.030 +/- 0.009	0.034 +/- 0.009
Sit to Stand	Vastus Lateralis	0.040 +/- 0.010	0.023 +/- 0.009	0.038 +/- 0.010	0.019 +/- 0.009	0.047 +/- 0.009	0.059 +/- 0.009
	Rectus Femoris	0.029 +/- 0.009	0.024 +/- 0.009	0.026 +/- 0.009	0.022 +/- 0.009	0.032 +/- 0.010	0.037 +/- 0.009
	Biceps Femoris	0.011 +/- 0.009	0.013 +/- 0.009	0.012 +/- 0.009	0.012 +/- 0.009	0.023 +/- 0.010	0.017 +/- 0.009
	Semitendinosus	0.018 +/- 0.010	0.012 +/- 0.009	0.016 +/- 0.010	0.015 +/- 0.009	0.026 +/- 0.009	0.021 +/- 0.009
Squats	Vastus Lateralis	0.043 +/- 0.009	0.019 +/- 0.011	0.056 +/- 0.009	0.017 +/- 0.011	0.078 +/- 0.009	0.083 +/- 0.009
	Rectus Femoris	0.050 +/- 0.009	0.039 +/- 0.009	0.034 +/- 0.009	0.028 +/- 0.009	0.076 +/- 0.009	0.085 +/- 0.011
	Biceps Femoris	0.008 +/- 0.009	0.029 +/- 0.009	0.010 +/- 0.009	0.022 +/- 0.009	0.026 +/- 0.009	0.017 +/- 0.011
	Semitendinosus	0.015 +/- 0.009	0.019 +/- 0.011	0.014 +/- 0.009	0.017 +/- 0.011	0.034 +/- 0.009	0.025 +/- 0.009

Table 4: RMS (Root Mean Squared) means with standard error. Best – best selected signal, Comp – composite signal, sEMG – traditional sEMG, Opt – optimally placed over muscle belly, Disp - displaced 1 cm distal from muscle belly

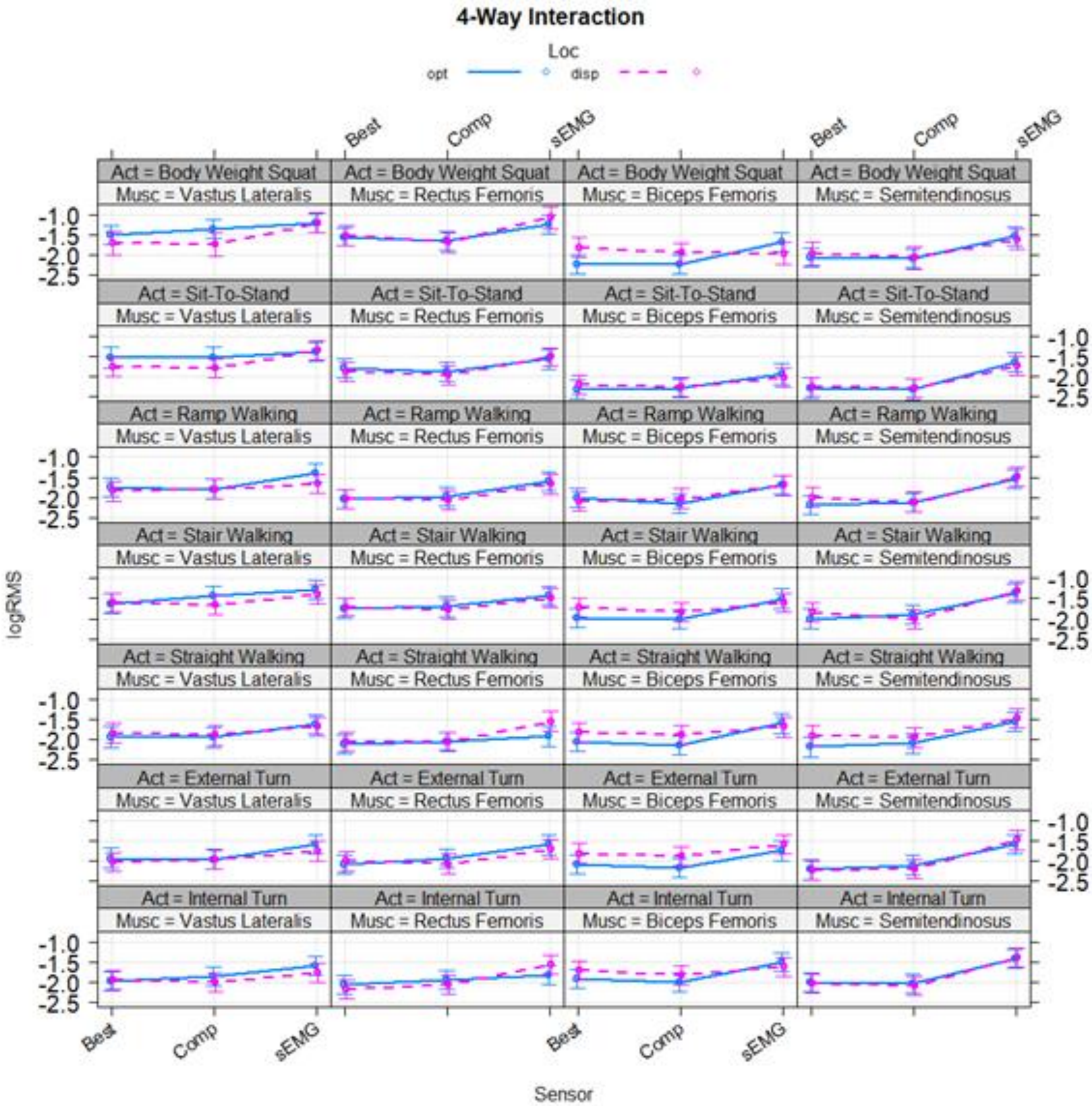

Figure 19: Effects plot for logRMS responses. Solid blue is optimal placement, dashed pink is displaced. Best is Best Signal, Comp is Composite Signal, sEMG is Traditional sEMG. –Note the higher values for Traditional sEMG (far right data point).

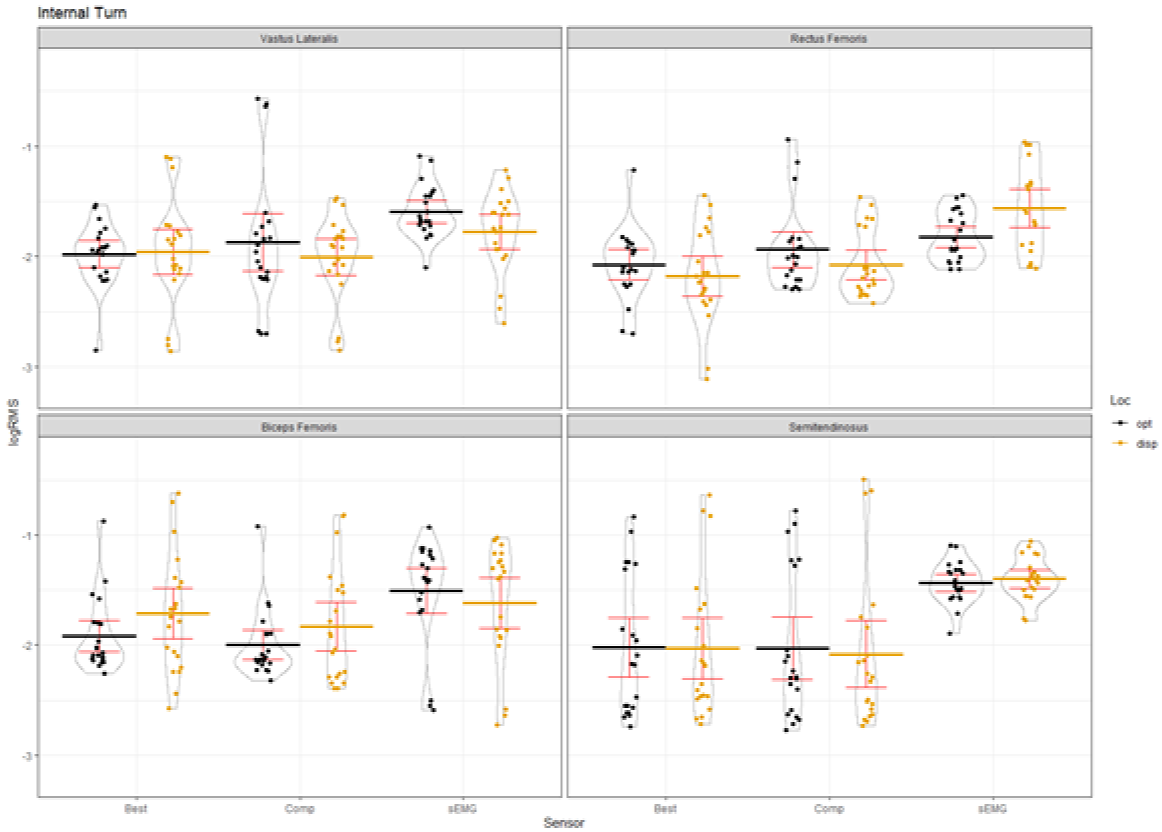

Figure 20: Violin graph of logRMS (Root Mean Squared) for Body Weight Squats. Opt is optimal placement, disp is displaced. Best (left) is Best Signal, Comp (middle) is Composite Signal, sEMG (right) is Traditional sEMG. –. Note higher means for Traditional sEMG, particularly for Semitendinosus (bottom right).

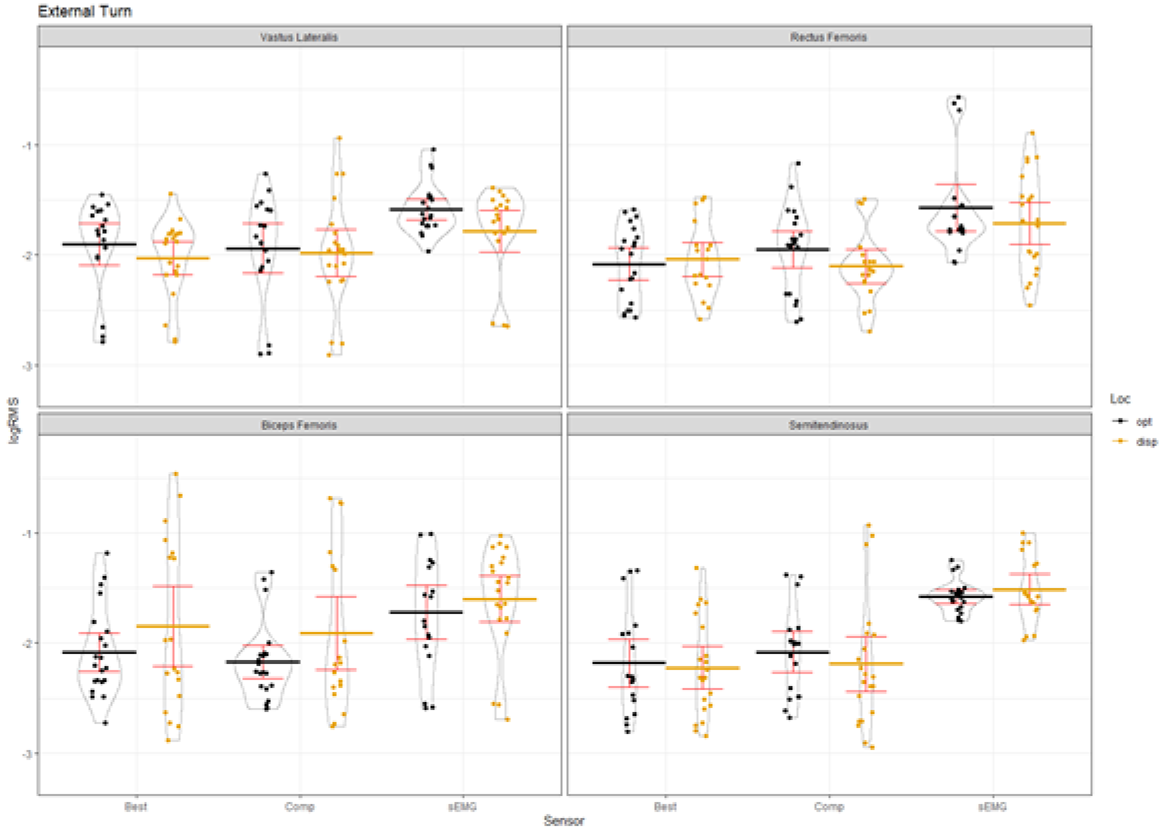

Figure 21: Violin graph of logRMS (Root Mean Squared) for Body Weight Squats. Opt is optimal placement, disp is displaced. Best (left) is Best Signal, Comp (middle) is Composite Signal, sEMG (right) is Traditional sEMG.. Note higher means for Traditional sEMG, particularly for Semitendinosus (bottom right).

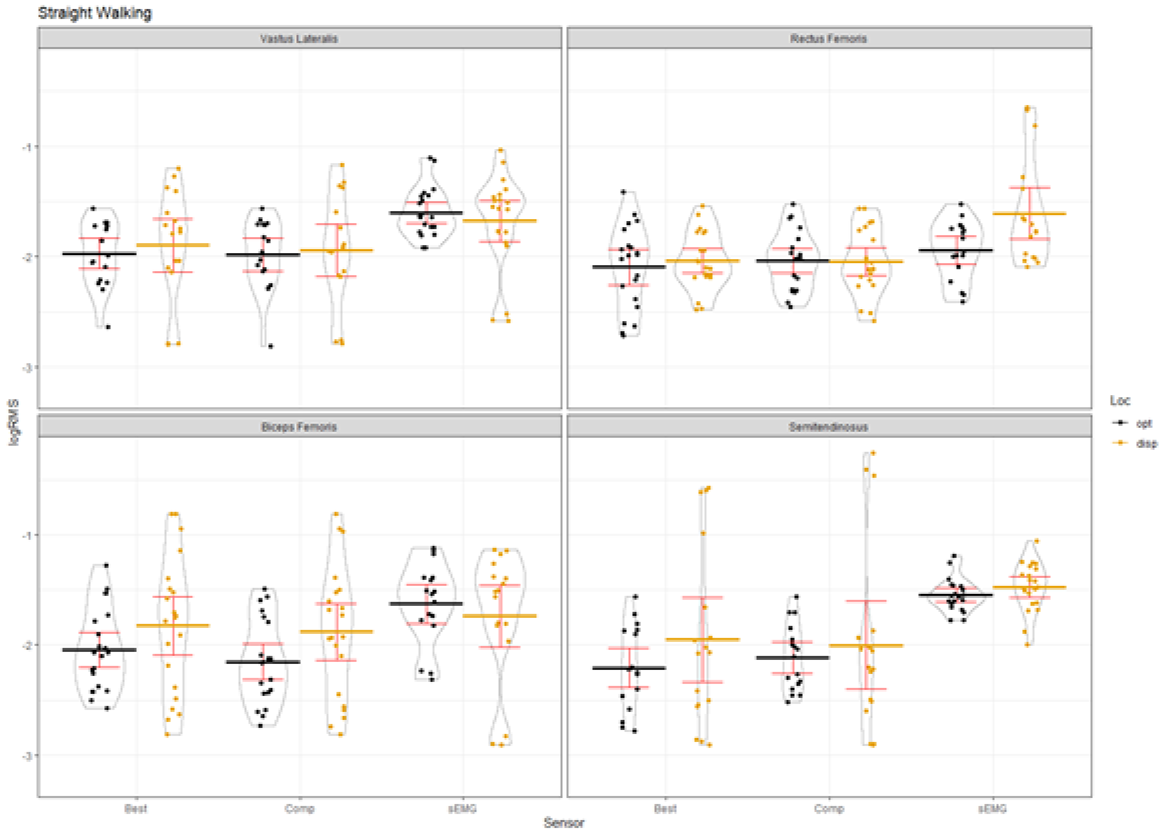

Figure 22: Violin graph of logRMS (Root Mean Squared) for Body Weight Squats. Opt is optimal placement, disp is displaced. Best (left) is Best Signal, Comp (middle) is Composite Signal, sEMG (right) is Traditional sEMG.. Note higher means for Traditional sEMG, particularly for Semitendinosus (bottom right).

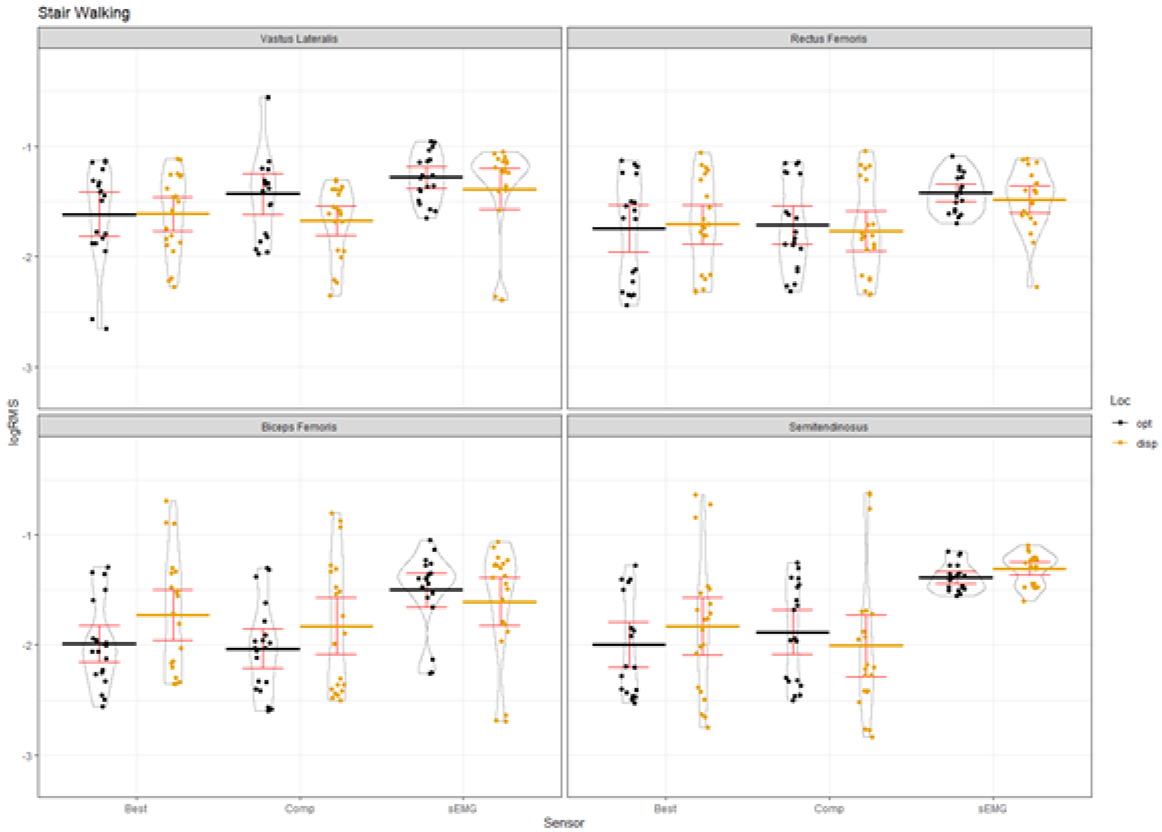

Figure 23: Violin graph of logRMS (Root Mean Squared) for Body Weight Squats. Opt is optimal placement, disp is displaced. Best (left) is Best Signal, Comp (middle) is Composite Signal, sEMG (right) is Traditional sEMG.. Note higher means for Traditional sEMG, particularly for Semitendinosus (bottom right).

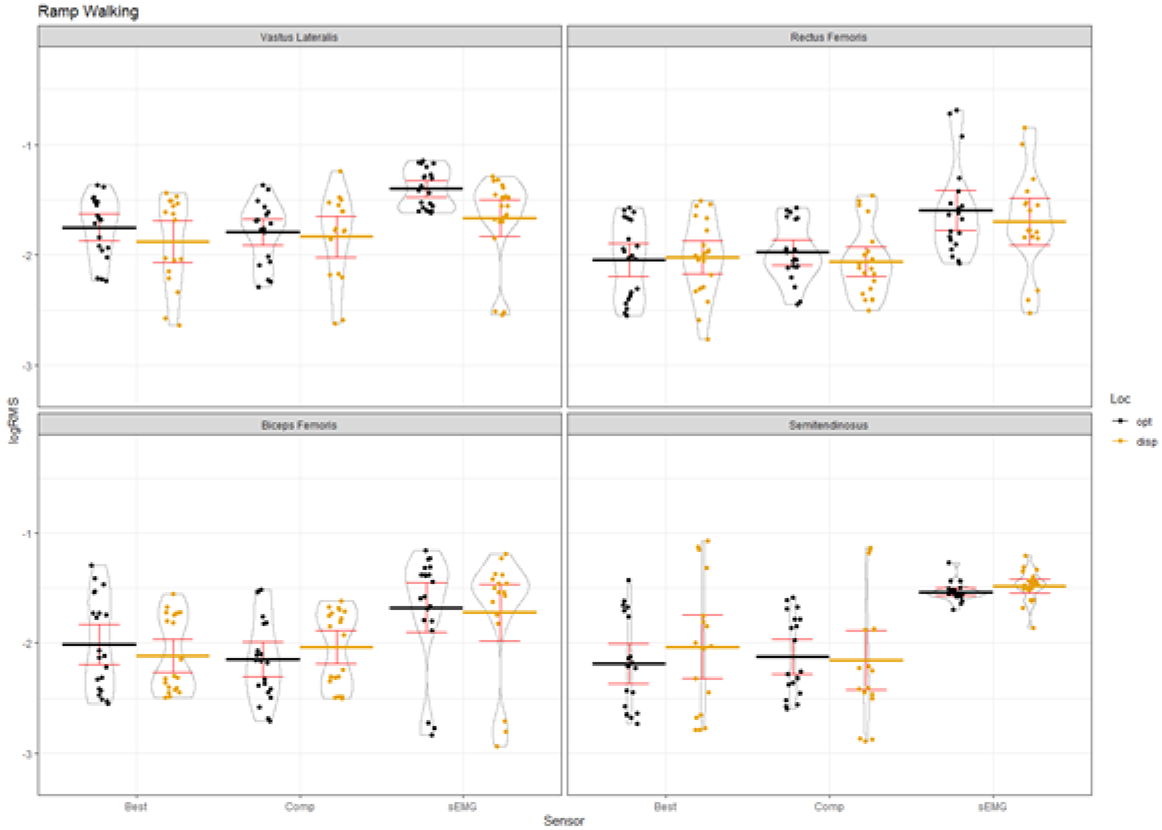

Figure 24: Violin graph of logRMS (Root Mean Squared) for Body Weight Squats. Opt is optimal placement, disp is displaced. Best (left) is Best Signal, Comp (middle) is Composite Signal, sEMG (right) is Traditional sEMG.. Note higher means for Traditional sEMG, particularly for Semitendinosus (bottom right).

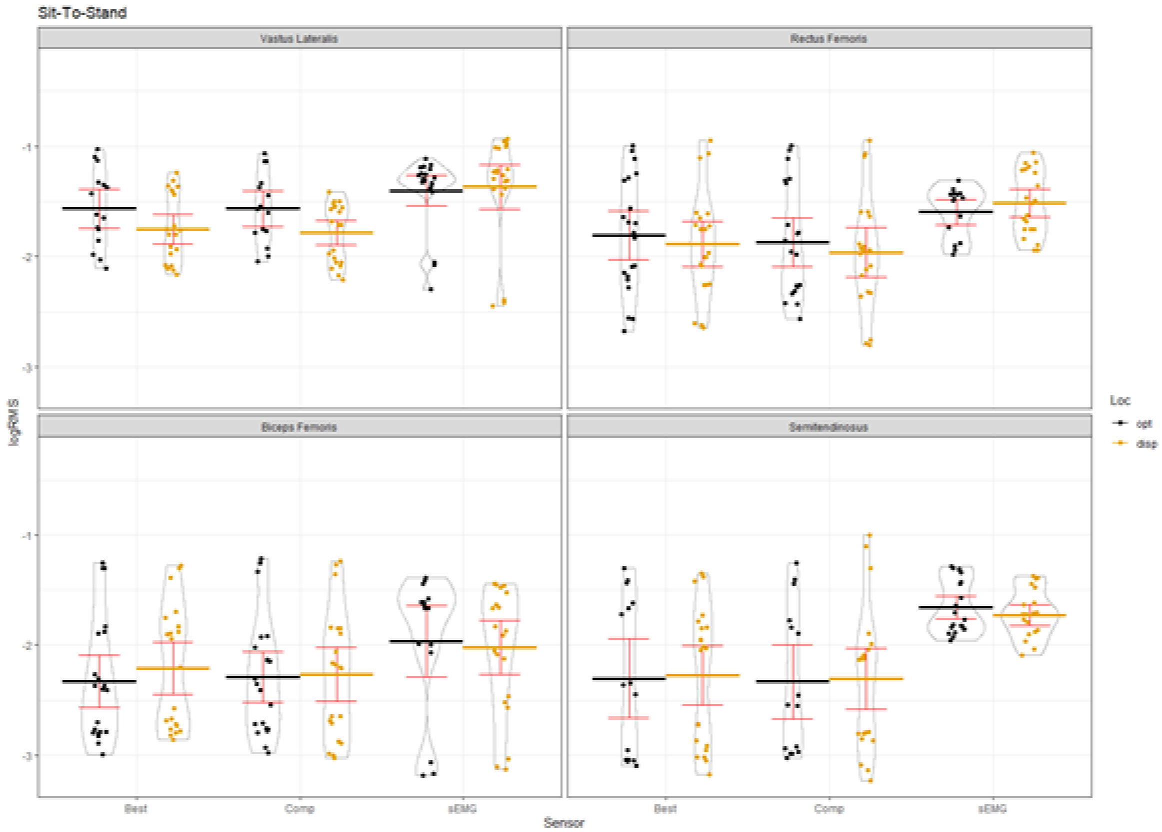

Figure 25: Violin graph of logRMS (Root Mean Squared) for Body Weight Squats. Opt is optimal placement, disp is displaced. Best (left) is Best Signal, Comp (middle) is Composite Signal, sEMG (right) is Traditional sEMG.. Note higher means for Traditional sEMG, particularly for Semitendinosus (bottom right).

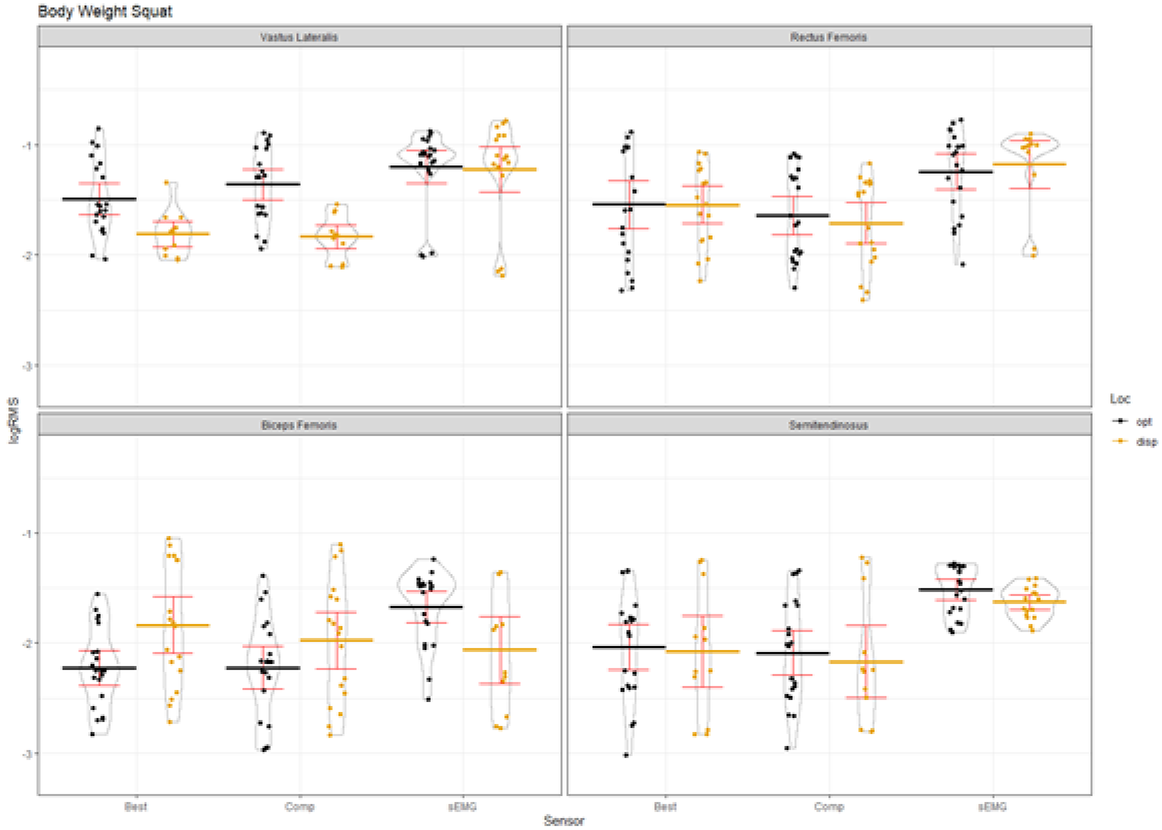

Figure 26: Violin graph of logRMS (Root Mean Squared) for Body Weight Squats. Opt is optimal placement, disp is displaced. Best (left) is Best Signal, Comp (middle) is Composite Signal, sEMG (right) is Traditional sEMG.. Note higher means for Traditional sEMG, particularly for Semitendinosus (bottom right).

DP Ratio

DP is measured in decibels (dB). Due to an increase in variance, a log10 transform of the DP data occurred to aid with statistical analysis (see Appendix 2). Single-level interactions were found with regards to muscle, signal, and activity ($p<0.01$), as well as two-way interactions between muscle and signal, location and signal, muscle and activity, and sensor and activity ($p<0.01$). The single three-way interaction was between muscle, location, and signal ($p<0.01$). There was a trend of higher DP levels for sEMG signals than for Best and Composite signals (Figures 27-34). Displaced sensors tended to display lower, yet not statistically significant means for DP than for optimally placed sensors ($p=0.09$). Effects analysis determined that 8% of variability was due to fixed effects and 99% of variability was due to a combination of fixed and random effects.

Activity	Muscle	Best - Opt	Best - Disp	Comp - Opt	Comp - Disp	sEMG - Opt	sEMG - Disp
Internal Turn	Vastus Lateralis	222.15 +/- 6562	650.93 +/- 6562	261.09 +/- 6562	388.42 +/- 6562	36082.34 +/- 6562	1688.36 +/- 6562
	Rectus Femoris	1573.62 +/- 6562	235.56 +/- 6562	1621.85 +/- 6562	730.51 +/- 6562	20949.51 +/- 6562	3048.13 +/- 6562
	Biceps Femoris	654.81 +/- 6562	457.3 +/- 6562	511.31 +/- 6562	606.39 +/- 6562	14104.3 +/- 6562	1127.39 +/- 6562
	Semitendinosus	548.06 +/- 6562	276.75 +/- 6562	462.32 +/- 6562	301.07 +/- 6562	1735.48 +/- 6562	5979.68 +/- 6562
External Turn	Vastus Lateralis	-161.66 +/- 6945	271.9 +/- 6562	166.42 +/- 6945	896.53 +/- 6562	28776.68 +/- 6562	1355.22 +/- 6947
	Rectus Femoris	1525.48 +/- 6562	442.89 +/- 6947	1795.37 +/- 6562	436.1 +/- 6947	791.63 +/- 6945	6503.61 +/- 6562
	Biceps Femoris	415.94 +/- 6562	-280.65 +/- 6947	287.05 +/- 6562	-41.72 +/- 6947	3763.06 +/- 6945	14407.91 +/- 6562
	Semitendinosus	-40.71 +/- 6945	1078.69 +/- 6562	-143.05 +/- 6945	1177.65 +/- 6562	1254.88 +/- 6562	2562.8 +/- 6947
Walking	Vastus Lateralis	3492.08 +/- 7074	385.16 +/- 7077	3595.53 +/- 7074	-91.25 +/- 7077	10456.67 +/- 6562	1499.05 +/- 6562
	Rectus Femoris	868.75 +/- 6562	164.09 +/- 6562	1060.05 +/- 6562	254.68 +/- 6562	3873.6 +/- 7074	3053.52 +/- 7077
	Biceps Femoris	236.82 +/- 6562	269.31 +/- 6562	158.74 +/- 6562	424.73 +/- 6562	5945.93 +/- 7074	1109.4 +/- 7077
	Semitendinosus	3398.91 +/- 7074	-616.73 +/- 7077	3655.95 +/- 7074	-666.79 +/- 7077	1003.14 +/- 6562	4473.41 +/- 6562
Stair Walking	Vastus Lateralis	108.87 +/- 6767	369.5 +/- 6562	1264.99 +/- 6767	504.02 +/- 6562	32529.96 +/- 6661	3644.14 +/- 6562
	Rectus Femoris	88.67 +/- 6661	511.87 +/- 6562	383.4 +/- 6661	593.61 +/- 6562	15815.41 +/- 6767	19150.45 +/- 6562
	Biceps Femoris	-9.66 +/- 6661	286.72 +/- 6562	-21.91 +/- 6661	582.16 +/- 6562	9118.22 +/- 6767	1968.25 +/- 6562
	Semitendinosus	-90.28 +/- 6767	4896.45 +/- 6562	345.95 +/- 6767	499.17 +/- 6562	3236.57 +/- 6661	4645.68 +/- 6562
Ramp Walking	Vastus Lateralis	367.42 +/- 6661	-339.53 +/- 7077	297.63 +/- 6661	605.07 +/- 7077	60176.68 +/- 6562	2656.98 +/- 6562
	Rectus Femoris	769.82 +/- 6562	613.32 +/- 6562	1806.49 +/- 6562	707.3 +/- 6562	8538.33 +/- 6661	9730.83 +/- 7077
	Biceps Femoris	263.43 +/- 6562	122.92 +/- 6660	247.78 +/- 6562	1268.26 +/- 6660	4465.19 +/- 6661	5515.81 +/- 7077
	Semitendinosus	63.69 +/- 6661	-57.49 +/- 7077	259.53 +/- 6661	-65.22 +/- 7077	1807.17 +/- 6562	3890.31 +/- 6562
Sit to Stand	Vastus Lateralis	3669.73 +/- 7450	318.75 +/- 6562	3665.58 +/- 7450	374.91 +/- 6562	10595.79 +/- 6562	2204.92 +/- 6562
	Rectus Femoris	353.27 +/- 6562	327.25 +/- 6562	588.19 +/- 6562	275.11 +/- 6562	4293.8 +/- 7450	7119.26 +/- 6562
	Biceps Femoris	207.56 +/- 6562	765.88 +/- 6562	242.13 +/- 6562	491.51 +/- 6562	4239.19 +/- 7450	1308.64 +/- 6562
	Semitendinosus	3726.25 +/- 7450	755.88 +/- 6562	3728.23 +/- 7450	1512.87 +/- 6562	1643.87 +/- 6562	2153.68 +/- 6562
Squats	Vastus Lateralis	318.05 +/- 6562	-2469.94 +/- 8148	836.97 +/- 6562	-2326.01 +/- 8148	2965.79 +/- 6562	2014.08 +/- 6947
	Rectus Femoris	143.34 +/- 6562	-266.57 +/- 6947	132.13 +/- 6562	-279.71 +/- 6947	2643.77 +/- 6562	1515.55 +/- 8148
	Biceps Femoris	409.64 +/- 6562	2357.1 +/- 6947	387.06 +/- 6562	1412.22 +/- 6947	11975.92 +/- 6562	2569.04 +/- 8148
	Semitendinosus	504.82 +/- 6562	-1806.14 +/- 8148	470.58 +/- 6562	-1895.3 +/- 8148	5625.64 +/- 6562	2365.99 +/- 6947

Table 5: DP ratio means (dB) with standard error. Best – best selected signal, Comp – composite signal, sEMG – traditional sEMG, Opt – optimally placed over muscle belly, Disp - displaced 1 cm distal from muscle belly

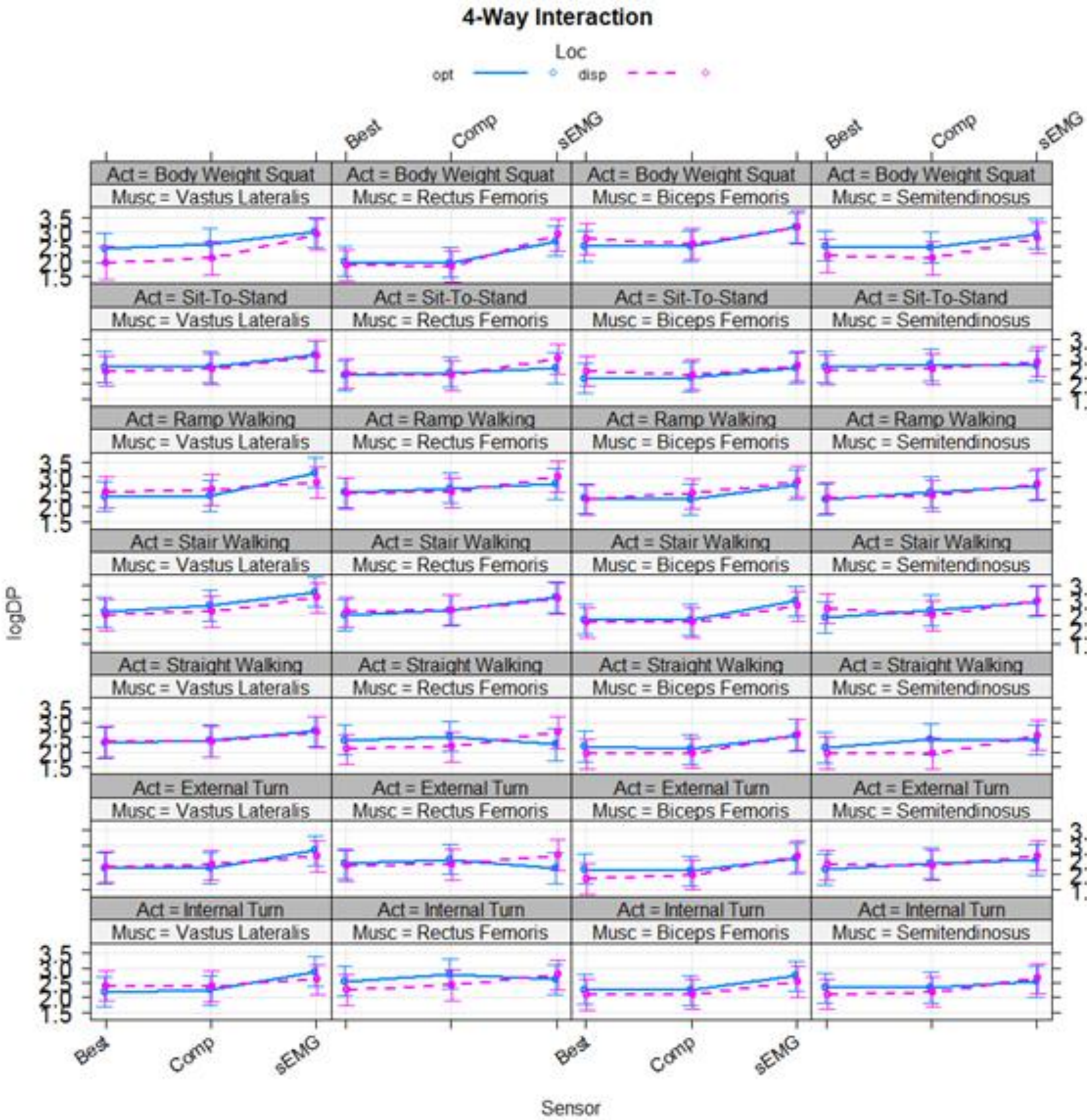

Figure 27: Effects plot of logDP Solid blue is optimal placement, dashed pink is displaced. Best is Best Signal, Comp is Composite Signal, sEMG is Traditional sEMG. Note the higher values for Traditional sEMG (far right data point), which is present for every activity for Biceps Femoris and Vastus Lateralis.

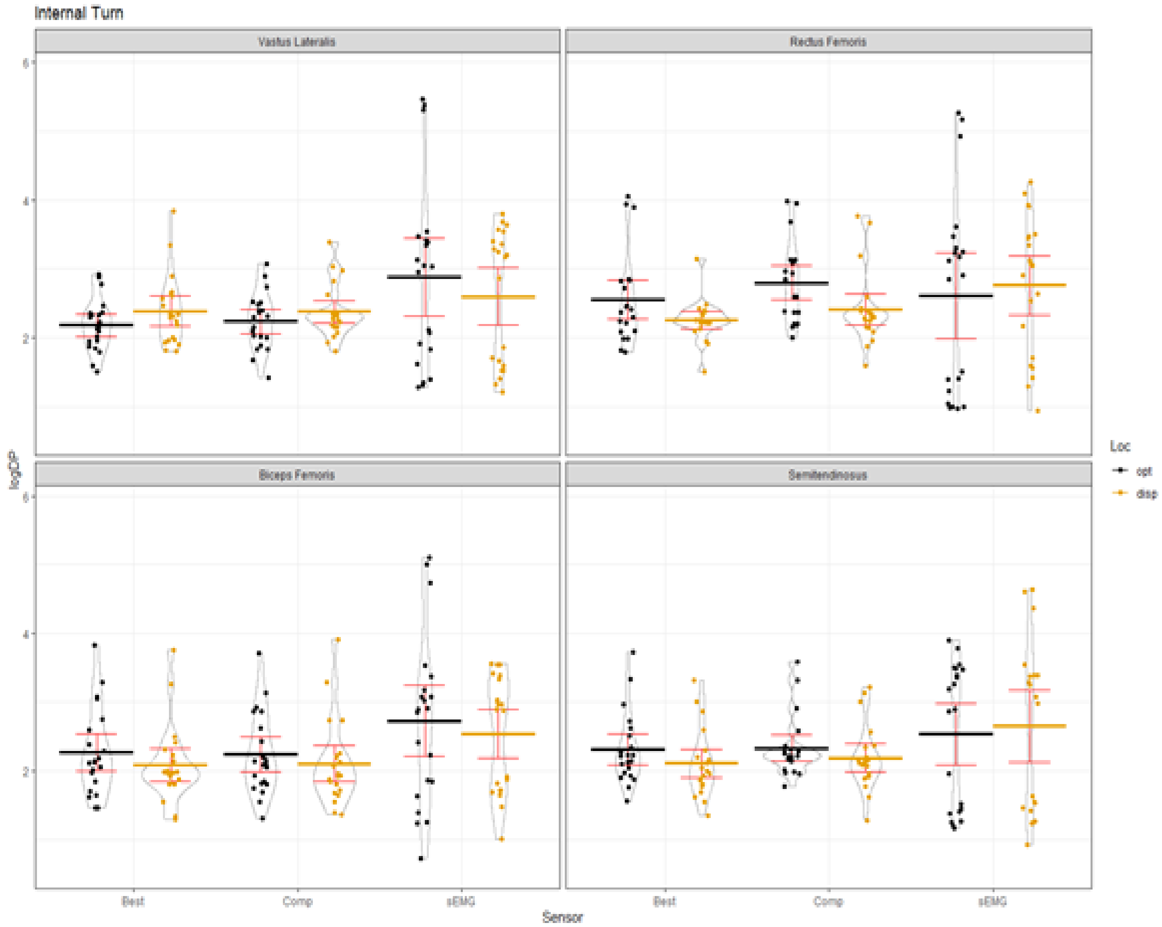

Figure 28: Violin graph of logDP for Internal Turn. Opt is optimal placement, disp is displaced. Best (left) is Best Signal, Comp (middle) is Composite Signal, sEMG (right) is Traditional sEMG.– Note higher means and higher spreads for Traditional sEMG.

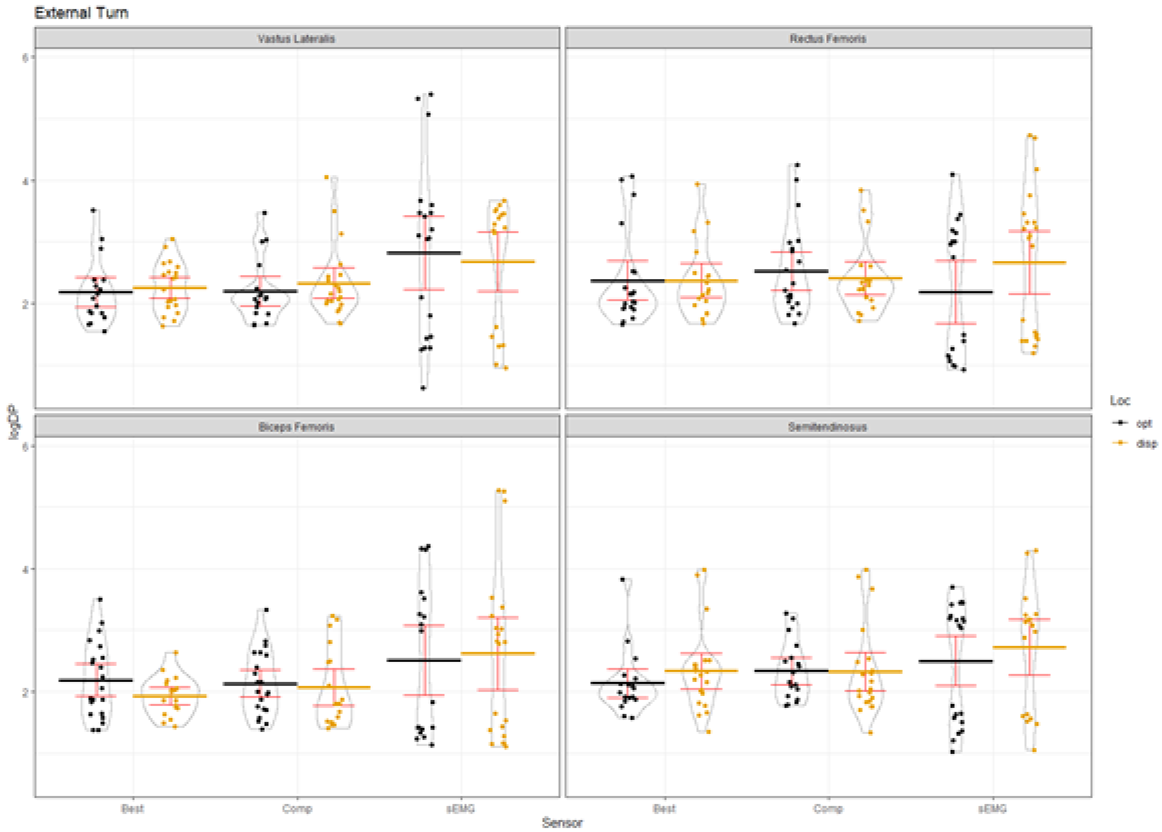

Figure 29: Violin graph of logDP for External Turn. Opt is optimal placement, disp is displaced. Best (left) is Best Signal, Comp (middle) is Composite Signal, sEMG (right) is Traditional sEMG. Note higher means and higher spreads for Traditional sEMG.

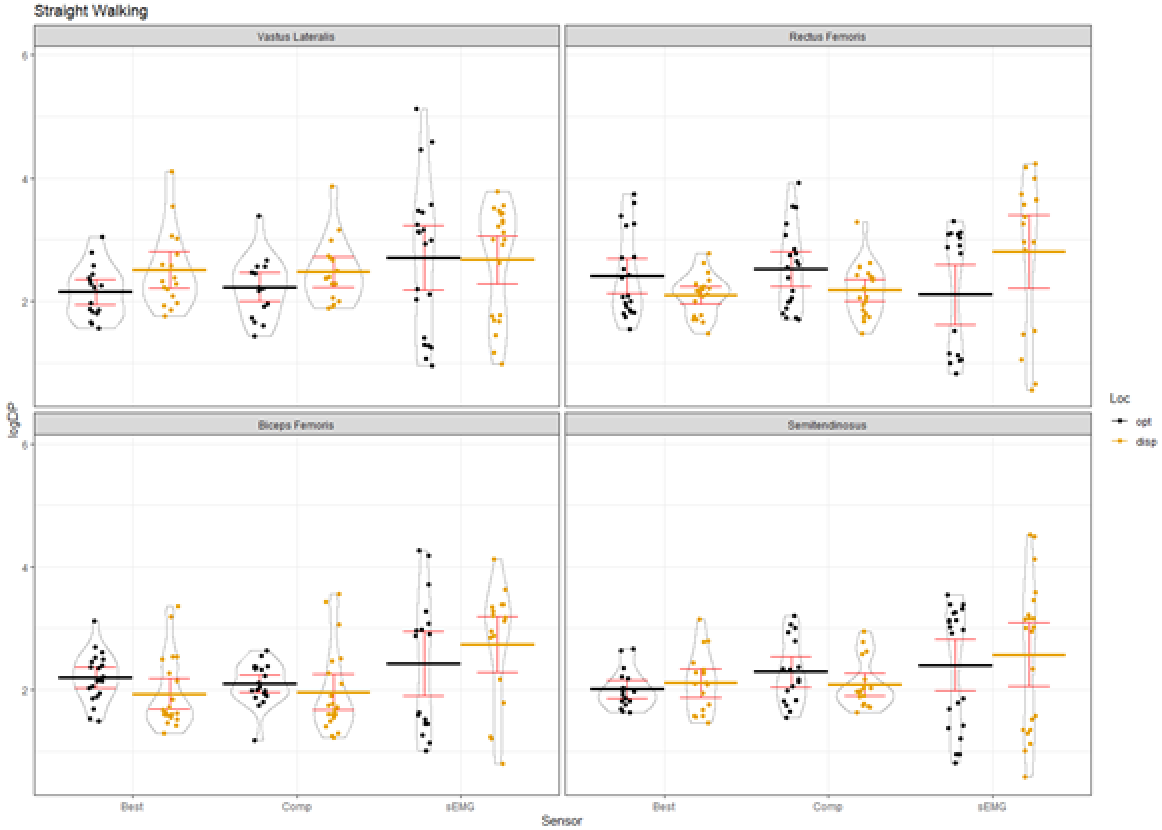

Figure 30: Violin graph of logDP for Straight Walking. Opt is optimal placement, disp is displaced. Best (left) is Best Signal, Comp (middle) is Composite Signal, sEMG (right) is Traditional sEMG. Note higher means and higher spreads for Traditional sEMG.

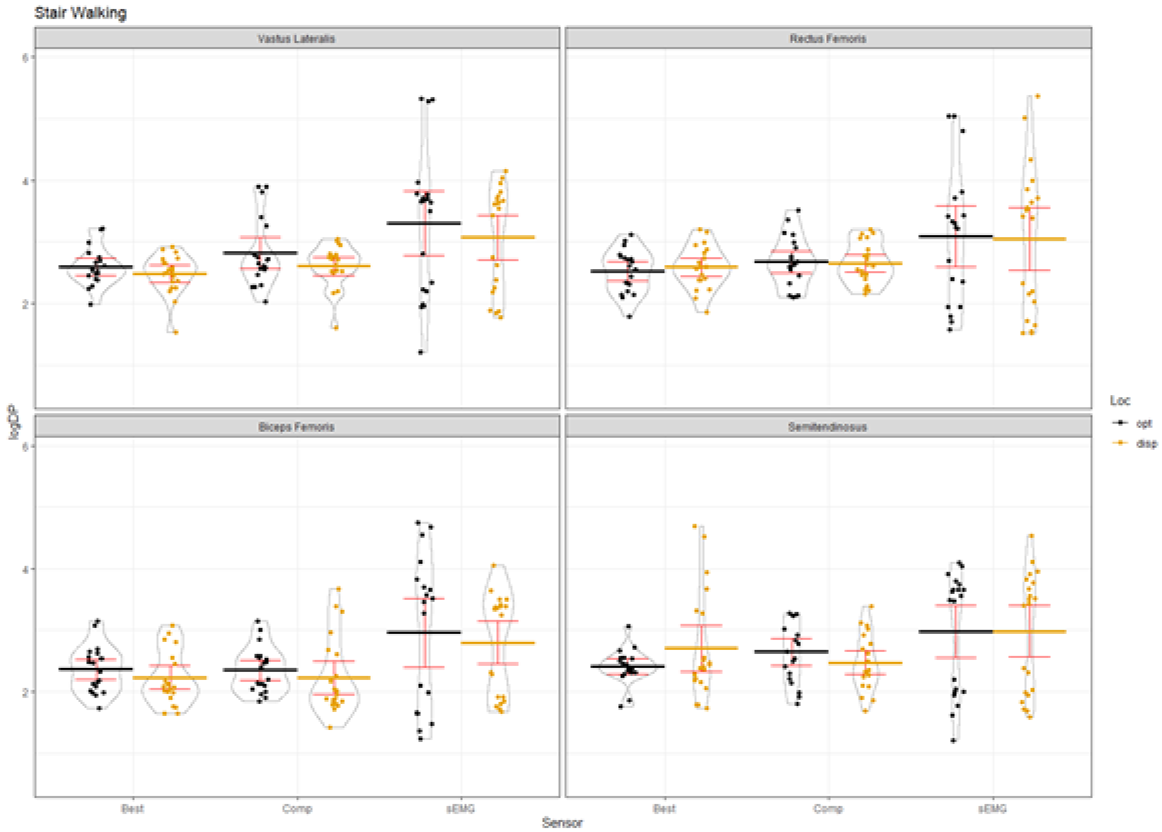

Figure 31: Violin graph of logDP for Stair Walking. Opt is optimal placement, disp is displaced. Best (left) is Best Signal, Comp (middle) is Composite Signal, sEMG (right) is Traditional sEMG. Note higher means and higher spreads for Traditional sEMG.

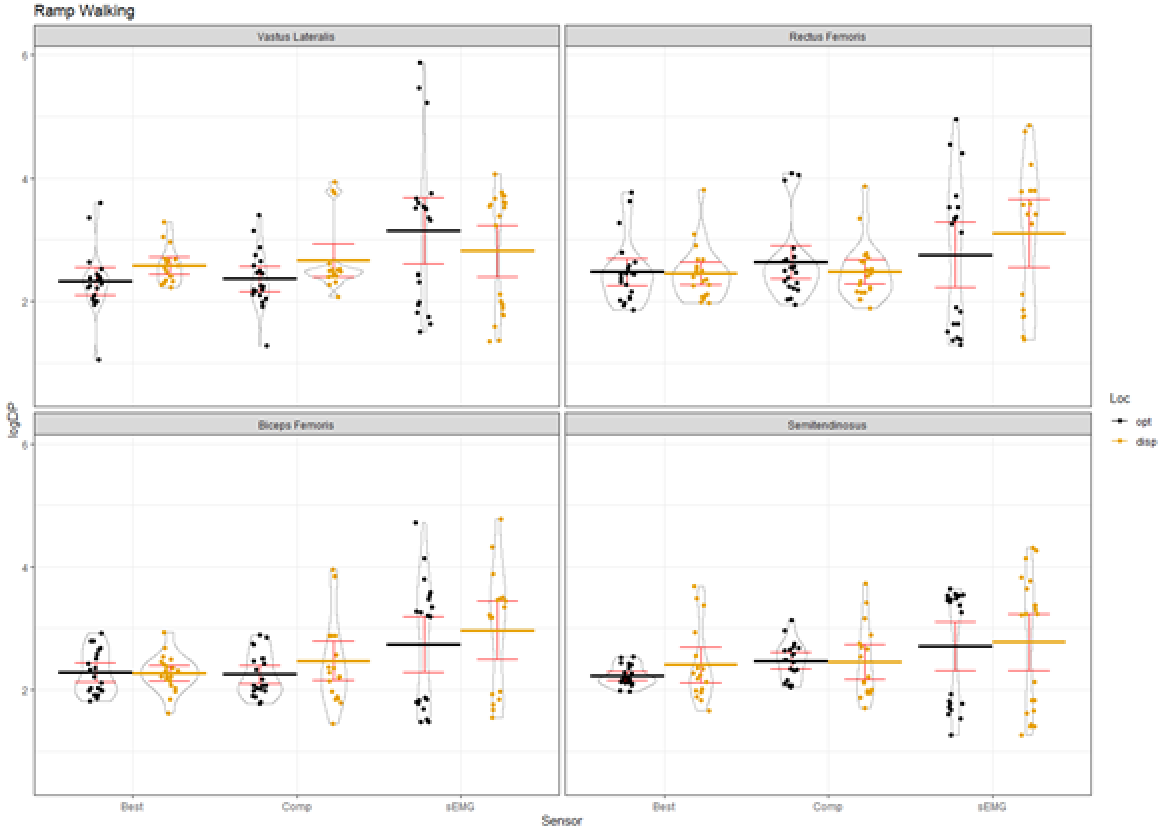

Figure 32: Violin graph of logDP for Ramp Walking. Opt is optimal placement, disp is displaced. Best (left) is Best Signal, Comp (middle) is Composite Signal, sEMG (right) is Traditional sEMG. Note higher means and higher spreads for Traditional sEMG.

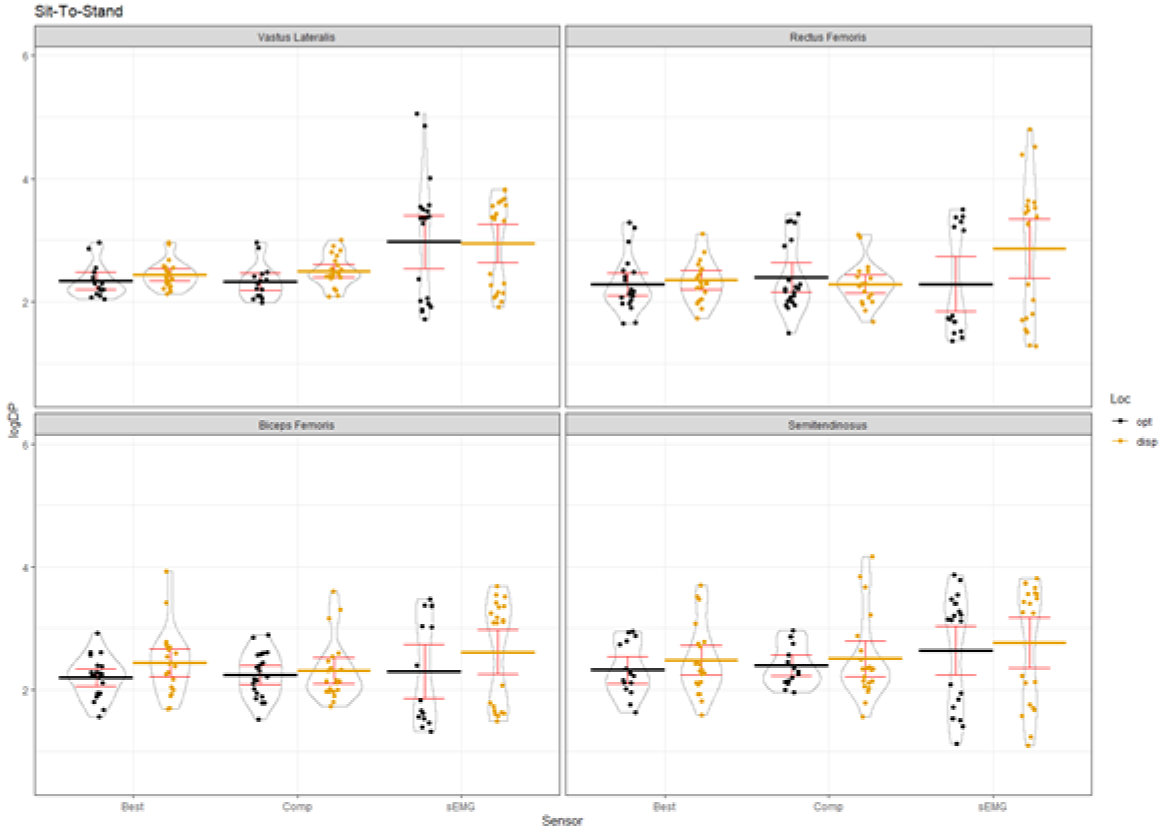

Figure 33: Violin graph of logDP for Sit to Stand. Opt is optimal placement, disp is displaced. Best (left) is Best Signal, Comp (middle) is Composite Signal, sEMG (right) is Traditional sEMG. Note higher means and higher spreads for Traditional sEMG for Vastus Lateralis (top left) and Rectus Femoris (top right).

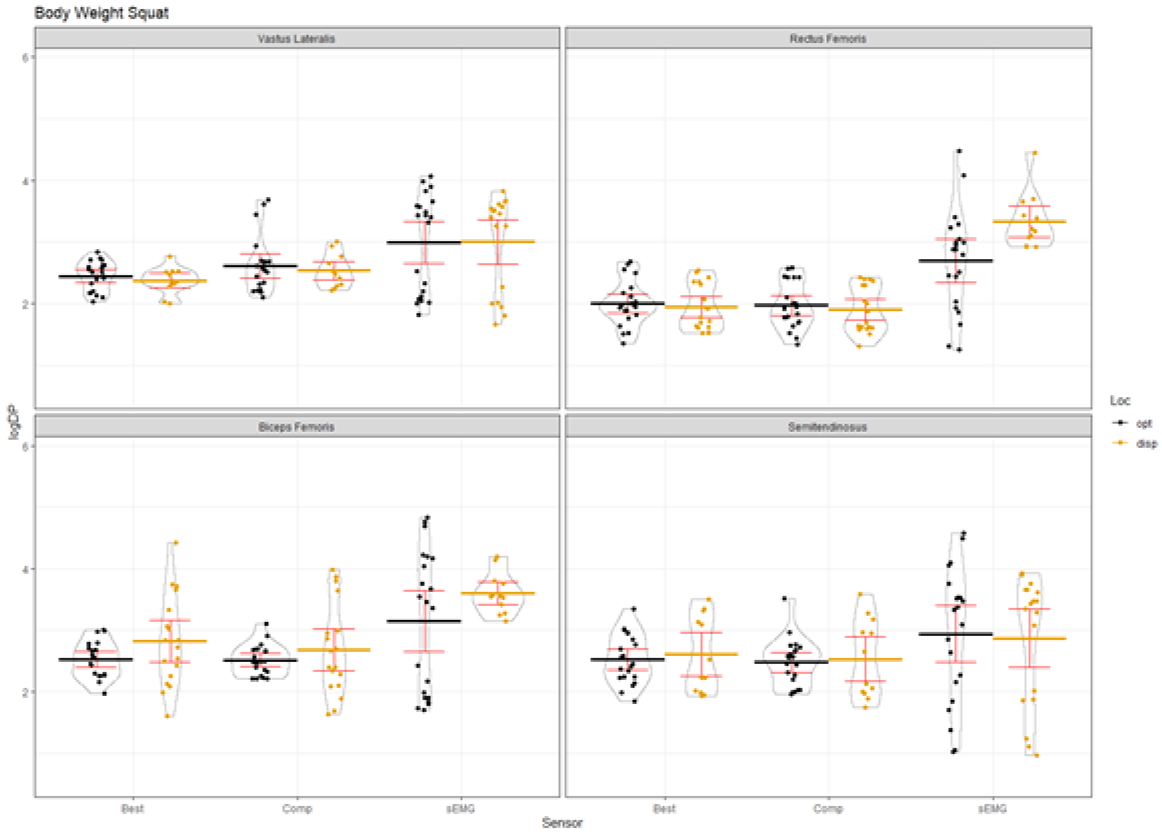

Figure 34: Violin graph of logDP for Body Weight Squats. Opt is optimal placement, disp is displaced. Best (left) is Best Signal, Comp (middle) is Composite Signal, sEMG (right) is Traditional sEMG. Note higher means and higher spreads for Traditional sEMG.

Ω Ratio

Statistical modeling revealed interactions based on muscle ($p<0.01$), signal ($p<0.01$), and activity ($p=0.022$), as well as two-way interactions between muscle and signal, muscle and activity, and signal and activity ($p<0.01$), and three-way interactions between muscle, location, and signal ($p<0.01$) and muscle, signal, and activity ($p=0.028$). Ω displayed higher values for sEMG sensors than for Best or Combined signals. Composite signals displayed equal or greater Ω levels than Best signals, but lower than sEMG signals (Figures 35-42). This measurement has no units. Effects analysis determined that 13% of variability was due to fixed effects and 77% of variability was due to a combination of fixed and random effects.

Activity	Muscle	Best - Opt	Best - Disp	Comp - Opt	Comp - Disp	sEMG - Opt	sEMG - Disp
Internal Turn	Vastus Lateralis	1.98 +/- 0.05	1.97 +/- 0.05	2.07 +/- 0.05	2.04 +/- 0.05	2.01 +/- 0.05	2.07 +/- 0.05
	Rectus Femoris	2.10 +/- 0.05	2.08 +/- 0.05	2.10 +/- 0.05	2.06 +/- 0.05	2.16 +/- 0.05	2.28 +/- 0.05
	Biceps Femoris	1.93 +/- 0.05	2.04 +/- 0.05	1.92 +/- 0.05	2.04 +/- 0.05	1.97 +/- 0.05	2.06 +/- 0.05
	Semitendinosus	2.00 +/- 0.05	2.05 +/- 0.05	2.06 +/- 0.05	2.07 +/- 0.05	2.12 +/- 0.05	2.07 +/- 0.05
External Turn	Vastus Lateralis	1.99 +/- 0.05	1.99 +/- 0.05	2.02 +/- 0.05	2.03 +/- 0.05	2.03 +/- 0.05	2.02 +/- 0.05
	Rectus Femoris	2.06 +/- 0.05	2.06 +/- 0.05	2.09 +/- 0.05	2.10 +/- 0.05	2.29 +/- 0.05	2.24 +/- 0.05
	Biceps Femoris	1.95 +/- 0.05	2.06 +/- 0.05	1.98 +/- 0.05	1.97 +/- 0.05	2.11 +/- 0.05	2.01 +/- 0.05
	Semitendinosus	1.99 +/- 0.05	1.99 +/- 0.05	2.06 +/- 0.05	2.03 +/- 0.05	2.02 +/- 0.05	2.15 +/- 0.05
Walking	Vastus Lateralis	2.02 +/- 0.05	2.03 +/- 0.05	2.04 +/- 0.05	2.07 +/- 0.05	2.06 +/- 0.05	2.01 +/- 0.05
	Rectus Femoris	2.06 +/- 0.05	2.06 +/- 0.05	2.09 +/- 0.05	2.07 +/- 0.05	2.20 +/- 0.05	2.16 +/- 0.05
	Biceps Femoris	1.98 +/- 0.05	2.02 +/- 0.05	2.07 +/- 0.05	2.00 +/- 0.05	2.10 +/- 0.05	2.01 +/- 0.05
	Semitendinosus	2.10 +/- 0.05	2.09 +/- 0.05	2.08 +/- 0.05	2.14 +/- 0.05	2.04 +/- 0.05	2.14 +/- 0.05
Stair Walking	Vastus Lateralis	2.09 +/- 0.05	2.09 +/- 0.05	2.17 +/- 0.05	2.13 +/- 0.05	2.08 +/- 0.05	2.06 +/- 0.05
	Rectus Femoris	2.1 +/- 0.05	2.07 +/- 0.05	2.12 +/- 0.05	2.11 +/- 0.05	2.11 +/- 0.05	2.15 +/- 0.05
	Biceps Femoris	2.01 +/- 0.05	2.10 +/- 0.05	2.04 +/- 0.05	2.02 +/- 0.05	2.13 +/- 0.05	2.06 +/- 0.05
	Semitendinosus	2.04 +/- 0.05	2.05 +/- 0.05	2.10 +/- 0.05	2.08 +/- 0.05	2.06 +/- 0.05	2.13 +/- 0.05
Ramp Walking	Vastus Lateralis	2.00 +/- 0.05	2.03 +/- 0.05	2.04 +/- 0.05	2.06 +/- 0.05	2.03 +/- 0.05	2.06 +/- 0.05
	Rectus Femoris	2.07 +/- 0.05	2.04 +/- 0.05	2.11 +/- 0.05	2.07 +/- 0.05	2.21 +/- 0.05	2.20 +/- 0.05
	Biceps Femoris	1.95 +/- 0.05	2.01 +/- 0.05	2.01 +/- 0.05	2.07 +/- 0.05	2.11 +/- 0.05	2.06 +/- 0.05
	Semitendinosus	2.04 +/- 0.05	1.99 +/- 0.05	2.12 +/- 0.05	2.07 +/- 0.05	2.14 +/- 0.05	2.13 +/- 0.05
Sit to Stand	Vastus Lateralis	2.04 +/- 0.05	2.06 +/- 0.05	2.09 +/- 0.05	2.08 +/- 0.05	2.10 +/- 0.05	2.08 +/- 0.05
	Rectus Femoris	2.06 +/- 0.05	2.04 +/- 0.05	2.10 +/- 0.05	2.05 +/- 0.05	2.10 +/- 0.05	2.23 +/- 0.05
	Biceps Femoris	2.08 +/- 0.05	2.08 +/- 0.05	2.09 +/- 0.05	2.12 +/- 0.05	2.10 +/- 0.05	2.13 +/- 0.05
	Semitendinosus	2.09 +/- 0.05	2.06 +/- 0.05	2.07 +/- 0.05	2.09 +/- 0.05	2.12 +/- 0.05	2.18 +/- 0.05
Squats	Vastus Lateralis	2.08 +/- 0.05	2.07 +/- 0.05	2.14 +/- 0.05	2.10 +/- 0.05	2.07 +/- 0.05	2.09 +/- 0.05
	Rectus Femoris	2.00 +/- 0.05	2.01 +/- 0.05	2.00 +/- 0.05	2.01 +/- 0.05	2.02 +/- 0.05	2.10 +/- 0.05
	Biceps Femoris	2.13 +/- 0.05	2.08 +/- 0.05	2.14 +/- 0.05	2.10 +/- 0.05	2.27 +/- 0.05	2.17 +/- 0.05
	Semitendinosus	2.00 +/- 0.05	2.00 +/- 0.05	2.07 +/- 0.05	2.07 +/- 0.05	2.16 +/- 0.05	2.16 +/- 0.05

Table 6: Ω ratio means and standard error. Best – best selected signal, Comp – composite signal, sEMG – traditional sEMG, Opt – optimally placed over muscle belly, Disp - displaced 1 cm distal from muscle belly

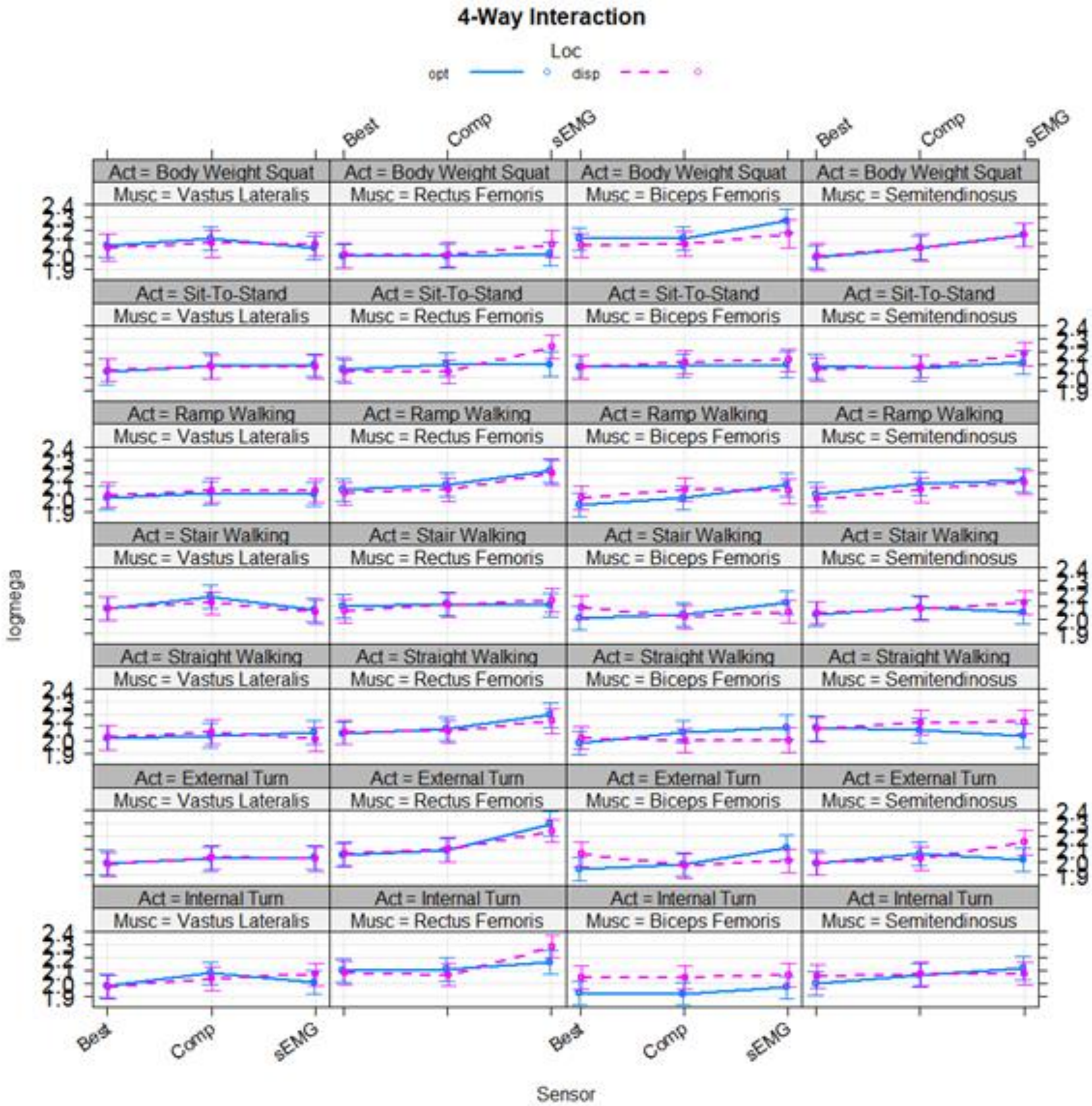

Figure 35: Effects plot of logΩ Solid blue is optimal placement, dashed pink is displaced. Best is Best Signal, Comp is Composite Signal, sEMG is Traditional sEMG. Note higher values for Traditional sEMG (far right data point). Unlike other quality measures, Omega should be low.

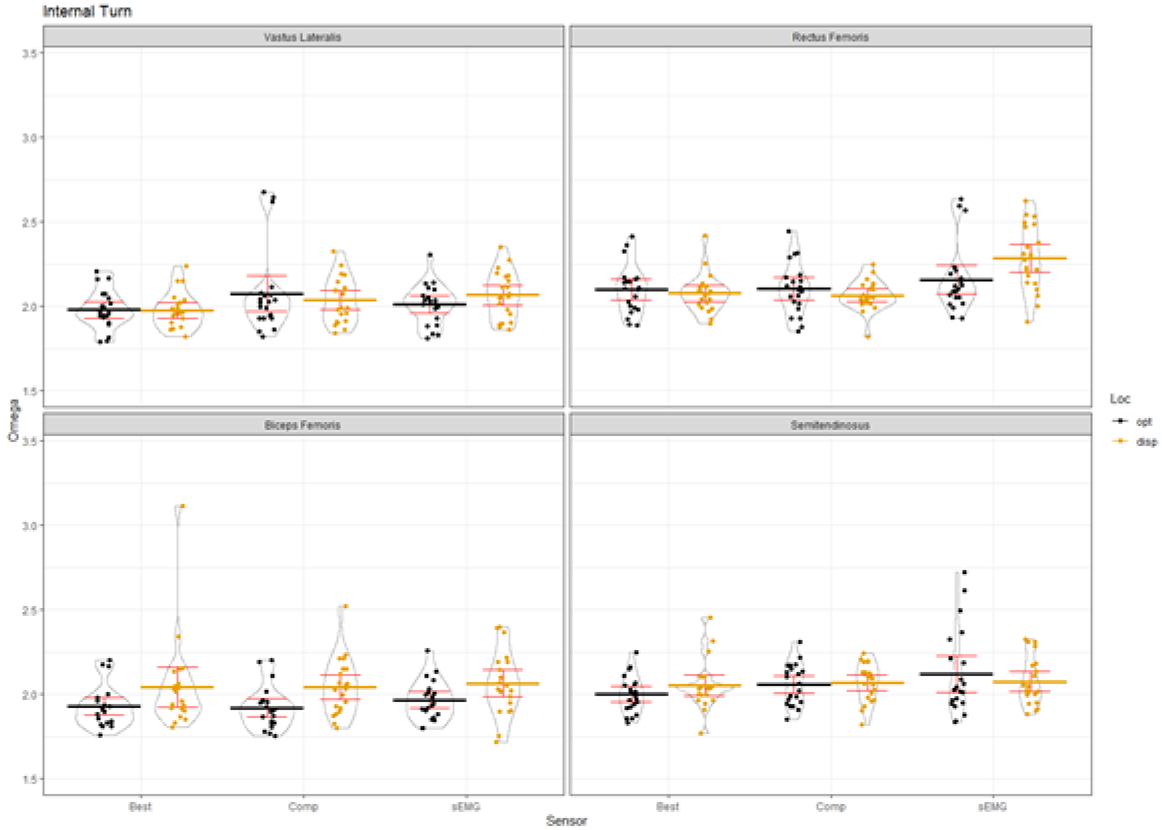

Figure 36: Violin graph of Ω for Internal Turn. Opt is optimal placement, disp is displaced. Best (left) is Best Signal, Comp (middle) is Composite Signal, sEMG (right) is Traditional sEMG.– Note higher means for Traditional sEMG, particularly for Rectus Femoris (top right).

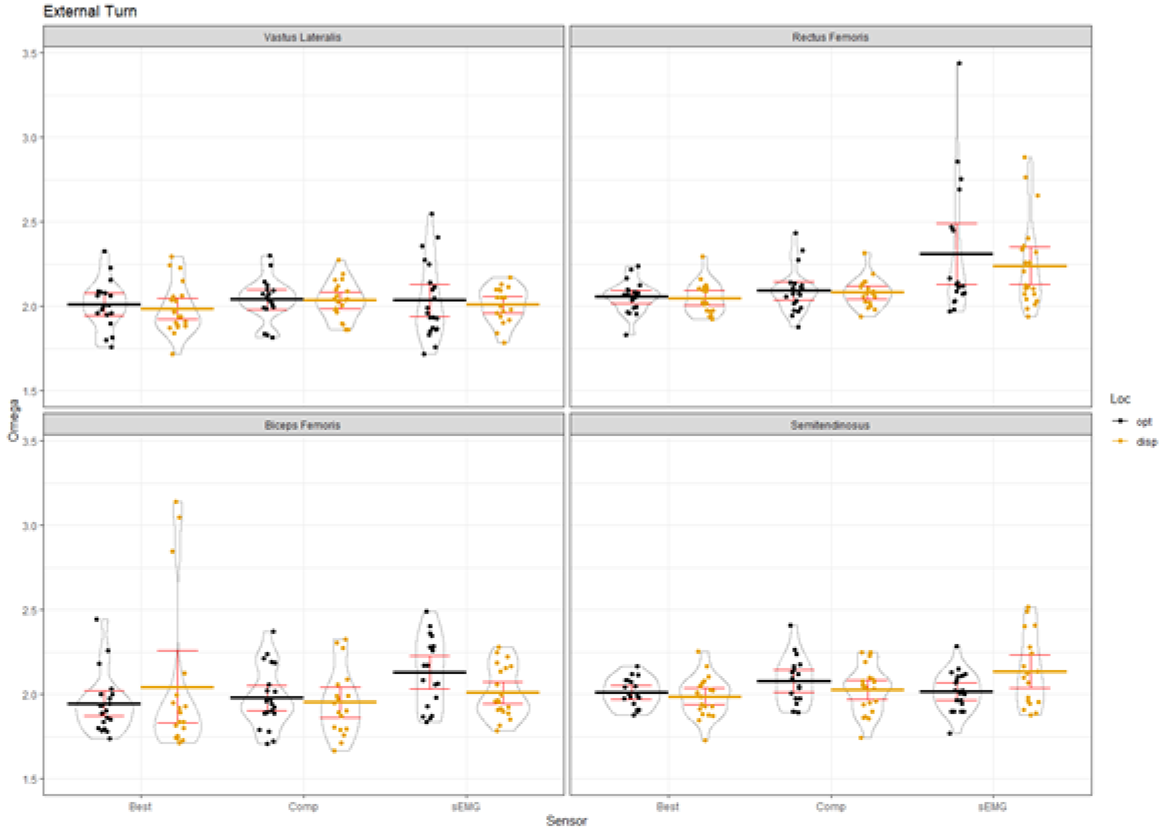

Figure 37: Violin graph of Ω for External Turn. Opt is optimal placement, disp is displaced. Best (left) is Best Signal, Comp (middle) is Composite Signal, sEMG (right) is Traditional sEMG. Note higher means for Traditional sEMG, particularly for Rectus Femoris (top right).

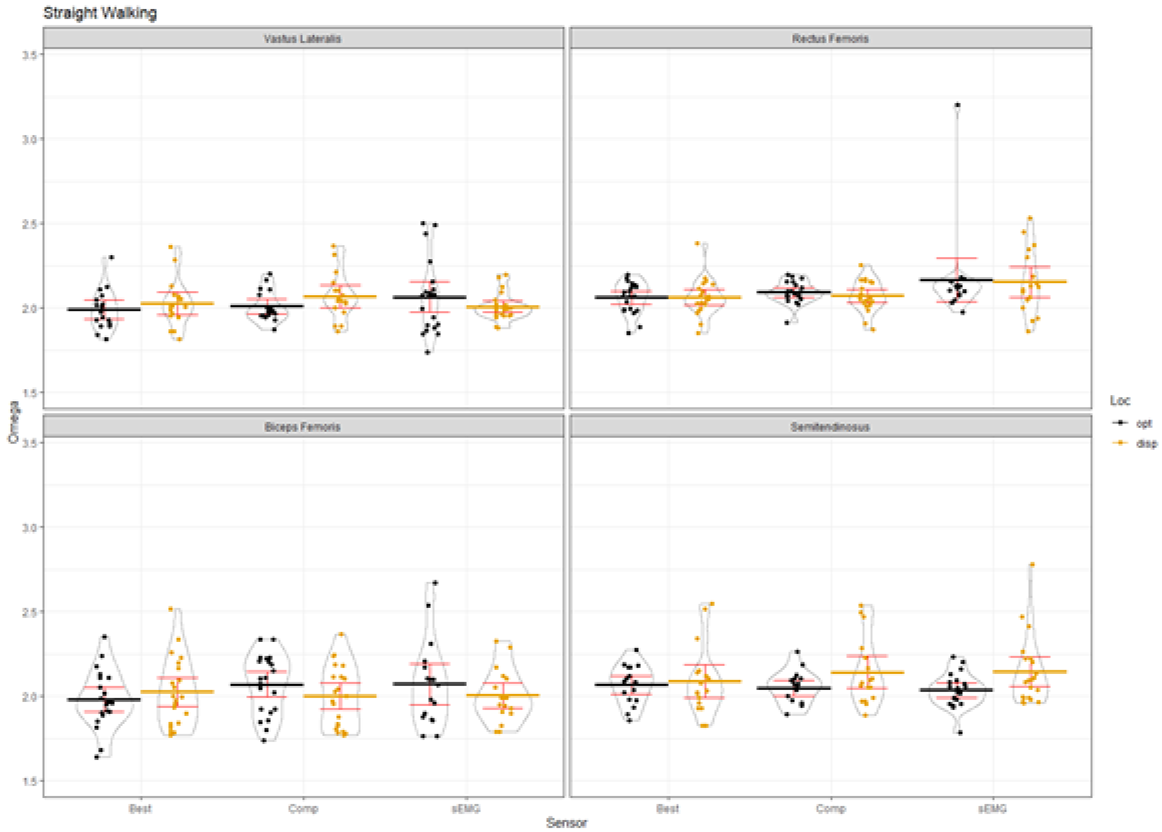

Figure 38: Violin graph of Ω for Straight Walking. Opt is optimal placement, disp is displaced. Best (left) is Best Signal, Comp (middle) is Composite Signal, sEMG (right) is Traditional sEMG. Note higher means for Traditional sEMG.

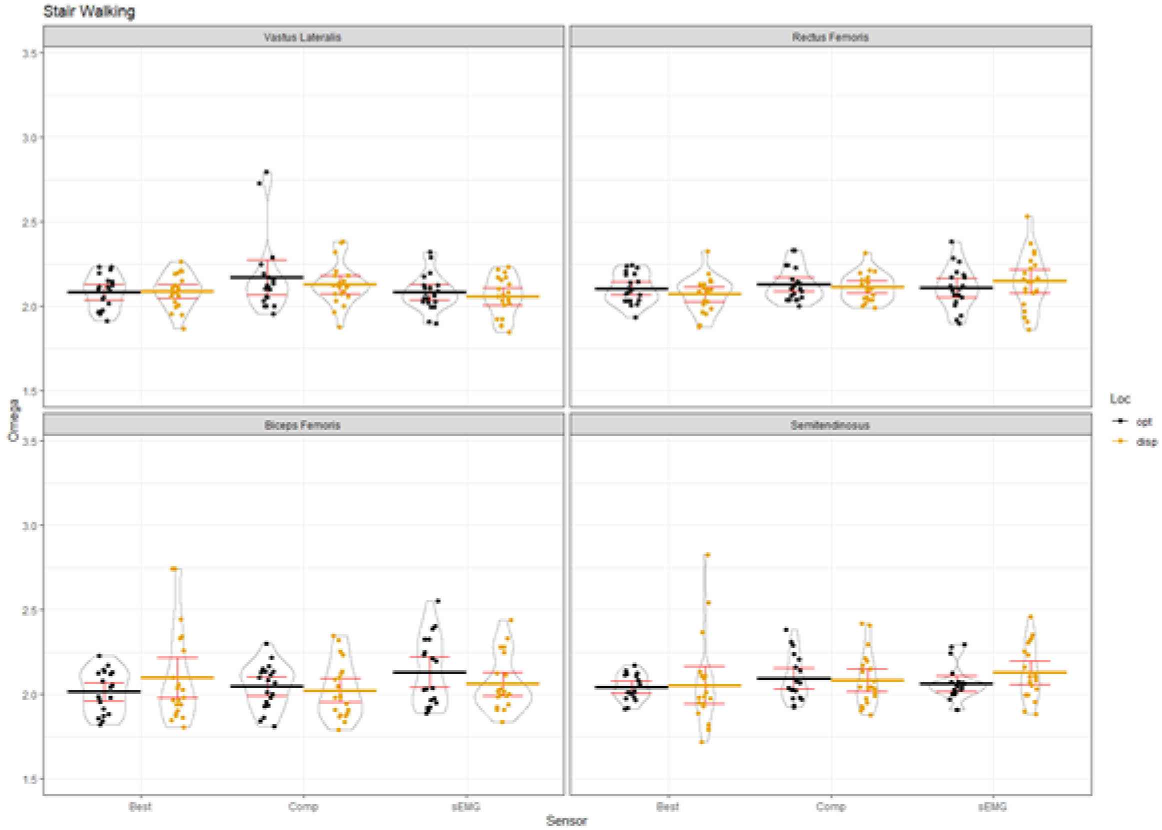

Figure 39: Violin graph of Ω for Stair Walking. Opt is optimal placement, disp is displaced. Best (left) is Best Signal, Comp (middle) is Composite Signal, sEMG (right) is Traditional sEMG. Note higher means for Traditional sEMG, as well as higher spreads for displaced Best Signal for Biceps Femoris (bottom left) and Semitendinosus (bottom right).

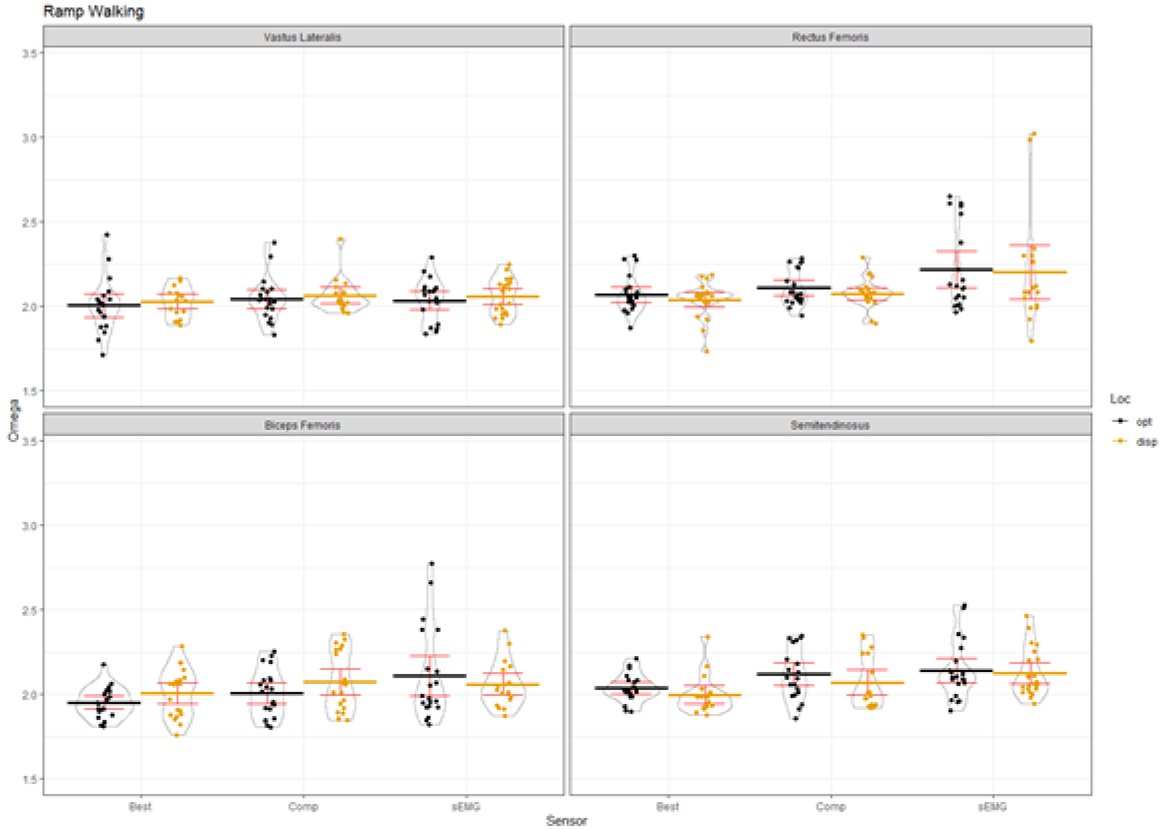

Figure 40: Violin graph of Ω for Ramp Walking. Opt is optimal placement, disp is displaced. Best (left) is Best Signal, Comp (middle) is Composite Signal, sEMG (right) is Traditional sEMG. Note higher means for Traditional sEMG, particularly for Rectus Femoris (top right).

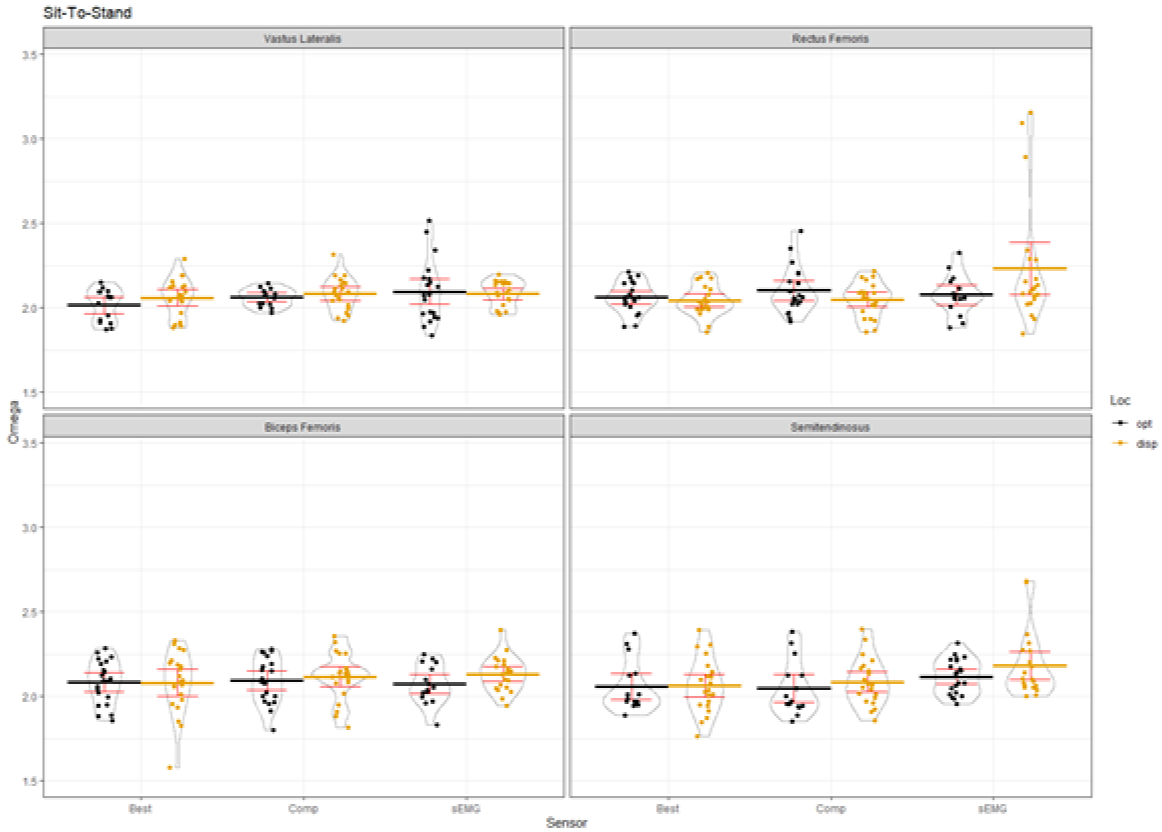

Figure 41: Violin graph of Ω for Sit to Stand. Opt is optimal placement, disp is displaced. Best (left) is Best Signal, Comp (middle) is Composite Signal, sEMG (right) is Traditional sEMG. Note higher means for Traditional sEMG, particularly for displaced Rectus Femoris (top right).

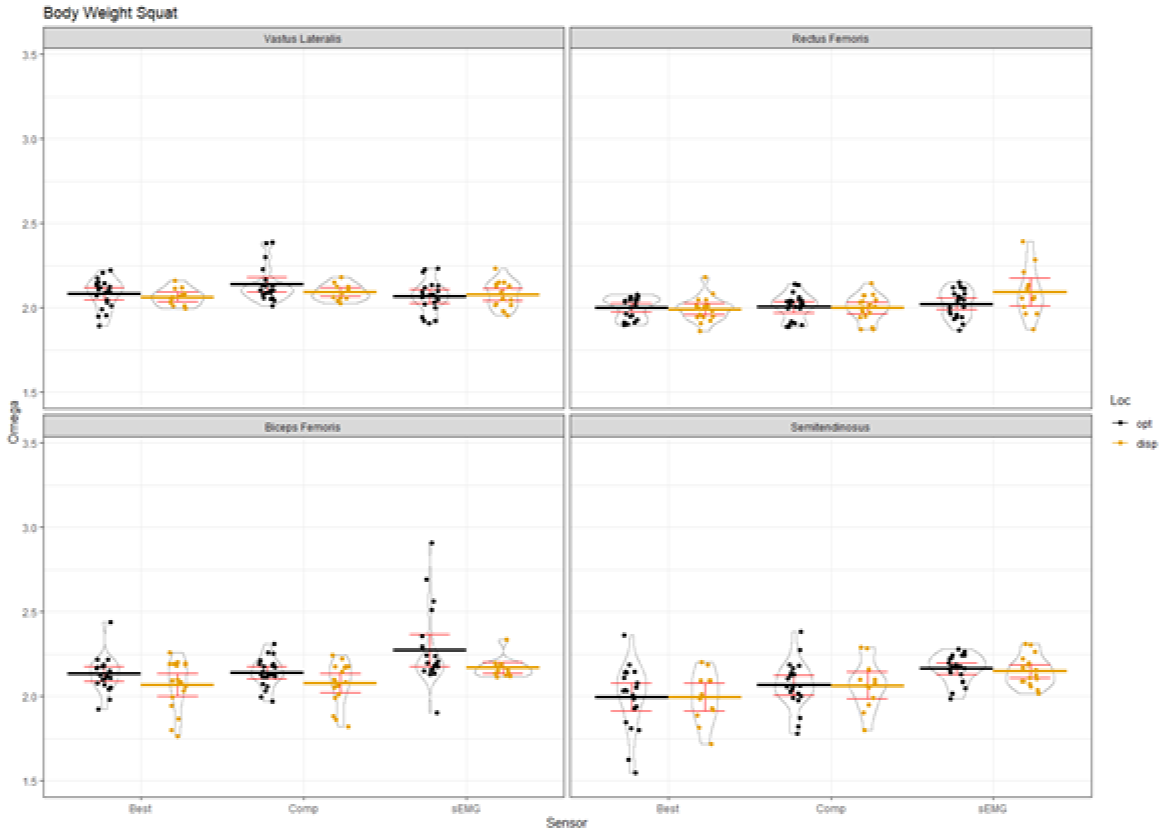

Figure 42: Violin graph of Ω for Body Weight Squats. Opt is optimal placement, disp is displaced. Best (left) is Best Signal, Comp (middle) is Composite Signal, sEMG (right) is Traditional sEMG. Note higher means for Traditional sEMG.

Signal and Location	SNR (dB)	RMS	DP (dB)	Ω
Best - Optimal	12.62 +/- 0.69	0.019 +/- 0.004	8.44E+02 +/- 3591	2.03 +/- 0.03
Best - Displaced	11.80 +/- 0.69	0.025 +/- 0.004	3.48E+02 +/- 3600	2.04 +/- 0.03
Composite - Optimal	10.29 +/- 0.69	0.021 +/- 0.004	.99E+03 +/- 3591	2.07 +/- 0.03
Composite - Displaced	9.43 +/- 0.69	0.024 +/- 0.004	3.10E+02 +/- 3600	2.07 +/- 0.03
Traditional - Optimal	5.01 +/- 0.69	0.038 +/- 0.004	1.10E+04 +/- 3591	2.10 +/- 0.03
Traditional - Displaced	5.26 +/- 0.69	0.039 +/- 0.004	4.62E+03 +/- 3600	2.11 +/- 0.03

Table 7: Total means of quality measures for each signal type and standard error.

Signal and Location	Muscle	SNR (dB)	RMS	DP (dB)	Ω
Best - Optimal	Vastus Lateralis	14.84 +/- 0.78	0.026 +/- 0.005	1.15E+03 +/- 4271	2.03 +/- 0.03
	Rectus Femoris	12.53 +/- 0.77	0.022 +/- 0.005	7.60E+02 +/- 4205	2.06 +/- 0.03
	Biceps Femoris	11.74 +/- 0.77	0.014 +/- 0.005	3.10E+02 +/- 4205	2.00 +/- 0.03
	Semitendinosus	11.36 +/- 0.78	0.016 +/- 0.005	1.16E+03 +/- 4271	2.04 +/- 0.03
Best - Displaced	Vastus Lateralis	14.21 +/- 0.78	0.021 +/- 0.005	-1.16E+02 +/- 4296	2.03 +/- 0.03
	Rectus Femoris	12.06 +/- 0.77	0.020 +/- 0.005	2.90E+02 +/- 4228	2.05 +/- 0.03
	Biceps Femoris	10.61 +/- 0.77	0.032 +/- 0.005	5.68E+02 +/- 4231	2.06 +/- 0.03
	Semitendinosus	10.31 +/- 0.78	0.028 +/- 0.005	6.50E+02 +/- 4296	2.03 +/- 0.03
Composite - Optimal	Vastus Lateralis	12.41 +/- 0.78	0.036 +/- 0.005	1.39E+03 +/- 4271	2.08 +/- 0.03
	Rectus Femoris	10.57 +/- 0.77	0.021 +/- 0.005	1.06E+03 +/- 4205	2.09 +/- 0.03
	Biceps Femoris	9.35 +/- 0.77	0.012 +/- 0.005	2.59E+02 +/- 4205	2.04 +/- 0.03
	Semitendinosus	8.83 +/- 0.78	0.017 +/- 0.005	1.25E+03 +/- 4271	2.08 +/- 0.03
Composite - Displaced	Vastus Lateralis	11.60 +/- 0.78	0.020 +/- 0.005	50.2 +/- 4296	2.07 +/- 0.03
	Rectus Femoris	10.36 +/- 0.77	0.017 +/- 0.005	3.88E+02 +/- 4228	2.07 +/- 0.03
	Biceps Femoris	8.39 +/- 0.77	0.027 +/- 0.005	6.78E+02 +/- 4231	2.05 +/- 0.03
	Semitendinosus	7.38 +/- 0.78	0.033 +/- 0.005	1.23E+02 +/- 4296	2.08 +/- 0.03
Traditional - Optimal	Vastus Lateralis	6.16 +/- 0.77	0.045 +/- 0.005	2.59E+04 +/- 4205	2.05 +/- 0.03
	Rectus Femoris	3.22 +/- 0.78	0.040 +/- 0.005	8.14E+03 +/- 4271	2.16 +/- 0.03
	Biceps Femoris	5.31 +/- 0.78	0.033 +/- 0.005	7.66E+03 +/- 4271	2.11 +/- 0.03
	Semitendinosus	5.36 +/- 0.77	0.033 +/- 0.005	2.33E+03 +/- 4205	2.09 +/- 0.03
Traditional - Displaced	Vastus Lateralis	6.12 +/- 0.77	0.043 +/- 0.005	2.15E+03 +/- 4228	2.06 +/- 0.03
	Rectus Femoris	3.73 +/- 0.78	0.046 +/- 0.005	7.16E+03 +/- 4296	2.19 +/- 0.03
	Biceps Femoris	5.79 +/- 0.78	0.030 +/- 0.005	5.43E+03 +/- 4296	2.07 +/- 0.03
	Semitendinosus	5.39 +/- 0.77	0.036 +/- 0.005	3.72E+03 +/- 4228	2.14 +/- 0.03

Table 8: Means of each quality measure by muscle with standard error

Signal and Location	Activity	SNR (dB)	RMS	DP (dB)	Ω
Best - Optimal	Internal Turn	11.41 +/- 0.76	0.017 +/- 0.006	7.47E+02 +/- 4489	2.00 +/- 0.04
	External Turn	11.49 +/- 0.76	0.012 +/- 0.006	4.34E+02 +/- 4757	2.00 +/- 0.04
	Straight Walking	10.31 +/- 0.77	0.013 +/- 0.006	1.99E+03 +/- 4601	2.04 +/- 0.04
	Stair Walking	13.26 +/- 0.76	0.024 +/- 0.006	24.4 +/- 4547	2.06 +/- 0.04
	Ramp Walking	12.02 +/- 0.76	0.015 +/- 0.006	3.66E+02 +/- 4508	2.01 +/- 0.04
	Sit to Stand	14.56 +/- 0.77	0.024 +/- 0.006	1.99E+03 +/- 4692	2.07 +/- 0.04
	Body Weight Squats	15.26 +/- 0076	0.029 +/- 0.006	3.44E+02 +/- 4489	2.05 +/- 0.04
Best - Displaced	Internal Turn	10.66 +/- 0.76	0.026 +/- 0.006	4.05E+02 +/- 4489	2.04 +/- 0.04
	External Turn	10.38 +/- 0.76	0.023 +/- 0.006	3.78E+02 +/- 4757	2.02 +/- 0.04
	Straight Walking	9.65 +/- 0.77	0.032 +/- 0.006	50.5 +/- 4602	2.05 +/- 0.04
	Stair Walking	13.34 +/- 0.76	0.035 +/- 0.006	1.52E+03 +/- 4489	2.08 +/- 0.04
	Ramp Walking	10.83 +/- 0.77	0.016 +/- 0.006	84.8 +/- 4611	2.02 +/- 0.04
	Sit to Stand	13.53 +/- 0.76	0.018 +/- 0.006	5.47E+02 +/- 4489	2.06 +/- 0.04
	Body Weight Squats	14.19 +/- 0.79	0.026 +/- 0.006	-5.46E+02 +/- 4943	2.04 +/- 0.04
Composite - Optimal	Internal Turn	9.32 +/- 0.76	0.027 +/- 0.006	7.14E+02 +/- 4489	2.04 +/- 0.04
	External Turn	9.34 +/- 0.76	0.013 +/- 0.006	4.43E+02 +/- 4757	2.04 +/- 0.04
	Straight Walking	8.03 +/- 0.77	0.013 +/- 0.006	2.12E+03 +/- 4601	2.07 +/- 0.04
	Stair Walking	10.91 +/- 0.76	0.031 +/- 0.006	4.93E+02 +/- 4547	2.11 +/- 0.04
	Ramp Walking	9.81 +/- 0.76	0.013 +/- 0.006	6.53E+02 +/- 4508	2.07 +/- 0.04
	Sit to Stand	12.34 +/- 0.77	0.023 +/- 0.006	2.06E+03 +/- 4692	2.09 +/- 0.04
	Body Weight Squats	12.28 +/- 0.76	0.028 +/- 0.006	4.57E+02 +/- 4489	2.09 +/- 0.04
Composite - Displaced	Internal Turn	8.00 +/- 0.76	0.025 +/- 0.006	5.06E+02 +/- 4489	2.05 +/- 0.04
	External Turn	8.03 +/- 0.76	0.024 +/- 0.006	6.17E+02 +/- 4757	2.03 +/- 0.04
	Straight Walking	7.64 +/- 0.77	0.036 +/- 0.006	-19.7 +/- 4602	2.07 +/- 0.04
	Stair Walking	11.45 +/- 0.76	0.031 +/- 0.006	5.45E+02 +/- 4489	2.09 +/- 0.04
	Ramp Walking	8.60 +/- 0.77	0.016 +/- 0.006	6.29E+02 +/- 4611	2.07 +/- 0.04
	Sit to Stand	10.89 +/- 0.76	0.017 +/- 0.006	6.64E+02 +/- 4489	2.08 +/- 0.04
	Body Weight Squats	11.42 +/- 0.79	0.021 +/- 0.006	-7.72E+02 +/- 4943	2.07 +/- 0.04
Traditional - Optimal	Internal Turn	5.03 +/- 0.76	0.033 +/- 0.006	1.82E+04 +/- 4489	2.06 +/- 0.04
	External Turn	4.57 +/- 0.76	0.036 +/- 0.006	8.65E+03 +/- 4575	2.11 +/- 0.04
	Straight Walking	4.02 +/- 0.77	0.028 +/- 0.006	5.32E+03 +/- 4601	2.10 +/- 0.04
	Stair Walking	6.11 +/- 0.76	0.045 +/- 0.006	1.52E+04 +/- 4547	2.10 +/- 0.04
	Ramp Walking	4.79 +/- 0.76	0.037 +/- 0.006	1.88E+04 +/- 4508	2.12 +/- 0.04
	Sit to Stand	3.96 +/- 0.77	0.032 +/- 0.006	5.19E+03 +/- 4692	2.10 +/- 0.04
	Body Weight Squats	6.61 +/- 0.76	0.054 +/- 0.006	5.80E+03 +/- 4489	2.13 +/- 0.04
Traditional - Displaced	Internal Turn	4.54 +/- 0.76	0.037 +/- 0.006	2.96E+03 +/- 4489	2.12 +/- 0.04
	External Turn	4.42 +/- 0.76	0.033 +/- 0.006	8.71E+03 +/- 4575	2.11 +/- 0.04
	Straight Walking	4.64 +/- 0.77	0.038 +/- 0.006	2.53E+03 +/- 4602	2.08 +/- 0.04
	Stair Walking	6.63 +/- 0.76	0.046 +/- 0.006	7.35E+03 +/- 4489	2.10 +/- 0.04
	Ramp Walking	4.84 +/- 0.77	0.032 +/- 0.006	5.45E+03 +/- 4602	2.11 +/- 0.04
	Sit to Stand	5.04 +/- 0.76	0.034 +/- 0.006	3.20E+03 +/- 4489	2.16 +/- 0.04
	Body Weight Squats	6.68 +/- 0.79	0.053 +/- 0.006	2.12E+03 +/- 4943	2.13 +/- 0.04

Table 9: Means of signal quality measures by activity and standard error

Cross Correlation and Cross Covariance

Cross correlation and cross covariance were calculated with Optimal placement as the baseline and Displaced placement as the comparison. Due to the internal comparative nature of this measurement, reported values have no units. Both cross correlation and cross covariance displayed values of 0 except for the singular instances of lags of 1 or -1 listed in Table 10. Because +/-1 is the lowest amount that can be shifted and result in a difference, time lag is minimal for outlier data points.

Activity	Muscle	Signal	Analysis Type	Value
Internal Turn	Vastus Lateralis	Traditional sEMG	Both	1
Internal Turn	Rectus Femoris	Best Signal	Both	1
External Turn	Vastus Lateralis	Best Signal	Cross Covariance	1
External Turn	Vastus Lateralis	Composite Signal	Cross Covariance	1
External Turn	Biceps Femoris	Best Signal	Both	1
External Turn	Semitendinosus	Best Signal	Both	1
External Turn	Semitendinosus	Composite Signal	Cross Covariance	1
Sit to Stand	Vastus Lateralis	Composite Signal	Both	-1
Sit to Stand	Rectus Femoris	Traditional sEMG	Both	-1
Sit to Stand	Semitendinosus	Best Signal	Both	-1
Body Weight Squats	Rectus Femoris	Best Signal	Both	-1
Body Weight Squats	Rectus Femoris	Composite Signal	Both	-1
Body Weight Squats	Biceps Femoris	Composite Signal	Both	-1
Body Weight Squats	Semitendinosus	Best Signal	Both	-1

Table 10: Specific instances where Cross Correlation and Covariance did not equal 0

Mean Squared Coherence - Means

Coherence means were calculated with Optimal placement as the baseline and Displaced placement as the comparison. Due to the internal comparative nature of this measurement, the values have no units. Significant interactions were seen for muscle, sensor, and activity ($p<0.01$). Two-way interactions were seen between muscle and activity, signal, and activity ($p<0.01$), and a three-way interaction between muscle, signal, and activity ($p=0.02$). All average coherence means were relatively high, at least over 0.8, with a large amount over 0.9 (Figures 43-50). Due to being a comparative measure, mean squared coherence does not have units. Higher means were seen for Traditional sEMG signals, although that was a relative difference as many had similar levels for all three signal types. Three activities: internal turn, external turn, and straight walking, displayed higher variation and differences in coherence between the signal types, along with lower coherence means in general. For these activities, Vastus Lateralis and Semitendinosus displayed higher coherence mean levels, while the Biceps Femoris displayed a loss in coherence mean during the process of creating the Composite Signal. Apart from those instances, compositing did not have much effect on coherence mean. Effects analysis determined that 49% of variability was due to fixed effects and 80% of variability was due to a combination of fixed and random effects.

Activity	Muscle	Best	Comp	sEMG
Internal Turn	Vastus Lateralis	0.847 +/- 0.015	0.854 +/- 0.015	0.904 +/- 0.015
	Rectus Femoris	0.901 +/- 0.015	0.907 +/- 0.015	0.949 +/- 0.015
	Biceps Femoris	0.845 +/- 0.015	0.835 +/- 0.015	0.870 +/- 0.015
	Semitendinosus	0.887 +/- 0.015	0.885 +/- 0.015	0.916 +/- 0.015
External Turn	Vastus Lateralis	0.849 +/- 0.015	0.844 +/- 0.015	0.889 +/- 0.015
	Rectus Femoris	0.890 +/- 0.015	0.890 +/- 0.015	0.946 +/- 0.015
	Biceps Femoris	0.843 +/- 0.015	0.812 +/- 0.015	0.924 +/- 0.015
	Semitendinosus	0.881 +/- 0.015	0.877 +/- 0.015	0.918 +/- 0.015
Walking	Vastus Lateralis	0.797 +/- 0.015	0.797 +/- 0.015	0.865 +/- 0.015
	Rectus Femoris	0.844 +/- 0.015	0.841 +/- 0.015	0.919 +/- 0.015
	Biceps Femoris	0.812 +/- 0.015	0.795 +/- 0.015	0.884 +/- 0.015
	Semitendinosus	0.864 +/- 0.015	0.860 +/- 0.015	0.898 +/- 0.015
Stair Walking	Vastus Lateralis	0.918 +/- 0.015	0.951 +/- 0.015	0.950 +/- 0.015
	Rectus Femoris	0.950 +/- 0.015	0.954 +/- 0.015	0.969 +/- 0.015
	Biceps Femoris	0.951 +/- 0.015	0.945 +/- 0.015	0.969 +/- 0.015
	Semitendinosus	0.957 +/- 0.015	0.955 +/- 0.015	0.975 +/- 0.015
Ramp Walking	Vastus Lateralis	0.946 +/- 0.015	0.947 +/- 0.015	0.958 +/- 0.015
	Rectus Femoris	0.951 +/- 0.015	0.951 +/- 0.015	0.957 +/- 0.015
	Biceps Femoris	0.95 +/- 0.015	0.941 +/- 0.015	0.959 +/- 0.015
	Semitendinosus	0.955 +/- 0.015	0.950 +/- 0.015	0.976 +/- 0.015
Sit to Stand	Vastus Lateralis	0.945 +/- 0.015	0.949 +/- 0.015	0.953 +/- 0.015
	Rectus Femoris	0.947 +/- 0.015	0.947 +/- 0.015	0.958 +/- 0.015
	Biceps Femoris	0.959 +/- 0.015	0.959 +/- 0.015	0.959 +/- 0.015
	Semitendinosus	0.961 +/- 0.015	0.959 +/- 0.015	0.979 +/- 0.015
Squats	Vastus Lateralis	0.913 +/- 0.017	0.917 +/- 0.017	0.954 +/- 0.015
	Rectus Femoris	0.918 +/- 0.015	0.919 +/- 0.015	0.963 +/- 0.016
	Biceps Femoris	0.950 +/- 0.015	0.946 +/- 0.015	0.993 +/- 0.016
	Semitendinosus	0.924 +/- 0.017	0.929 +/- 0.017	0.981 +/- 0.015

Table 11: Coherence Means and standard error. Best – Best Signal, Comp – Composite Signal, sEMG – Traditional sEMG

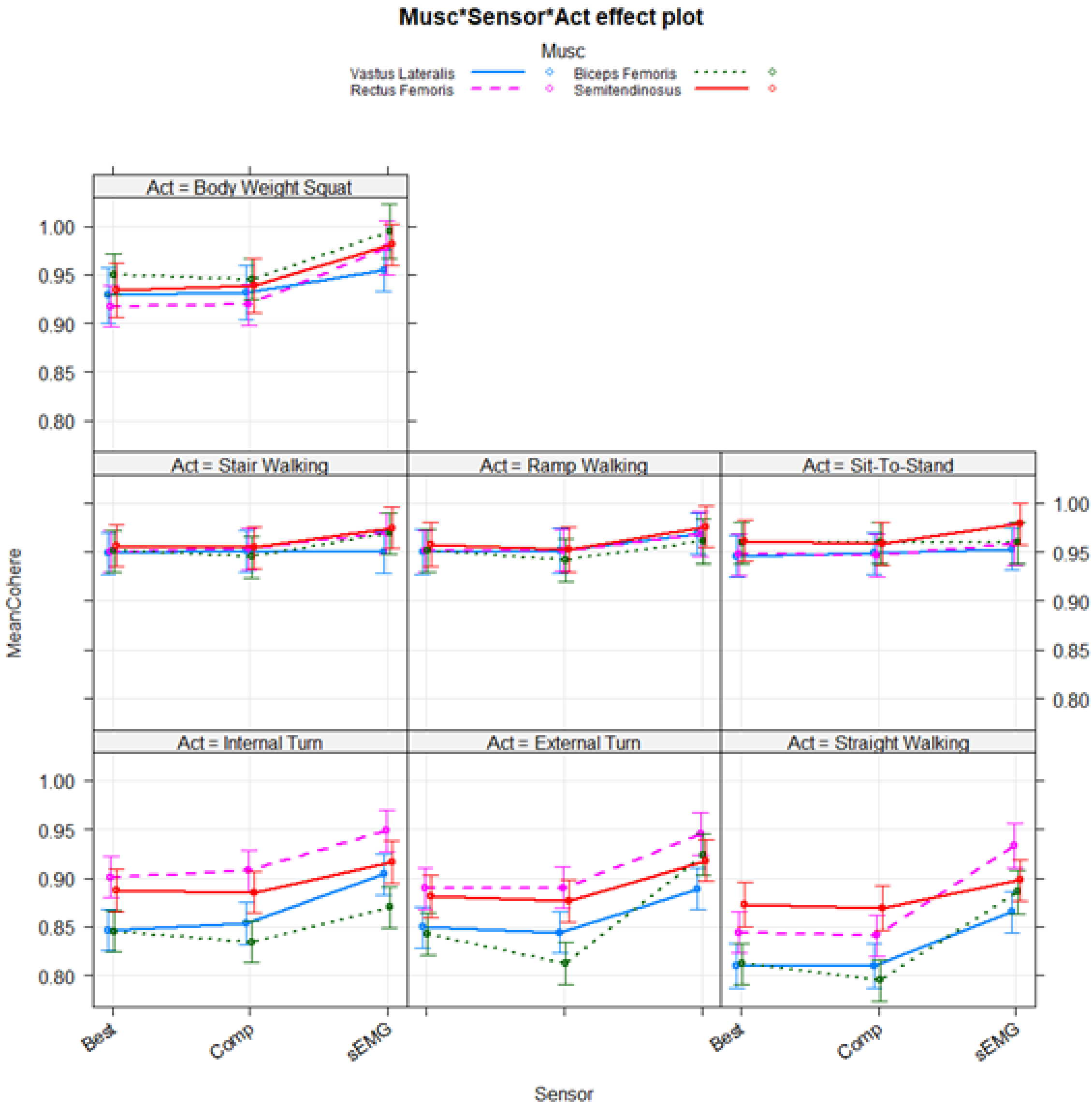

Figure 43: Effects plot of Coherence Means. Solid blue is Vastus Lateralis, dashed pink is Rectus Femoris, dotted green is Biceps Femoris, solid red is Semitendinosus. Best is Best Signal, Comp is Composite Signal, sEMG is traditional sEMG. Note the higher values for Traditional sEMG and higher spread between muscles for Internal Turn, External Turn, and Straight Walking (bottom row).

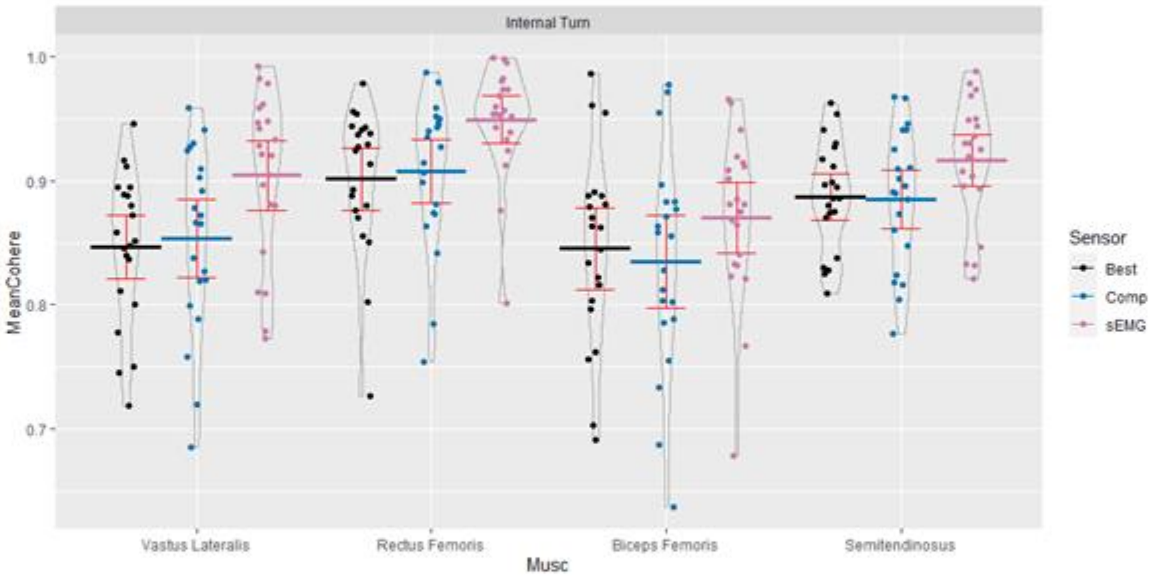

Figure 44: Violin plot of coherence means for Internal Turn. Best is Best Signal, Comp is Composite Signal, sEMG is Traditional sEMG. Note the higher means for Traditional sEMG and the lower Best Signal and Composite Signal values for Biceps Femoris (2nd from right).

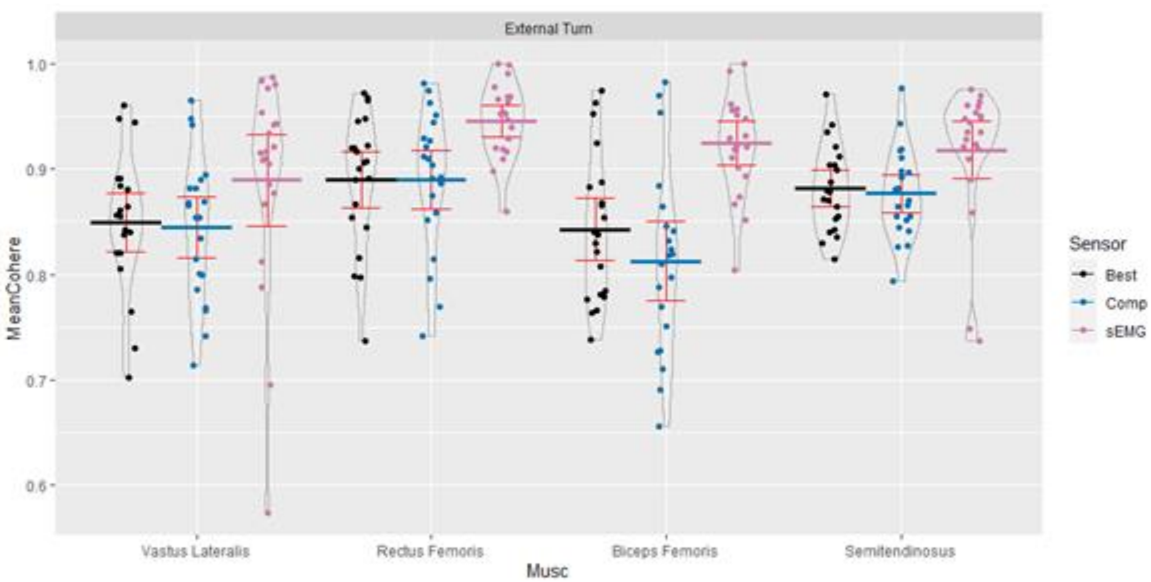

Figure 45: Violin plot of coherence means for External Turn. Best is Best Signal, Comp is Composite Signal, sEMG is Traditional sEMG. Note the higher means for Traditional sEMG and the lower Best Signal and Composite Signal values for Biceps Femoris (2nd from right).

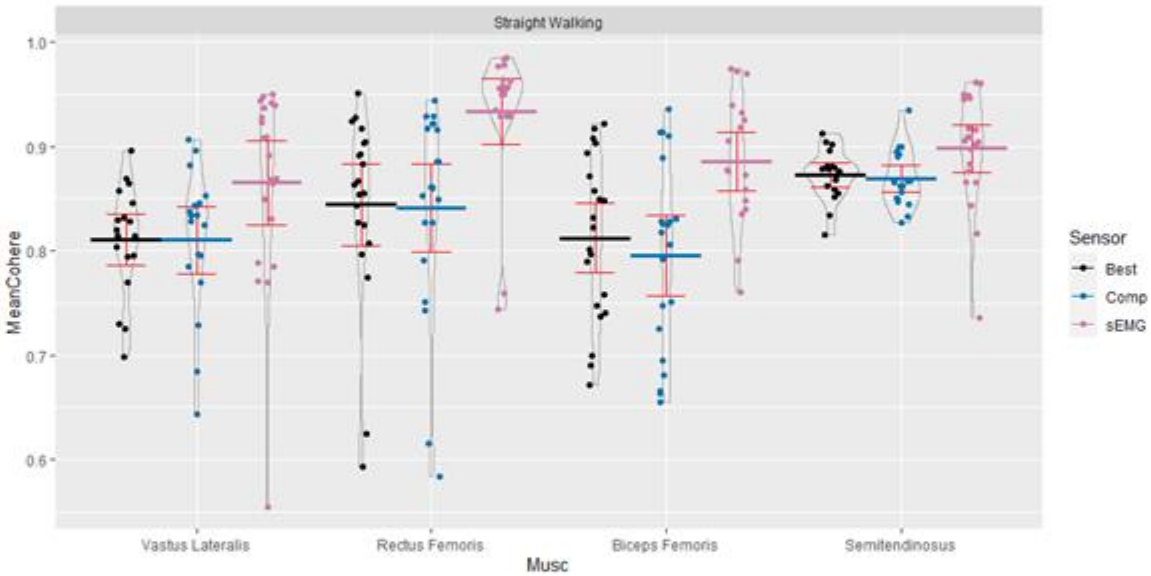

Figure 46: Violin plot of coherence means for straight walking. Best is Best Signal, Comp is Composite Signal, sEMG is Traditional sEMG. Note the higher means for Traditional sEMG and the lower Best Signal and Composite Signal values for Biceps Femoris (2nd from right).

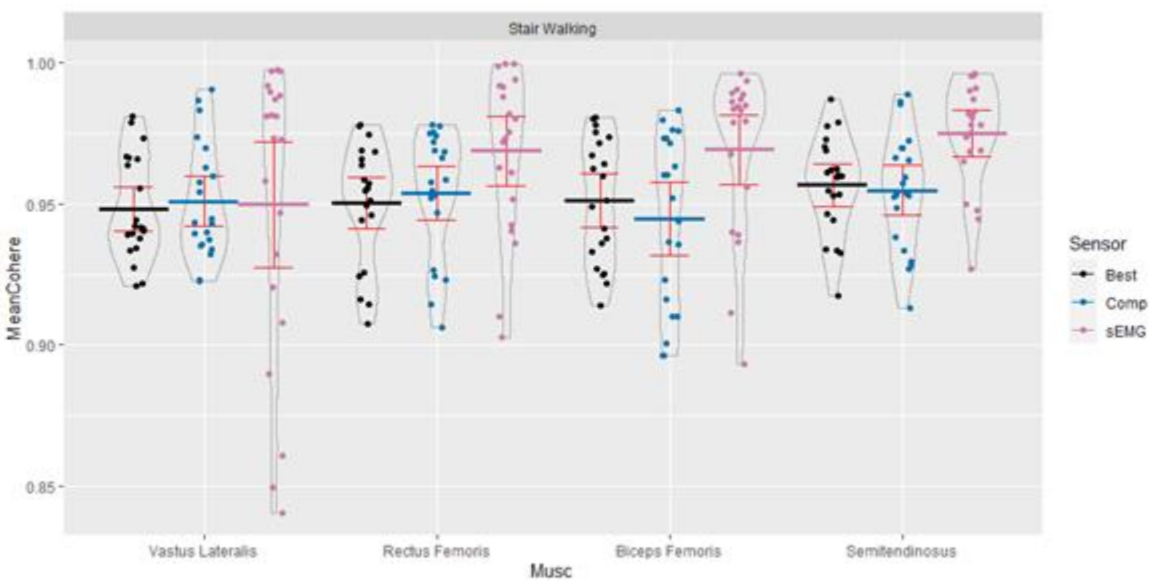

Figure 47: Violin plot of coherence means for Stair Walking. Best is Best Signal, Comp is Composite Signal, sEMG is Traditional sEMG. Note the higher means for Traditional sEMG.

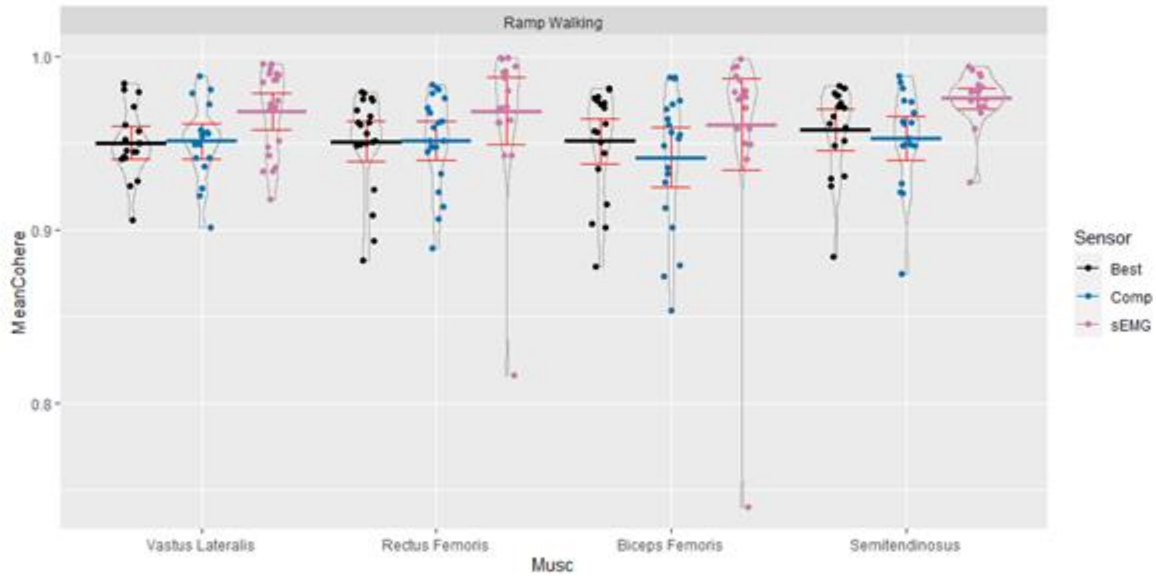

Figure 48: Violin plot of coherence means for Ramp Walking. Best is Best Signal, Comp is Composite Signal, sEMG is Traditional sEMG. Note the higher means for Traditional sEMG and the lower Best Signal and Composite Signal values for Biceps Femoris (2nd from right).

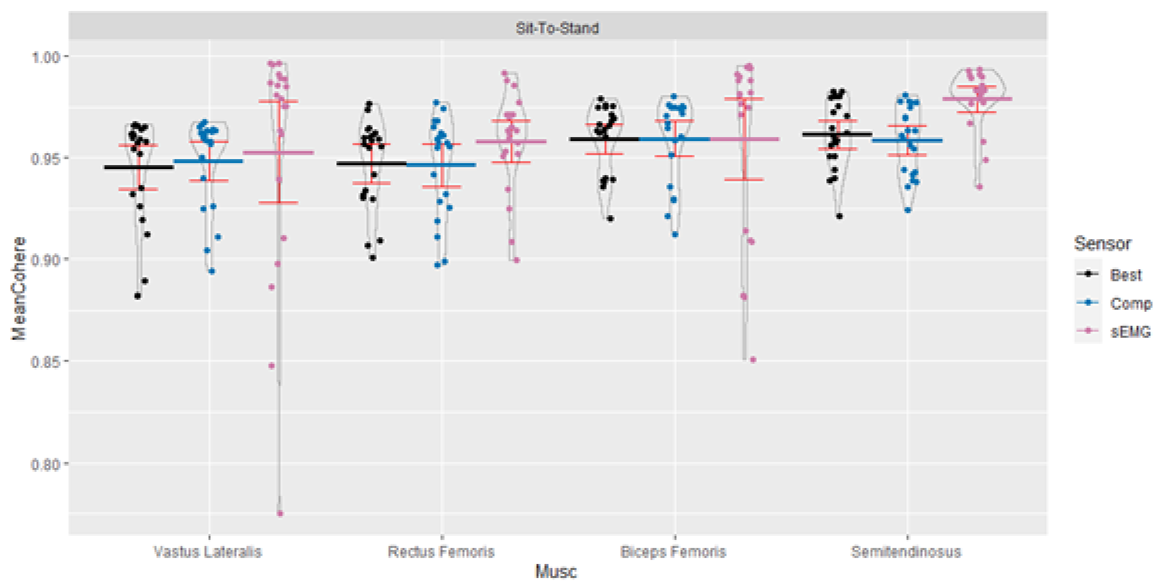

Figure 49: Violin plot of coherence means for Sit to Stand. Best is Best Signal, Comp is Composite Signal, sEMG is Traditional sEMG. Note the higher means for Traditional sEMG.

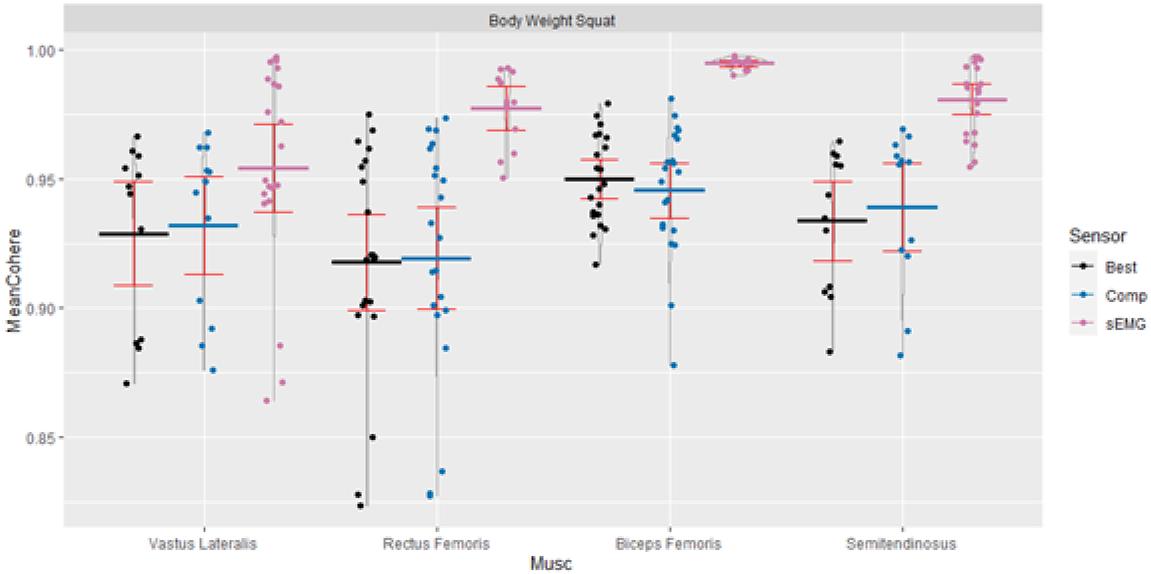

Figure 50: Violin plot of coherence means for Body Weight Squat. Best is Best Signal, Comp is Composite Signal, sEMG is Traditional sEMG. Note the higher means for Traditional sEMG.

Mean Squared Coherence - Standard Deviation

Coherence means were calculated with Optimal placement as the baseline and Displaced placement as the comparison. Since mean squared coherence creates multiple data points, outliers within the coherence spectrum can affect the calculated mean. To create a better image of the coherence spectrum, the standard deviation of each calculated coherence was determined. Due to the internal comparative nature of this measurement, the values have no units. Every measure was found to be of significant level for coherence deviation, including muscle, signal, and activity, as well as the two-way interactions between muscle and signal, muscle and activity, and sensor and activity, and the three-way interaction between muscle, signal, and activity. All p-values were less than 0.01. Trends from coherence means held through coherence deviation as well, with internal and external turns, along with straight walking, displaying higher deviations, as well as a larger spread in deviations, while stair, ramp, and sit-to-stand displayed low levels and little variation. All deviation levels were low, with the highest mean being 0.15, while the lowest values were centered around 0.03 (Figures 51-58). sEMG signals displayed lower deviations, and Rectus Femoris displayed lower deviation levels on the varying activity types, while Biceps Femoris was more likely to increase in deviation when composited. Effects analysis determined that 51% of variability was due to fixed effects and 70% of variability was due to a combination of fixed and random effects.

Activity	Muscle	Best	Comp	sEMG
Internal Turn	Vastus Lateralis	0.149 +/- 0.011	0.146 +/- 0.011	0.111 +/- 0.011
	Rectus Femoris	0.119 +/- 0.011	0.115 +/- 0.011	0.0728 +/- 0.011
	Biceps Femoris	0.119 +/- 0.011	0.152 +/- 0.011	0.139 +/- 0.011
	Semitendinosus	0.149 +/- 0.011	0.126 +/- 0.011	0.0992 +/- 0.011
External Turn	Vastus Lateralis	0.149 +/- 0.011	0.149 +/- 0.011	0.108 +/- 0.011
	Rectus Femoris	0.116 +/- 0.011	0.120 +/- 0.011	0.0723 +/- 0.011
	Biceps Femoris	0.116 +/- 0.011	0.155 +/- 0.011	0.0859 +/- 0.011
	Semitendinosus	0.149 +/- 0.011	0.145 +/- 0.011	0.0969 +/- 0.011
Walking	Vastus Lateralis	0.160 +/- 0.011	0.156 +/- 0.011	0.130 +/- 0.011
	Rectus Femoris	0.140 +/- 0.011	0.143 +/- 0.011	0.0703 +/- 0.011
	Biceps Femoris	0.140 +/- 0.011	0.155 +/- 0.011	0.116 +/- 0.011
	Semitendinosus	0.159 +/- 0.011	0.128 +/- 0.011	0.105 +/- 0.011
Stair Walking	Vastus Lateralis	0.0696 +/- 0.011	0.0650 +/- 0.011	0.0632 +/- 0.011
	Rectus Femoris	0.0559 +/- 0.011	0.0502 +/- 0.011	0.0417 +/- 0.011
	Biceps Femoris	0.0559 +/- 0.011	0.0529 +/- 0.011	0.0393 +/- 0.011
	Semitendinosus	0.0696 +/- 0.011	0.0490 +/- 0.011	0.0350 +/- 0.011
Ramp Walking	Vastus Lateralis	0.0570 +/- 0.011	0.0588 +/- 0.011	0.0370 +/- 0.011
	Rectus Femoris	0.0562 +/- 0.011	0.0529 +/- 0.011	0.0366 +/- 0.011
	Biceps Femoris	0.0573 +/- 0.011	0.0612 +/- 0.011	0.0440 +/- 0.011
	Semitendinosus	0.0569 +/- 0.011	0.0532 +/- 0.011	0.0281 +/- 0.011
Sit to Stand	Vastus Lateralis	0.0725 +/- 0.011	0.0706 +/- 0.011	0.0624 +/- 0.011
	Rectus Femoris	0.0746 +/- 0.011	0.0776 +/- 0.011	0.0655 +/- 0.011
	Biceps Femoris	0.0746 +/- 0.011	0.0564 +/- 0.011	0.0552 +/- 0.011
	Semitendinosus	0.0725 +/-0.011	0.0551 +/- 0.011	0.0398 +/- 0.011
Squats	Vastus Lateralis	0.0989 +/- 0.013	0.1037 +/- 0.013	0.0596 +/- 0.011
	Rectus Femoris	0.0833 +/- 0.011	0.0804 +/- 0.011	0.0441 +/- 0.013
	Biceps Femoris	0.0833 +/- 0.011	0.0745 +/- 0.011	0.0269 +/- 0.013
	Semitendinosus	0.0984 +/- 0.013	0.0813 +/- 0.013	0.0316 +/- 0.011

Table 12: Coherence Deviation Means and standard error. Best – Best Signal, Comp – Composite Signal, sEMG – Traditional sEMG

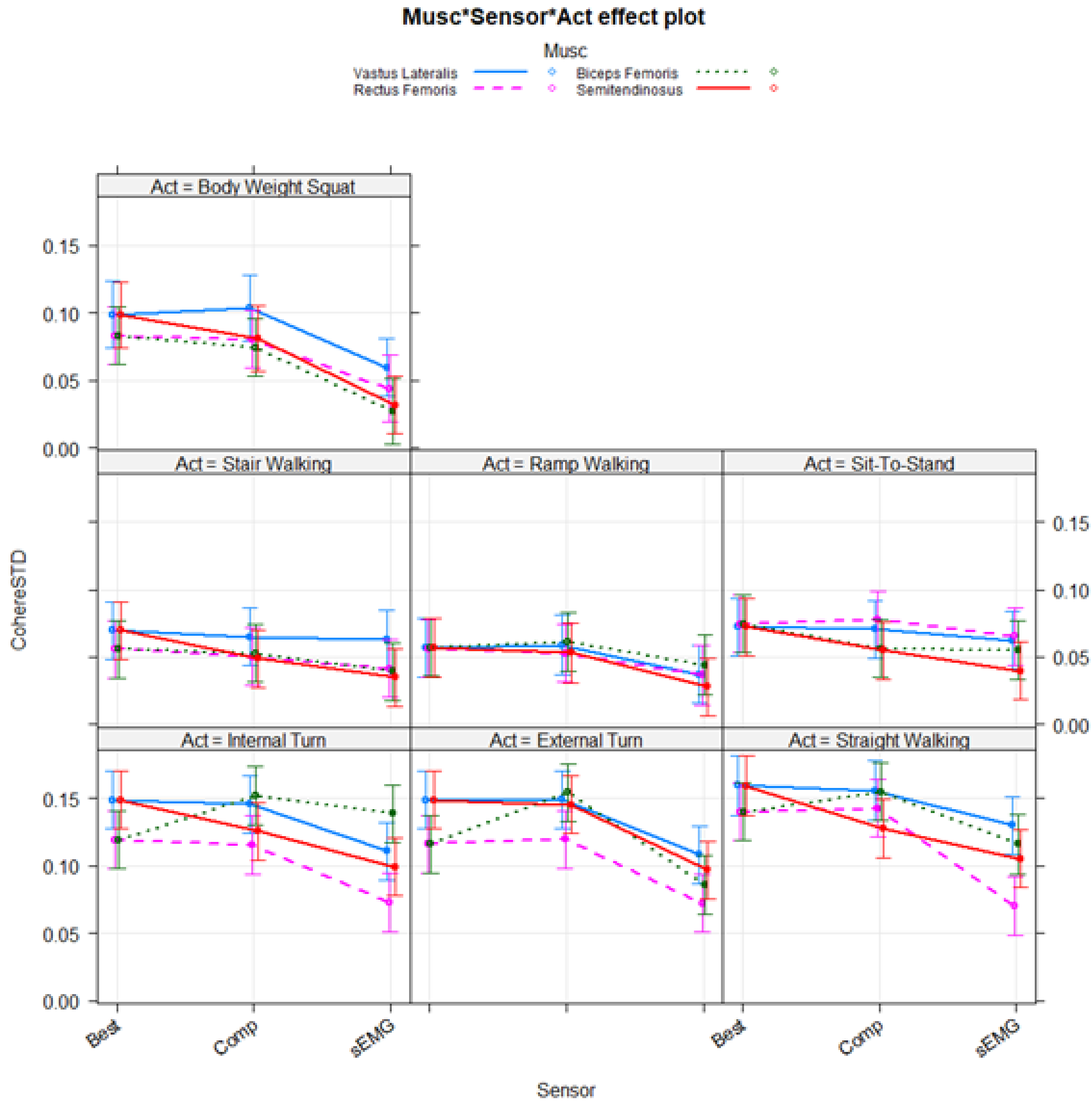

Figure 51: Effects plot for Coherence Deviation. Solid blue is Vastus Lateralis, dashed pink is Rectus Femoris, dotted green is Biceps Femoris, solid red is Semitendinosus. Best is Best Signal, Comp is Composite Signal, sEMG is traditional sEMG. Note the lower values for Traditional sEMG and higher spread between muscles for Internal Turn, External Turn, and Straight Walking (bottom row).

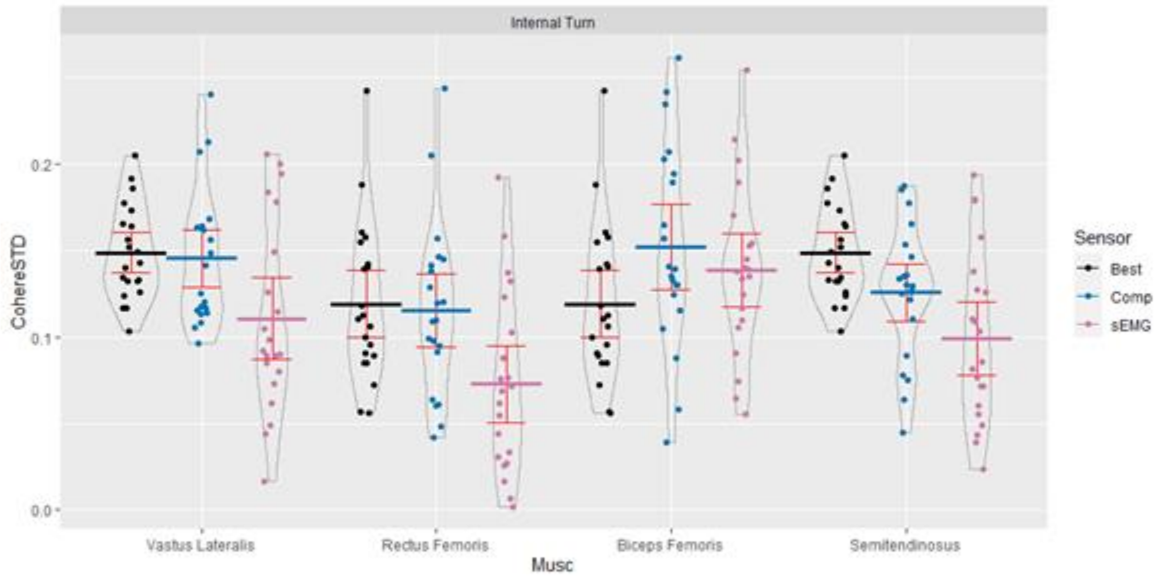

Figure 52: Violin plot of coherence standard deviation for Stair Walking. Best is Best Signal, Comp is Composite Signal, sEMG is Traditional sEMG.   Note the lower values for Traditional sEMG and the higher Composite Signal mean for Biceps Femoris (2nd from right).

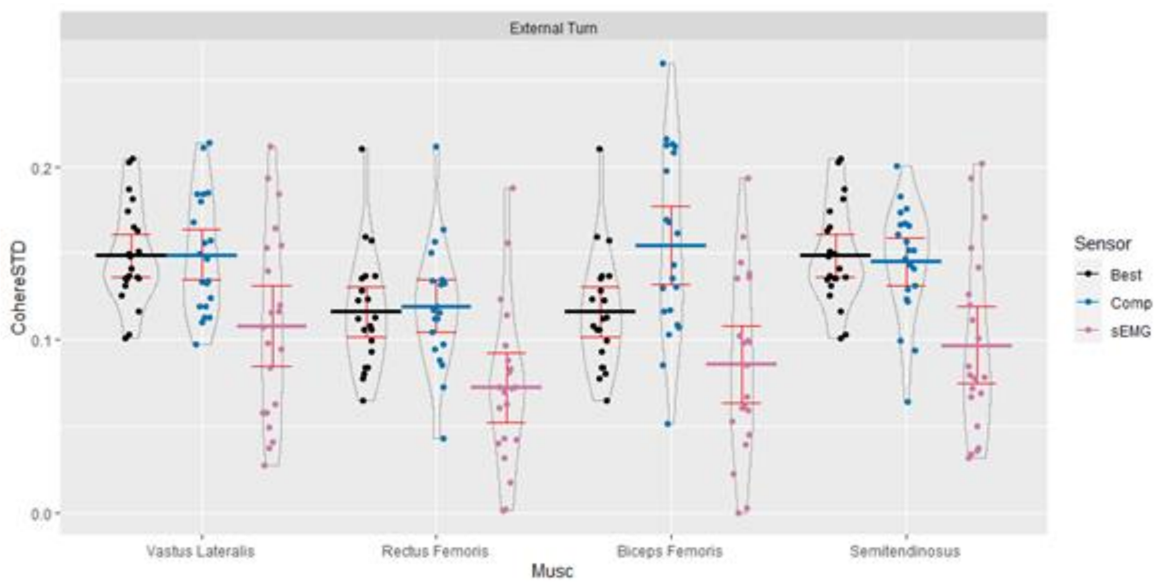

Figure 53: Violin plot of coherence standard deviation for Stair Walking. Best is Best Signal, Comp is Composite Signal, sEMG is Traditional sEMG.   Note the lower values for Traditional sEMG and the higher Composite Signal mean for Biceps Femoris (2nd from right).

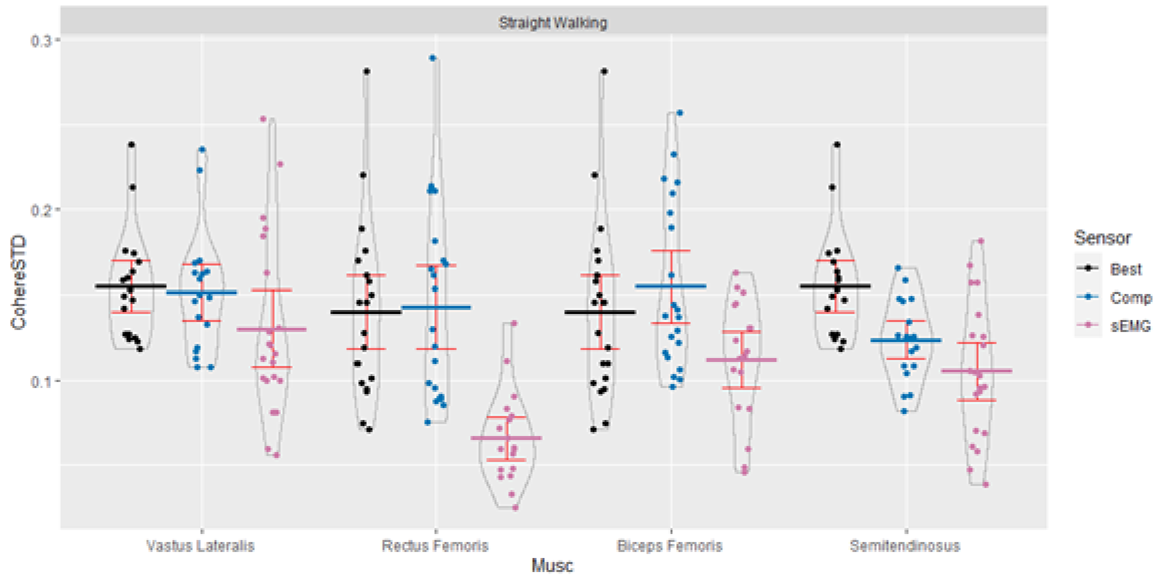

Figure 54: Violin plot of coherence standard deviation for Stair Walking. Best is Best Signal, Comp is Composite Signal, sEMG is Traditional sEMG. Note the lower values for Traditional sEMG and the higher Composite Signal mean for Biceps Femoris (2nd from right).

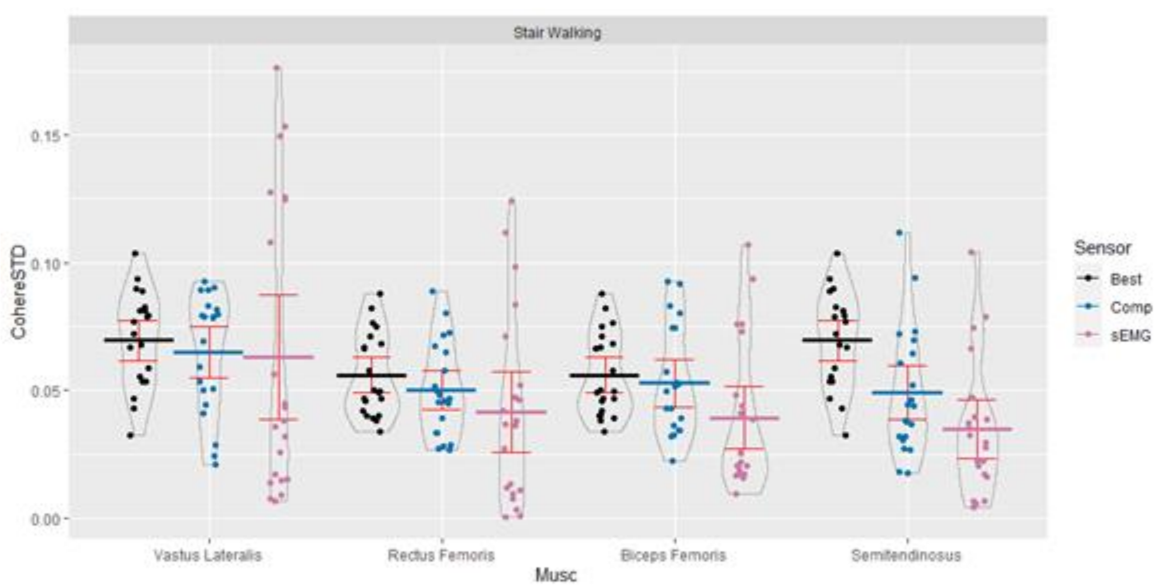

Figure 55: Violin plot of coherence standard deviation for Stair Walking. Best is Best Signal, Comp is Composite Signal, sEMG is Traditional sEMG. Note the lower values for Traditional sEMG.

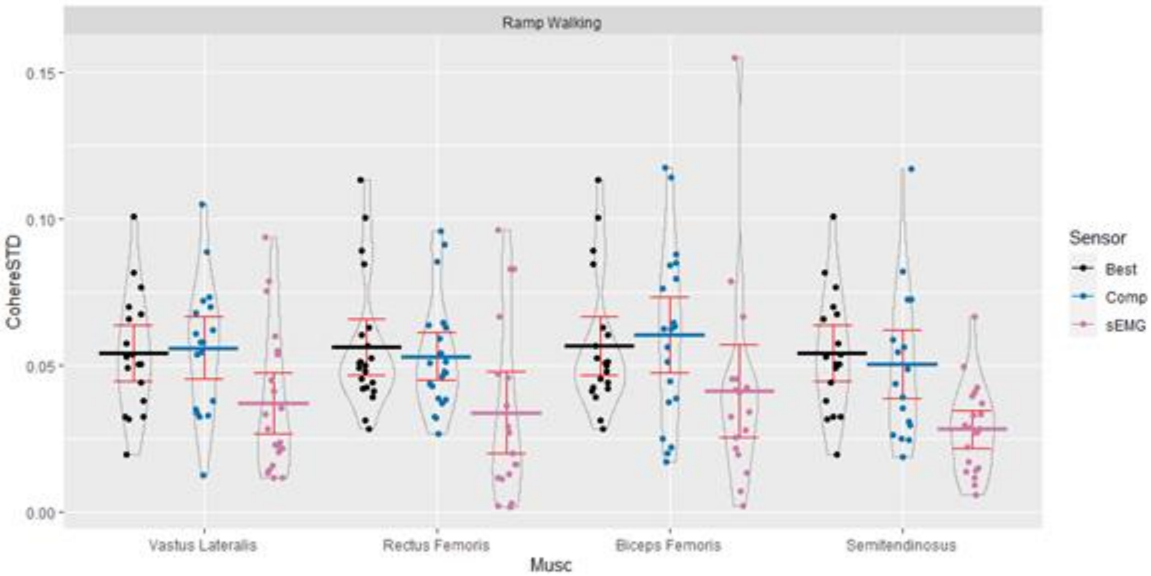

Figure 56: Violin plot of coherence standard deviation for Ramp Walking. Best is Best Signal, Comp is Composite Signal, sEMG is Traditional sEMG. Note the lower values for Traditional sEMG and the higher Composite Signal mean for Biceps Femoris (2nd from right).

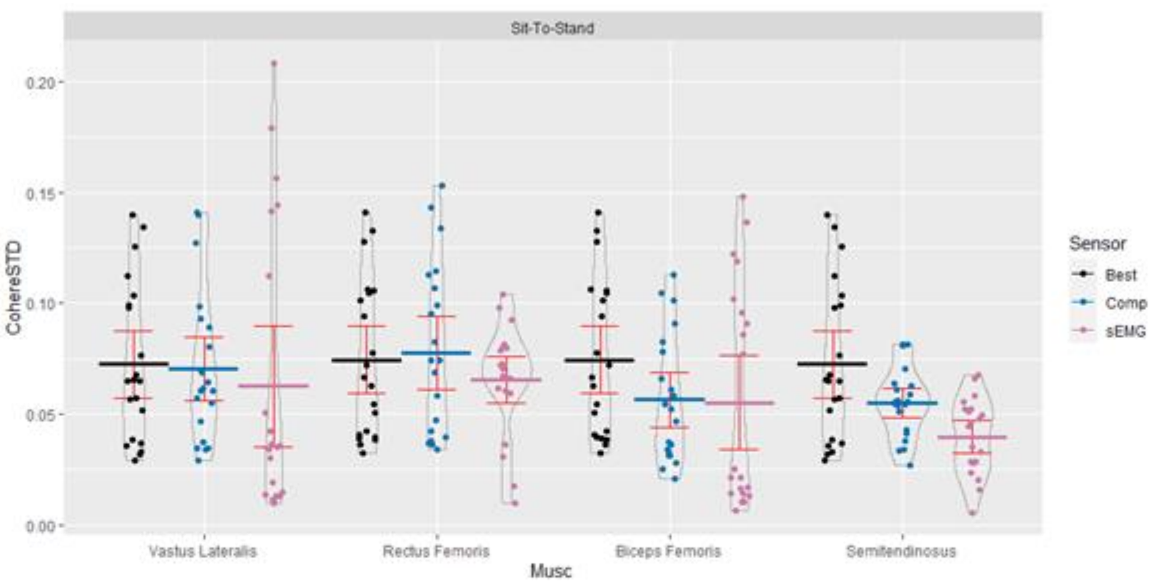

Figure 57: Violin plot of coherence standard deviation for Sit to Stand. Best is Best Signal, Comp is Composite Signal, sEMG is Traditional sEMG. Note the lower values for Traditional sEMG.

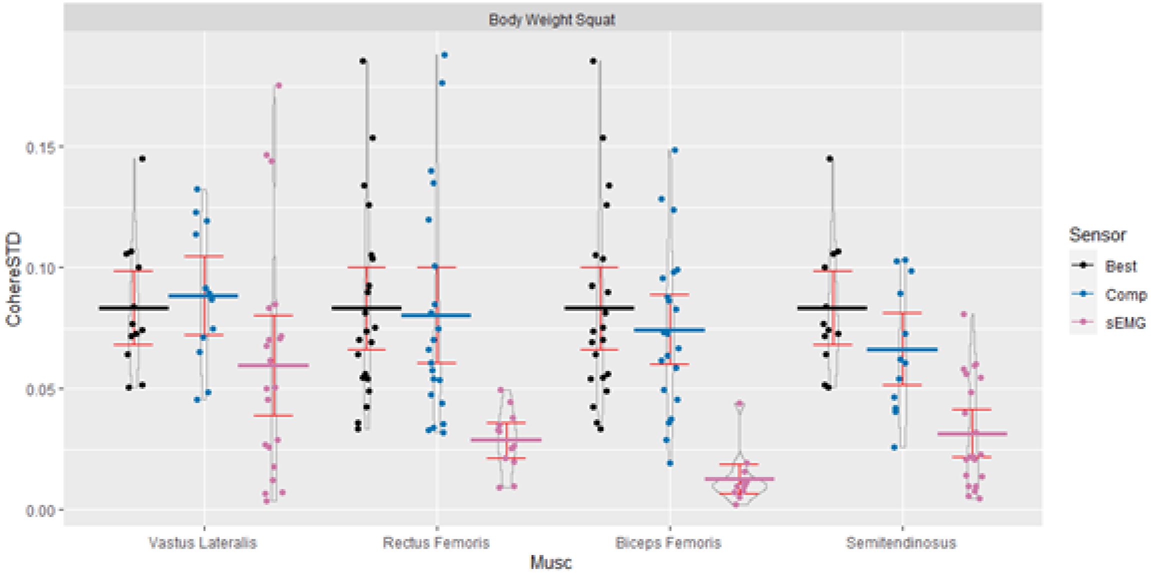

Figure 58: Violin plot of coherence standard deviation for Body Weight Squat. Best is Best Signal, Comp is Composite Signal, sEMG is Traditional sEMG. Note the lower values for Traditional sEMG.

Signal	Coherence Mean	Coherence Deviation
Best Signal	0.906 +/- 0.010	0.100 +/- 0.007
Composite Signal	0.904 +/- 0.010	0.0975 +/- 0.007
Traditional sEMG	0.941 +/- 0.010	0.0684 +/- 0.007

Table 13: Total means of coherence values and standard error

Signal	Muscle	Coherence Mean	Coherence Deviation
Best Signal	Vastus Lateralis	0.892 +/- 0.011	0.108 +/- 0.008
	Rectus Femoris	0.914 +/- 0.011	0.0922 +/- 0.008
	Biceps Femoris	0.902 +/- 0.011	0.0924 +/- 0.008
	Semitendinosus	0.918 +/- 0.011	0.108 +/- 0.008
Composite Signal	Vastus Lateralis	0.894 +/- 0.011	0.107 +/- 0.008
	Rectus Femoris	0.916 +/- 0.011	0.0912 +/- 0.008
	Biceps Femoris	0.890 +/- 0.011	0.101 +/- 0.008
	Semitendinosus	0.916 +/- 0.011	0.0910 +/- 0.008
Traditional sEMG	Vastus Lateralis	0.926 +/- 0.011	0.0816 +/- 0.008
	Rectus Femoris	0.953 +/- 0.011	0.0576 +/- 0.008
	Biceps Femoris	0.937 +/- 0.011	0.0723 +/- 0.008
	Semitendinosus	0.949 +/- 0.011	0.0622 +/- 0.008

Table 14: Means of coherence values and standard error by muscle

Signal	Activity	Coherence Mean	Coherence Deviation
Best	Internal Turn	0.870 +/- 0.013	0.134 +/- 0.009
	External Turn	0.866 +/- 0.013	0.133 +/- 0.009
	Straight Walking	0.829 +/- 0.013	0.150 +/- 0.009
	Stair Walking	0.952 +/- 0.013	0.0628 +/- 0.009
	Ramp Walking	0.951 +/- 0.013	0.0569 +/- 0.009
	Sit to Stand	0.953 +/- 0.013	0.0735 +/- 0.009
	Body Weight Squats	0.926 +/- 0.013	0.0910 +/- 0.010
Composite	Internal Turn	0.870 +/- 0.013	0.135 +/- 0.009
	External Turn	0.856 +/- 0.013	0.142 +/- 0.009
	Straight Walking	0.823 +/- 0.013	0.145 +/- 0.009
	Stair Walking	0.951 +/- 0.013	0.0543 +/- 0.009
	Ramp Walking	0.947 +/- 0.013	0.0565 +/- 0.009
	Sit to Stand	0.953 +/- 0.013	0.0649 +/- 0.009
	Body Weight Squats	0.928 +/- 0.013	0.0850 +/- 0.010
Traditional sEMG	Internal Turn	0.910 +/- 0.013	0.105 +/- 0.009
	External Turn	0.919 +/- 0.013	0.0908 +/- 0.009
	Straight Walking	0.891 +/- 0.013	0.105 +/- 0.009
	Stair Walking	0.966 +/- 0.013	0.0448 +/- 0.009
	Ramp Walking	0.968 +/- 0.013	0.0364 +/- 0.009
	Sit to Stand	0.962 +/- 0.013	0.0557 +/- 0.009
	Body Weight Squats	0.973 +/- 0.013	0.0405 +/- 0.010

Table 15: Mean coherence values and standard error by activity

DISCUSSION AND CONCLUSIONS

The purpose of this Thesis was to 1: quantify signal quality differences between HDsEMG and traditional sEMG, 2: quantify signal variations during non-optimal placement for HDsEMG and traditional sEMG, and 3: identify effective processing methods when using HDsEMG signals for prosthesis control. An experimental study with human participants was performed to collect sEMG data using both single channel Traditional sEMG sensors and 16 channel HDsEMG sensors from four leg muscles (Vastus Lateralis, Rectus Femoris, Biceps Femoris, Semitendinosus) across seven different activities of daily living (Internal Turning, External Turning, Straight Walking, Ramp Walking, Stair Walking, Sit to Stand, and Body Weight Squats). Three different signals were created from HDsEMG data: an individual channel with the highest signal to noise ratio (Best Signal), a time series mean of all HDsEMG channels (Composite Signal), and a time series mean of all HDsEMG channels with a signal to noise ratio greater than 2 dB (Threshold Signal). The Threshold signal was found to be the same as the Composite Signal, so quality and similarity measures were only analyzed for the Composite Signal.

Aim 1: Quantify signal quality differences between HDsEMG and traditional sEMG

The hypothesis was that HDsEMG-derived signals would produce higher quality through increased SNR, RMS, and DP values while producing lower Ω values. The mean SNR values including all muscles and activities was 12.6 +/- 2.5 dB for Best Signal, 10.3 +/- 2.6 dB for Composite Signal, and 5.0 +/- 2.0 dB for traditional sEMG, all in optimal positions ($p<0.01$). Most works focusing on SNR use artificial signals with known noise contents, and little work has been done on HDsEMG SNR values. Both HDsEMG-derived signals had SNR values over twice the SNR value of the traditional sEMG sensors, indicating that HDsEMG-derived signals have less noise than sEMG signals. A value of 10 dB has been presented as the threshold at which a signal can be considered free of major sources of noise[61], and a value of 2 dB as the point where a signal is considered unusable due to excess noise. Both the specific muscle and activity type had significant impact on the SNR and RMS values (both, $p<0.01$). SNR values for Rectus Femoris (10.57-12.52 dB) and Vastus Lateralis (12.4-14.8 dB) were higher for the optimally placed HDsEMG-derived signals than for traditional sEMG signals (7.38-11.74 dB). Simulated signals are created on a band of 5-30 dB SNR[68], and clinical measurements have reported values between 2 and 40 dB for sEMG[69,70]. Thus, Traditional sEMG presents values on the low end of expected values, and HDsEMG-derived signals presented values in the middle range. Therefore, HDsEMG, particularly Best Signal, presents better SNR values than Traditional sEMG.

Root mean squared averages, a measure of signal strength for optimally placed signals was 0.0192 +/- 0.0110 for Best Signals, 0.0213 +/- 0.0139 for Composite Signals, and 0.0387 +/- 0.0148 for traditional sEMG. These values were reported with regard to the maximum individual electrode reading across all activities and trials for the given muscle. Traditional sEMG sensors displayed higher signal strength with regard to peak recorded values, making the features used in feature detection more prominent[17,18]. The Vastus Lateralis displayed HDsEMG-derived RMS than other muscles at 0.036. Therefore, Traditional sEMG presents one advantage over HDsEMG.

DP values were $8.44*10^2$ +/- $1.21*10^3$ dB for Best Signals, $1.00*10^3$ +/- $1.22*10^3$ dB for Composite Signals, and $1.10*10^4$ +/- $1.36*10^4$ dB for traditional sEMG sensors ($p<0.01$), all optimally placed. The cutoff for DP was 30 dB[61], denoting signal power was sufficiently peaked over noise. Higher values than expected were seen due to the averaging process being sensitive to low values. While DP did not produce values of the expected magnitude, the fact that they were large places them over the 30 dB cutoff, meaning all signals peaked in power to a desired level.

Ω values indicate signal symmetry and the presence of high frequency noise. Total averaged Ω values were 2.03 +/- 0.05 for optimally placed Best Signals, 2.07 +/- 0.05 for optimally placed Composite Signals, and 2.1 +/- 0.08 for optimally placed traditional sEMG sensors ($p<0.01$). The cutoff for Ω values given for a simulated diaphragm EMG system was 1.4[62], values over which contained high frequency noise. Collected Ω values were greater than this desired level, but little work has been done for Ω values in other muscles leaving the cutoff unknown. Further work is desired, but HDsEMG presents Ω values denoting less noise content than Traditional sEMG.

With regards to activities, Stair Walking, Ramp Walking, Sit to Stand, and Body Weight Squats displayed higher SNR values, consistently displaying over 9.8 dB in the optimal position for Composite Signals and over 12 dB for Best Signals. Straight walking, internal turning, and external turning SNR values were less than 9.5 dB for Composite Signals and less than 10.5 dB for Best Signals.

The first hypothesis is partially confirmed. HD-derived signals displayed higher SNR values to a great degree, confirming that the baseline quality and noise were less than traditional sEMG signals. A slightly lower Ω value matched the hypothesis, but the values of Ω were greater than the theoretical cutoff for all signals. The higher signal strength in traditional sEMG signals did not match the initial hypothesis for signal quality. Thus, HDsEMG sensors present signals with less noise, but traditional sEMG sensors generate stronger signals after processing. The cleaner HDsEMG signal will lead to increased accuracy in classification of features during prosthesis control, as the desired features will not be distorted by extra noise. Having stronger features due to a higher signal strength means the control system will notice them with more ease, but if they are distorted the signal could be misclassified.

Aim 2: Quantify signal variations during non-optimal placement for HDsEMG and traditional sEMG

It was predicted that the three HDsEMG-derived signals would display less change in quality when displaced. Displacement alone had no effect on any metric, with $p>0.05$ for SNR, RMS, DP, and Ω. Displacement did show significance when interacting with other factors, including muscle, activity, and signal type ($p<0.05$). Sensor displacement resulted in decreased SNR levels for the HDsEMG-derived signals, with the Best Signal decreasing from 12.6 dB to 11.8 +/- 2.9 dB and the Composite Signal decreasing from 10.3 dB to 9.4 +/- 2.9 dB. The traditional sEMG SNR values increased from 5.0 to 5.3 +/- 1.9 dB. Displacement alone was not a significant factor ($p=0.27$) but interacted with signal type ($p<0.01$). Even with this increase in SNR for traditional sEMG and the decrease in SNR for the HDsEMG-derived sensors, the HDsEMG-derived sensors still had lower levels of noise before processing. The Best Signal was able to remain above the 10 dB level, retaining the status of being functionally noise free, unlike the Composite Signal, which dropped below the 10 dB level. RMS values increased with displacement for all signal types, with the Best Signal going from 0.0192 to 0.0251 +/- 0.0136, Composite going from 0.0213 to 0.0243 +/- 0.0149, and traditional sEMG going from 0.0378 to

0.0387 +/- 0.0167. This was not significant based on displacement alone ($p=0.82$) but on interactions between displacement and muscle ($p<0.01$), signal type ($p<0.01$), a three-way interaction between displacement, signal type, and muscle ($p<0.01$), and a combination of all four factors ($p=0.02$). Generally, an increase in RMS is considered good, as that denotes an increase in signal strength. However, an increase in RMS coupled with a decrease in SNR means that the higher average magnitude is coming from extra noise in areas with low amplitudes. DP values trended to decrease with displacement, with Best Signal going from $8.44*10^2$ dB to $3.47*10^2$ +/- $1.23*10^3$ dB, Composite Signal going from $1.00*10^3$ dB to $3.1*10^2$ +/- 840 dB, and traditional sEMG going from $1.10*10^4$ dB to $4.26*10^3$ +/- $4.15*10^3$ dB. However, it was not found to be statistically significant based on displacement alone ($p=0.09$), but based on interactions with the signal type ($p<0.01$) and a three-way interaction with muscle and signal type ($p<0.01$). This means that the increase in RMS is not due to an increase in high amplitude signal, but due to an increase in persistent low amplitude noise throughout the recorded signal. This noise deforms the signal, making the resulting features deviate from the expected form for intent detection. Therefore, while general trends can be determined for displacement, the exact degree of quality change, and whether it is significant, depends on the muscle and activity considered.

Besides changes in quality, crosstalk must be considered. Crosstalk operates on the same frequencies as the intended muscles and can persist through filtering. To detect crosstalk, the similarity between the optimally placed sensors (low probability of crosstalk) and the displaced sensors (high probability of crosstalk) was calculated as a proxy measurement. Due to a lack of specific papers focusing on similarity between displaced EMG signals, general signal similarity measures were used. The majority of cross correlation and cross covariance measurements displayed phase lag values of 0, with a few outliers displaying values of -1. A value of 0 means that the signals did not have to be shifted to achieve maximum similarity, and a value of -1 only denotes minor shifting. The fact that both methods agreed confirms the irrelevance of phase lag[62,63]. Because of this, compositing methods or multiple channel analysis methods do not have to correct for the presence of phase lag, leading to simpler and faster models.

Mean squared coherence measures similarity in the frequency domain. If no crosstalk is present, then the signals should have greater similarity, while if crosstalk is present then the signals will not be as similar. Similarity is also desired as the more similar two signals are, the greater chance that the control program will categorize them in the same manner and respond with the same methods. This measurement was simplified to coherence mean and coherence deviation. Coherence mean represents the mean of all calculated mean squared coherence values across the entire frequency domain. Coherence deviation is the standard deviation of that mean. The coherence means +/- coherence deviations for all activities and muscles were 0.906+/-0.100 for Best Signals, 0.904+/-0.098 for Composite Signals, and 0.941+/-0.068 for Traditional sEMG ($p<0.01$). The mean similarities between all signals were greater than 90%, with the lowest possible value within the standard deviation being 80%. This high level of similarity is expected, due to lower levels of signal change seen with displacement for other muscles. More research needs to be done to determine the optimum similarity level needed for a control system to consistently recognize the desired features. The difference between the two types of sensors is just above 0.03, or 3% in the favor of the traditional sEMG sensors. Applying this standard deviation to the coherence means, the majority of frequency coherence values for the Best Signal are located between 0.8 and 1.0, Composite Signals are located between 0.8 and 1.0, and traditional sEMGs are between 0.87 and 1.0. Thus, traditional sEMG presents a closer grouping of frequency similarities at a higher mean, denoting higher similarity overall. However, the HDsEMG-derived signals were over 80% similar in the frequency space. Similarity can drop due to the presence of random noise and inherent variation in human movement, so a similarity value of less than 1 is to be expected.

Activity had a significant impact on the coherence values ($p<0.01$). The coherence means for Internal Turning, External Turning, and Straight Walking were 0.87 at highest for Best and Composite Signals and 0.919 at highest for the traditional sEMG signal. This should be compared to the lowest value of 0.926 for the other activities seen in Best and Composite Signals, and the lowest value of 0.962 for traditional sEMG. The three activities with lower coherence means displayed higher deviations, with the lowest HD-derived signal deviation being 0.132 compared to the highest of the other activities being 0.091, and the lowest of the three activities being 0.091 for the traditional sEMG signal, with the highest of the other four being 0.055. Thus, straight walking, internal turning, and external turning display both lower overall coherence levels and higher variation in original coherence values. A control system would need to accept a wider degree of signal variance to accurately predict these activities. Muscle significantly interacted with activity for coherence ($p<0.01$). All muscles except one maintained similar coherence means between Best Signal and Composite Signal. The Biceps Femoris displayed lower coherence values when composited, dropping from 0.901 to 0.890 on average, with notable drops seen in the straight walking (0.812 to 0.795), external turn (0.843 to 0.812), and internal turn trials (0.845 to 0.835). This means that the Biceps Femoris muscle can be more prone to interference due to crosstalk for certain activities.

The second hypothesis was disproven. While HDsEMG-derived signals display better quality measures after displacement, it is caused by the initial lack of noise instead of mitigating an increase in noise. Traditional sEMG signals were able to maintain higher similarity values compared HDsEMG derived signals when displaced. Both crosstalk and signal variance were affected by muscle and activity, with straight walking and internal/external turns displaying lower coherence values.

Aim 3: Identify effective processing methods when using HDsEMG signals for prosthesis control

Control systems look for various features from their inputs. The analysis methods can range from amplitude-based feature detection[71] to fractal vector analysis[72]. Thus, the input signals need to be free from distortion and have clear, consistent changes related to the activity. Three different HDsEMG-derived signals were created. The hypothesis was that the Threshold Signal would present a higher quality signal with less crosstalk than Composite and Best Signals and that the Best Signal would present the least quality of the HDsEMG-derived signals. The majority of HDsEMG papers focus on differences in content between individual electrodes, instead of analyzing a combined HDsEMG signal.

Threshold Signal

When Composite and Threshold Signals were compared, the quality outputs were the same, with only minor differences. This means that the resulting signals were the same, which was not expected. The 2 dB threshold was set too low meaning that all HDsEMG signals were not overwhelmed by noise. Thresholding at this level is not relevant for prosthesis control. The computational power can be saved for more accurate control measures or more comprehensive signal combination processes.

<u>Best Signal</u>

The best signal presented the highest SNR values, with an optimal average value of 12.6 dB. The high SNR values were to be expected, as SNR was the selection criteria. This value decreased by less than 1 dB when displaced, maintaining high SNR. These values fall within the range expected for sEMG sensors[69,70] and are above the 10 dB threshold. RMS changed when displaced by 0.006, moving form 0.019 +/- 0.011 to 0.025 +/- 0.014 which was the highest change of the three analyzed channels. Ω values were the lowest of the three analyzed signal types, with an optimal value of 2.03, above the 1.4 threshold but consistent with all experimental readings. This increased to 2.04 with displacement, alongside the decrease in SNR showing an increase in high frequency noise with displacement. The overall coherence mean was 0.906, with a standard deviation of 0.100, denoting coherence greater than 80% after displacement. The Best Signal creates a signal with a high level of quality and a low level of noise.

<u>Composite Signal</u>

The Composite Signal displayed lower SNR values than the Best Signal, with an optimal placement mean of 10.3 dB and a displaced mean of 9.4 dB ($p<0.01$). This means that the Composite Signal creation process allows more noise into the signal, dipping slightly below the 10 dB threshold, but still in the low end of the expected range. The time mean process did not account for individual noise, so extra noise could have entered through multiple noisy channels.

However, the decrease of 0.8 dB was similar to the Best Signal decrease of the same amount. This means that displacement introduces a constant amount of noise into the HDsEMG signal. However, these values fall within the range expected for sEMG sensors, even with the decrease. Ω in the Composite Signal decreased with displacement dropping from 2.071 to 2.066, still above the threshold but in line with the other readings in this experiment. The coherence mean was 0.904 with a deviation of 0.097. The compositing process used can mitigate the effects of one or a few individual signals but allowed in extra noise.

The hypothesis was disproven due to Threshold Signal presenting the same values as the Composite Signal, and the Composite Signal presenting less quality than the Best Signal. If compositing methods are to be used, they need to be more comprehensive than time series mean processing.

Conclusion

HDsEMG presents signals with less noise than traditional sEMG, but traditional sEMG signals have higher relative signal strength. The initially high signal quality means that signal degradation due to displacement, while still present, has comparatively less effect on HDsEMG sensors than traditional sEMG sensors. HDsEMG channels have the potential to be combined to produce better signals, but more advanced methods are needed than those presented here. Traditional sEMG sensors were able to preserve the original signal more than HDsEMG sensors when displaced, but specific activity and motion had more of an impact on signal similarity than sensor type alone. Muscle selection affects the quality of the resulting data, with knee extensors, and the Rectus Femoris in general presenting higher quality data. Therefore, future research on HDsEMG based control methods should focus on creating new methods of combining the 16 channels and using the extensors, particularly the Rectus Femoris, for intent detection. If flexors are used, the Biceps Femoris should be avoided due to the potential for crosstalk when displaced. HDsEMG presents a method to get a more usable signal, but further experimentation with processing methods is needed to determine the full potential of this technology.

FUTURE WORK

Thresholding Methods

The thresholding method used in this project was simple, removing any channel that SNR values less than 2 dB. However, that did not prove to be adequate, as the threshold signal output was the same as the straight composite signal output. Different methods of setting the threshold should be considered, as removing low quality channels can improve the resulting composite signal.

One of the ways to improve thresholding would be to raise the SNR level. Because HDsEMG sensors have 16 channels, stricter quality measures can be used. A signal with an SNR value greater than 10 dB can be considered free of major sources of noise, which presents an intuitive level to set the SNR threshold.

Another method of creating a better threshold would be to include other criteria. The already presented quality measurements would make good candidates for inclusion, particularly if one specific source of noise is leading to corruption. The relative weight of each factor presents in the signal would need to be considered. Muscle-specific or device-specific thresholding methods could be created to improve accuracy.

Another method of thresholding is comparing the similarity of each incoming signal and removing those that display less similarity to the total group. This would work well for local detachments, individual motion artifacts, or bursts of noise. However, if the entire sensor is displaced, this method would fail. Testing to see the displacement needed to result in signal loss for the majority of channels needs to be accomplished.

The more complex a thresholding system gets, the more computationally intensive it is compared to simpler systems. Prosthesis control must function in real time, presenting a limit to how sophisticated this system can be. A cost-benefit analysis must be considered for future threshold work.

Compositing Methods

Another area for improvement with HDsEMG signals is compositing methods. This study used a very basic time series mean which did not fully remove all noise. More advanced methods could create a signal with less noise. To accomplish this, the field of blind source selection should be looked at[72]. This is the method of finding the underlying signal from multiple sources when the original signal is unknown. Many different methods exist to accomplish this. Machine learning mechanisms that have been trained to combine the HDsEMG signals can be created to make more accurate composite signals. The most promising one is canonical correlation analysis. This method uses statistics and linear relationships to determine whether features are part of the underlying signal or caused by noise[74]. This method has been used to successfully remove EMG artifacts from EEG signals, proving that it is relevant to biological signal processing[75]. Another method of compositing that was discovered is beam forming. The Delay Multiply and Sum (DMAS) version of this uses an algorithm to combine signals[75]. However, this method is mostly used for image data, such as ultrasound, and is focused on distortion caused by distance, which does not seem to be much of a problem for HDsEMG. Therefore, while beam forming might provide a solution, it is best to look towards other methods of compositing. Most HDsEMG work has been focused on the differences between nearby sensor channels, and less on creating an overall composite signal, this area is open for experimentation.

However, as with thresholding, the compositing method used is restricted by time and computational power. This would be particularly true for machine learning methods, as those have to both be trained and need to work in real time. Therefore, the method chosen would need to work on a limited window of data that is constantly moving, instead of creating a pre-made composite signal. The size of that window and the speed at which the compositing happens would need to be tested for effectiveness. Like with thresholding, a cost-benefit analysis of the accuracy of the method compared with the time needed would need to be done, particularly if a thresholding process is in effect.

Other Metrics to Consider

Specific mean squared coherence frequency values could be investigated, to determine the specific frequencies causing dissimilarity. This would both show where crosstalk is happening and the specific frequencies where noise is coming from. This could improve HDsEMG filter design. Other similarity methods exist to be considered, such as wavelet coherence analysis[77]. This analysis type provides a method of time domain similarity based on magnitude squared methods in the time domain. It would be useful to use for prosthesis control, as that occurs in real time, so time-domain similarity would be more important than power-domain similarity.

Another factor to consider would be interactions between the 16 channels of the HDsEMG array. Running similarity measures on all 16 compared to each other and compared to a mean would reveal which channels are most likely to cause problems during compositing. If it is found that quality and similarity correlate to locations, then thresholding could be improved, particularly if the areas of displacement showed an increase in crosstalk. This could eventually lead to a control device being trained to recognize displacement or initial misplacement. It would help to see whether different types of noise are more prevalent in different areas and whether displacement changes the locations of that noise. Medial-lateral displacement could be considered, as well as loss of contact caused by displacement.

Testing Measures

Signal quality and similarity are irrelevant if HDsEMG is not able to run a control system. Determining cost-benefit analysis is a large part of this, but there would need to be testing to see what can be predicted. This would start with predicting what activities are being accomplished and then testing whether specific parts of those activities can be detected. This is where factors such as window length would be tested. This initial testing would start with the data collected, using the subjects and trials as a base to see if HDsEMG works as an intent detection system. If a machine learning approach is taken, then some of that data would be used as training data, and some would be used for testing. It would be of interest to determine how much each individual subject's data works with the control system and to see how much training would be needed. Eventually, amputee data would be collected and tested by the same metrics to confirm the use of the control system.

The Final Device

The final goal is to develop a prosthesis that has a control mechanism included based on HDsEMG. Because the focus of this project is the control system, a device such as the Open Source Leg can be used as a base, with the developed control system attached. Due to limited computational strength, the HDsEMG sensors would most likely be attached to knee extensors due to their higher SNR levels, but a more advanced device would have HDsEMG attached to all muscles. The control system developed in the real time testing would be loaded into the device and tested using the same metrics as the real time testing. Once this has been successful, then additional activities and movement types could be added. This provides an opportunity to see how to adapt this system to amputees' specific cases, and to determine whether the robustness holds up in multiple situations. This device is still far away, but the data collected and presented here are the first steps in that direction.

APPENDICES

APPENDIX A

MOTION CAPTURE MARKER LOCATIONS

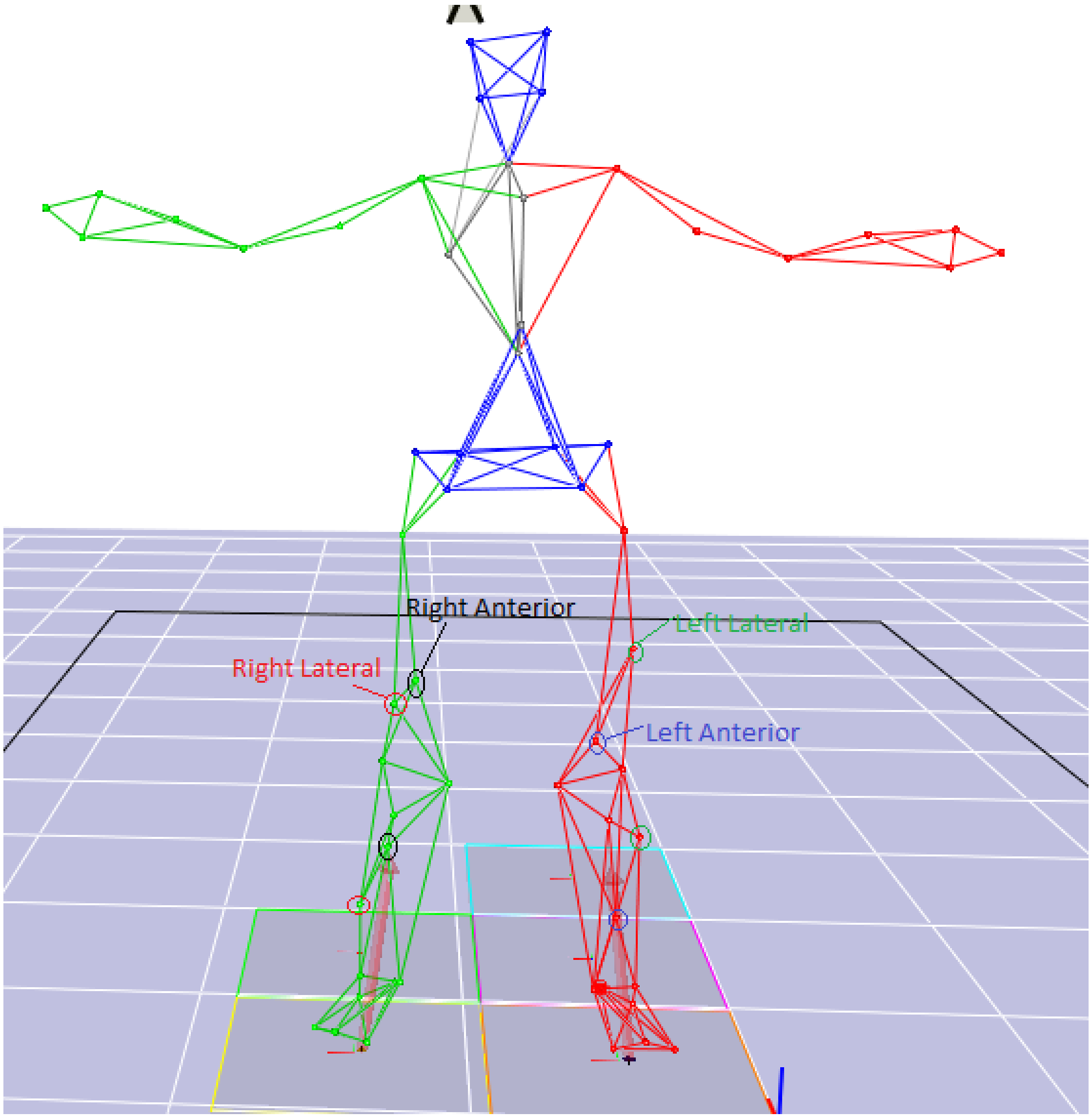

Figure 59: Skeleton created from motion capture markers. Markers were attached prior to calibration of force plates and cameras and before sEMG sensor placement. Anterior and lateral thigh and shank markers were used to determine body direction.

The following markers were added to the participants for motion capture purposes. Overall placements were based on a modified version of the plug-in gait marker setup used by Visual3D used for previous studies in the lab. No direct data was taken from motion capture for this thesis, but the data has potential to be correlated with force plate and EMG data in future studies. See earlier figure for the computer model generated in Cortex from this setup. Markers were worn for all activities and sensor conditions, and sensor location was measured first to prevent marker interference.

- RFHD - Right Forward Head, placed on headband
- LFHD - Left Forward Head, placed on headband
- LBHD - Left Behind Head, placed on headband
- RBHD - Right Behind Head, based on headband
- C7 - Vertebrae at base of back of neck
- CLAV - Clavicle, placed on bone in center of bone V
- RBAK - Right Back, midway between C7 and T10
- STRN - Sternum, at bottom of breastbone
- T10 - Vertebrae on lower back, midway down
- RSHO - Right Shoulder, on bony process on upper part
- RUPA - Right Upper Arm, midway between shoulder and elbow, on exterior side
- RELB - Right Elbow, placed on exterior point of joint
- RFRA - Right Forearm, midway between elbow and wrist, on exterior side
- RWRA - Right Wrist, on bony process. Should be pointing upwards in T pose.
- RWRB - Right Wrist, on bony process. Should be pointing downwards in T pose

- RFIN - Right Finger, placed on top of the middle knuckle
- LSHO - Left Shoulder, on bony process on upper part
- LUPA - Left Upper Arm, midway between shoulder and elbow, on exterior side
- LELB - Left Elbow, placed on exterior point of joint
- LFRA - Left Forearm, midway between elbow and wrist, on exterior side
- LWRA - Left Wrist, on bony process. Should be pointing upwards in T pose.
- LWRB - Left Wrist, on bony process. Should be pointing downwards in T pose
- LFIN - Left Finger, placed on top of the middle knuckle
- RASI - Right Front Hip, on bony curve
- LASI - Left Front Hip, opposite RASI
- LPSI - Left Back Hip, on bony protrusion near tailbone
- RPSI - Right Back Hip, across from LPSI
- RILC - Right Iliac Crest, top of hip bone on person’s side
- LILC - Left Iliac Crest, top of hip bone on person’s side
- RGTR - Right Greater Trochanter, placed on bony area where hip rotates
- RTHI - Right Thigh, on outside of thigh, placed lower than RATH
- RATH - Right Anterior Thigh, front of thigh, placed higher than RTHI
- RKNE - Right Knee, Outside
- RMFC - Right Knee, Inside
- RTTB - Right Tibial Tuberosity, placed on front, just below knee
- RLSH - Right Lateral Shank, on outside shank, lower than RASH
- RASH - Right Anterior Shank, on front of shank, higher than RLSH

- RANK - Right Ankle, Outside
- RMMA - Right Ankle, Inside
- RMT1 - Right Big Toe
- RTOE - Right Middle Toe
- RMT5 - Right Pinky Toe
- RLCC - Right Foot, below and slightly behind heel marker on lateral side
- RHEE - Right Heel, placed on back of shoe and facing backwards
- LGTR - Left Greater Trochanter, placed on bony area where hip rotates
- LTHI - Left Thigh, on outside of thigh, higher than LATH
- LATH - Left Anterior Thigh, on forward side of thigh, lower than LTHI
- LKNE - Left Knee, Outside
- LMFC - Left Knee, Inside
- LTTB - Left Tibial Tuberosity, placed on front, just below knee
- LLSH - Left Lateral Shank, outside of shank, higher than LASH
- LASH - Left Anterior Shank, front of shank, lower than LLSH
- LANK - Left Ankle, Outside
- LMMA - Left Ankle, Inside
- LMT1 - Left Big Toe
- LTOE - Left Middle Toe
- LMT5 - Left Pinky Toe
- LLCC - Left Foot, below and slightly behind heel marker on lateral side
- LHEE - Left Heel, placed on back of shoe and facing backwards

APPENDIX B

NON-LOG DATA FOR RMS AND DP

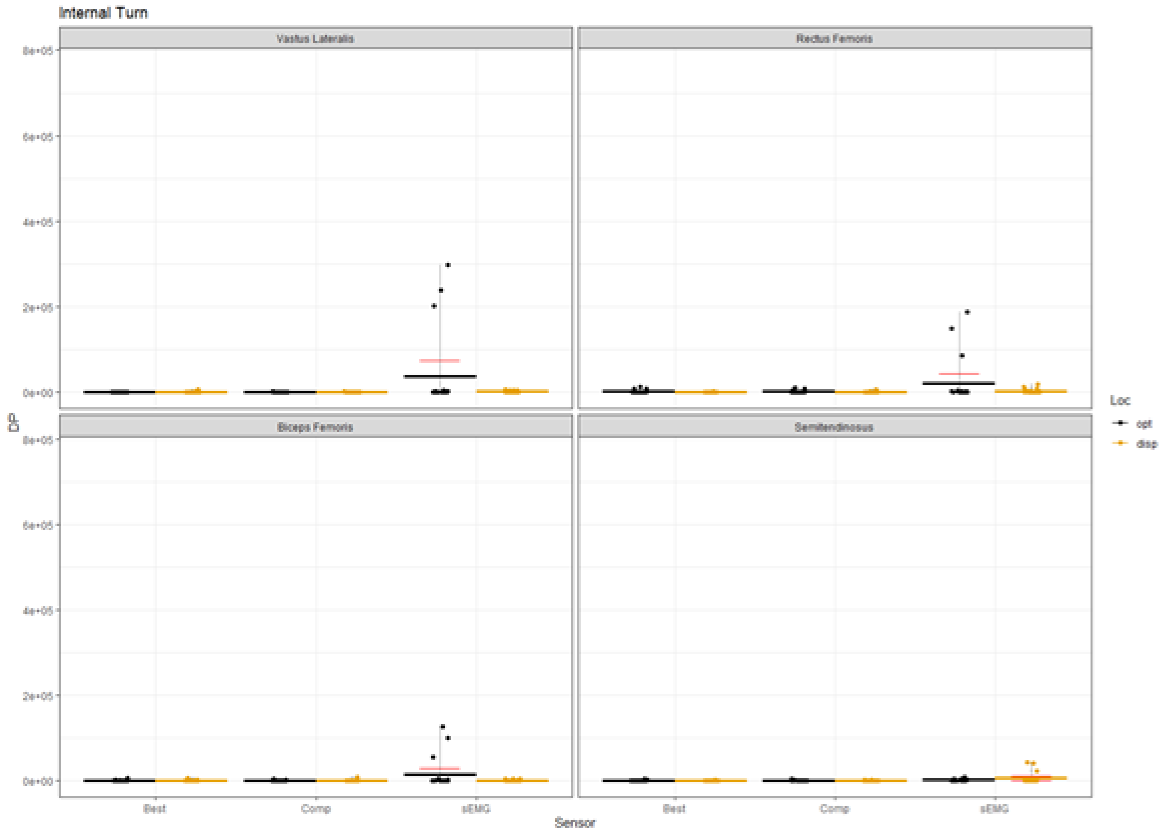

Figure 60: Violin graph of raw DP for Internal Turn. Opt is optimal placement, disp is displaced. Best (left) is Best Signal, Comp (middle) is Composite Signal, sEMG (right) is Traditional sEMG. Note presence of outliers for Vastus Lateralis (top left), Biceps Femoris (bottom left), and Rectus Femoris (top right).

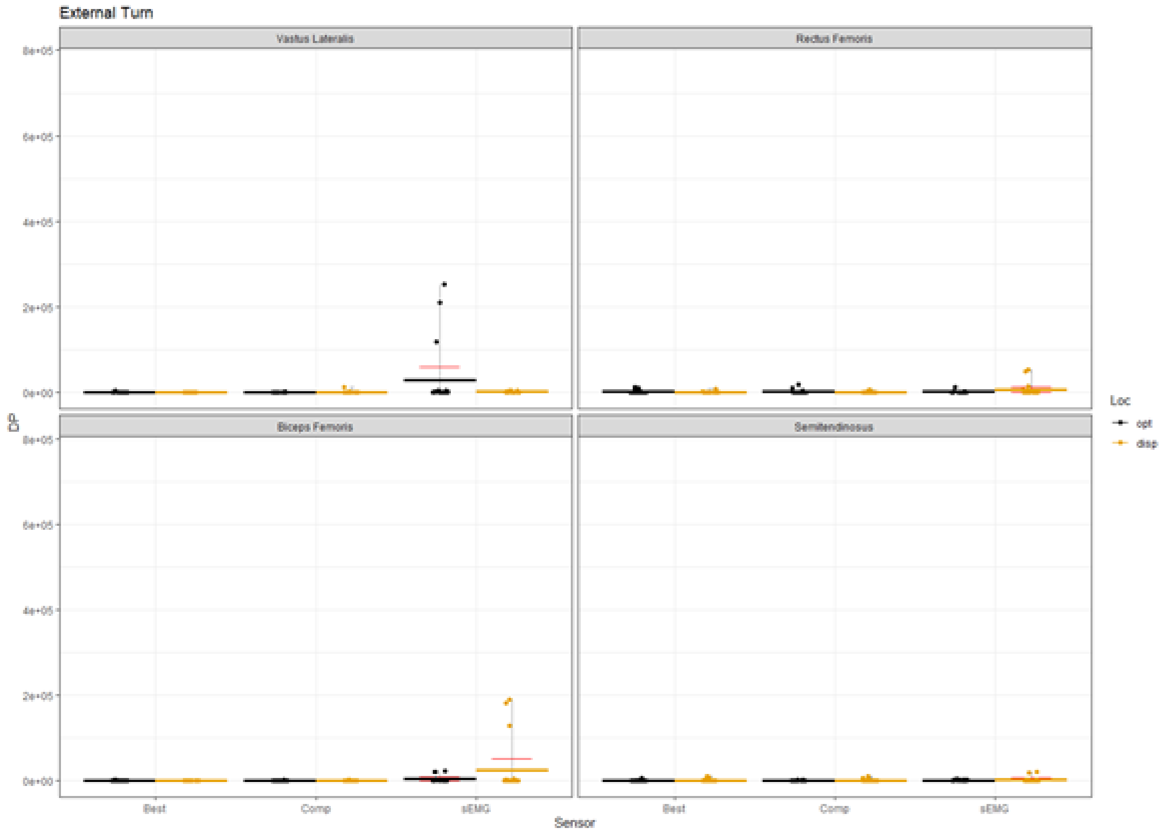

Figure 61: Violin graph of raw DP for External Turn. Opt is optimal placement, disp is displaced. Best (left) is Best Signal, Comp (middle) is Composite Signal, sEMG (right) is Traditional sEMG. Note presence of outliers for Vastus Lateralis (top left) and Biceps Femoris (bottom right).

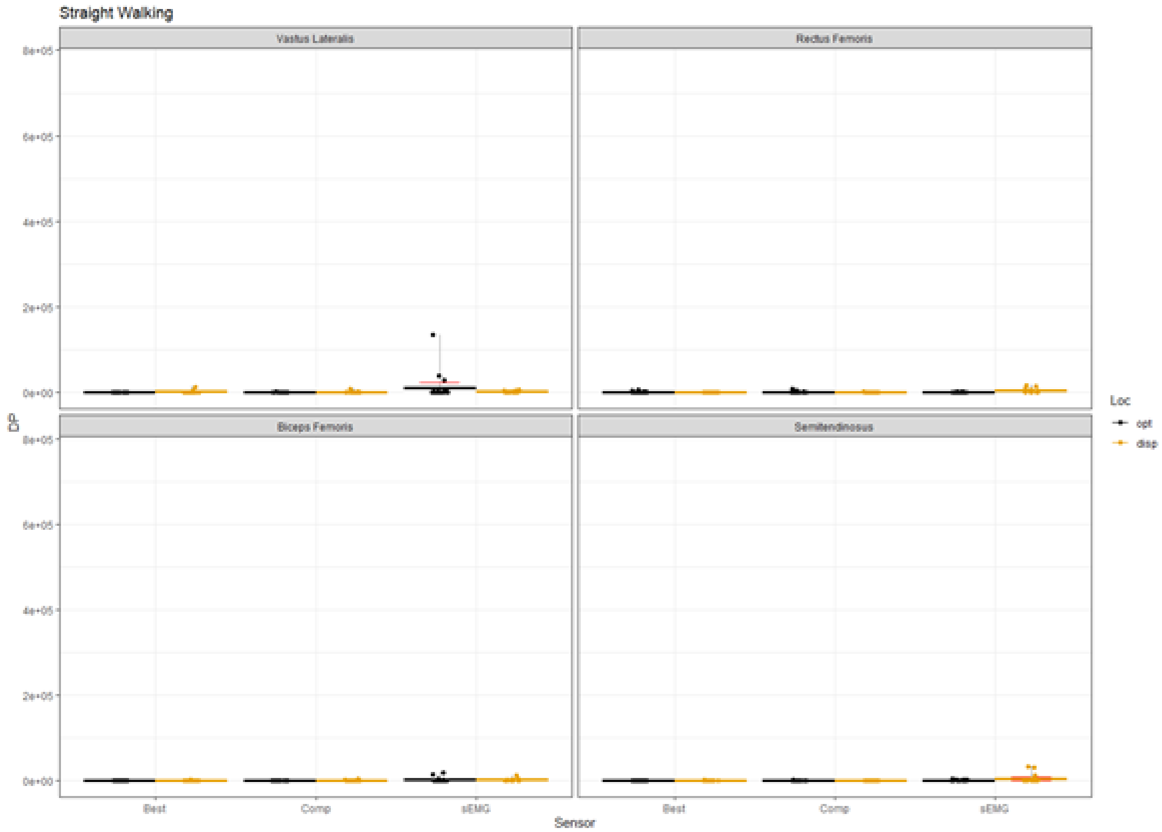

Figure 62: Violin graph of raw DP for Straight Walking. Opt is optimal placement, disp is displaced. Best (left) is Best Signal, Comp (middle) is Composite Signal, sEMG (right) is Traditional sEMG. Note presence of outliers for Vastus Lateralis (top left).

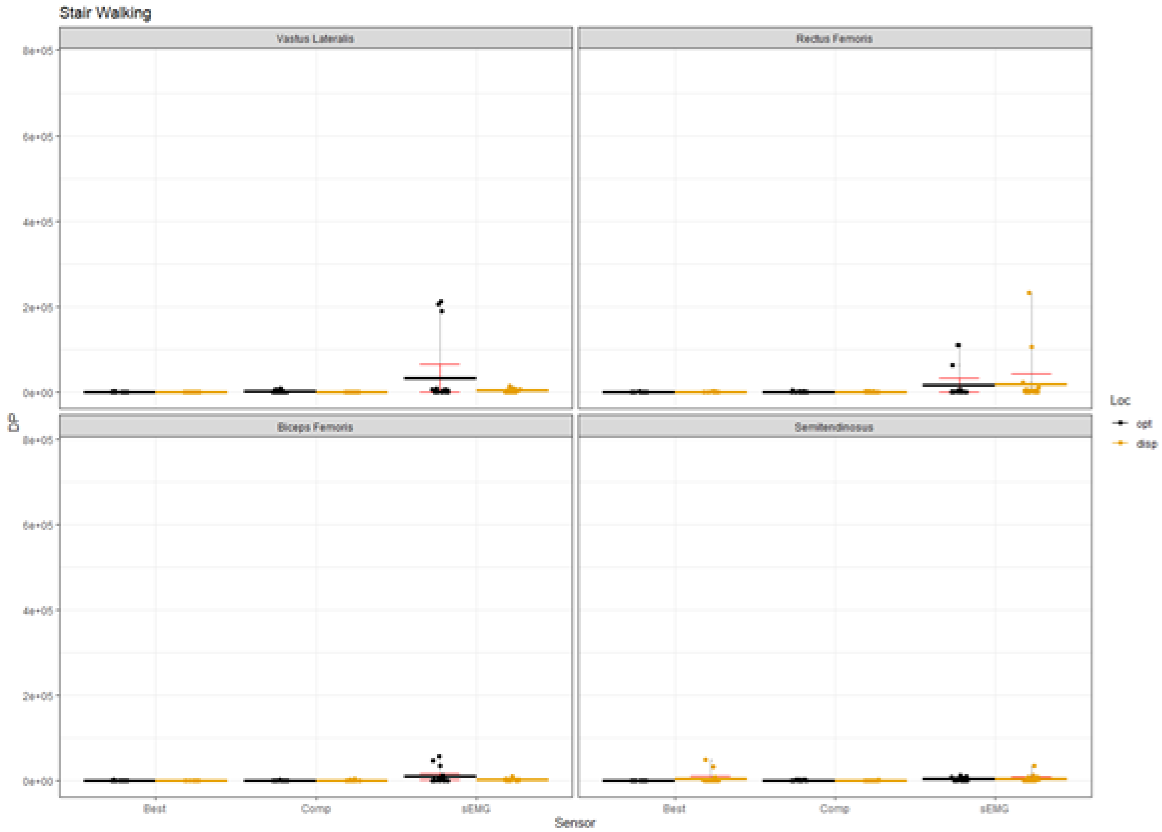

Figure 63: Violin graph of raw DP for Stair Walking. Opt is optimal placement, disp is displaced. Best (left) is Best Signal, Comp (middle) is Composite Signal, sEMG (right) is Traditional sEMG. Note presence of outliers for Vastus Lateralis (top left) and Rectus Femoris (top right).

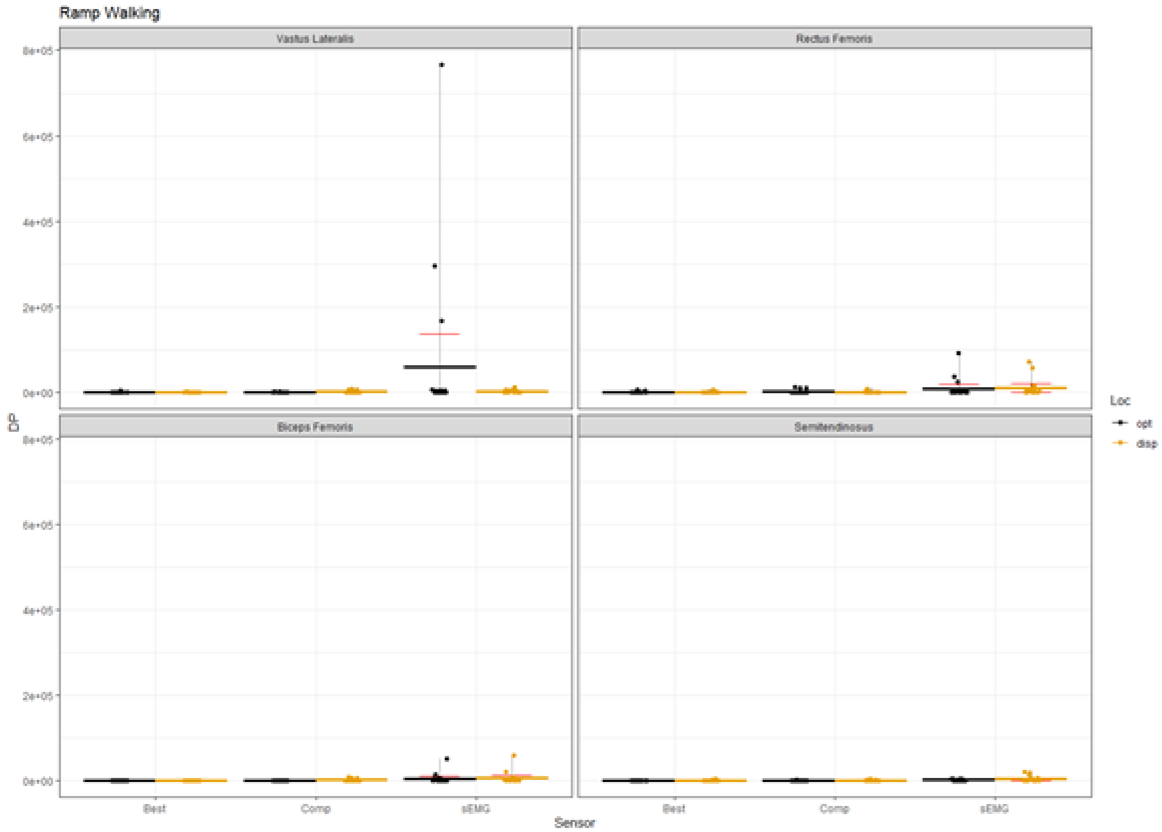

Figure 64: Violin graph of raw DP for Ramp Walking. Opt is optimal placement, disp is displaced. Best (left) is Best Signal, Comp (middle) is Composite Signal, sEMG (right) is Traditional sEMG. Note extreme outliers for Vastus Lateralis (top left).

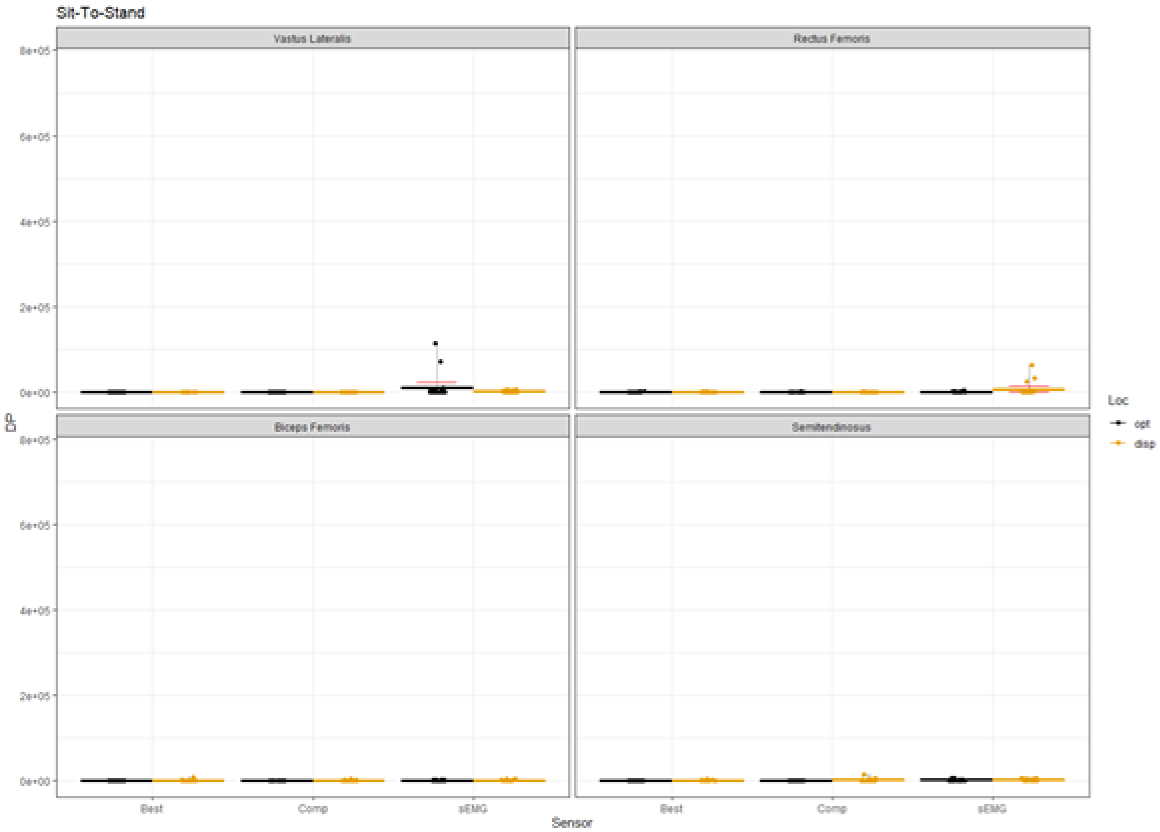

Figure 65: Violin graph of raw DP for Sit to Stand. Opt is optimal placement, disp is displaced. Best (left) is Best Signal, Comp (middle) is Composite Signal, sEMG (right) is Traditional sEMG. Note presence of outliers for Vastus Lateralis (top left) and Rectus Femoris (top right).

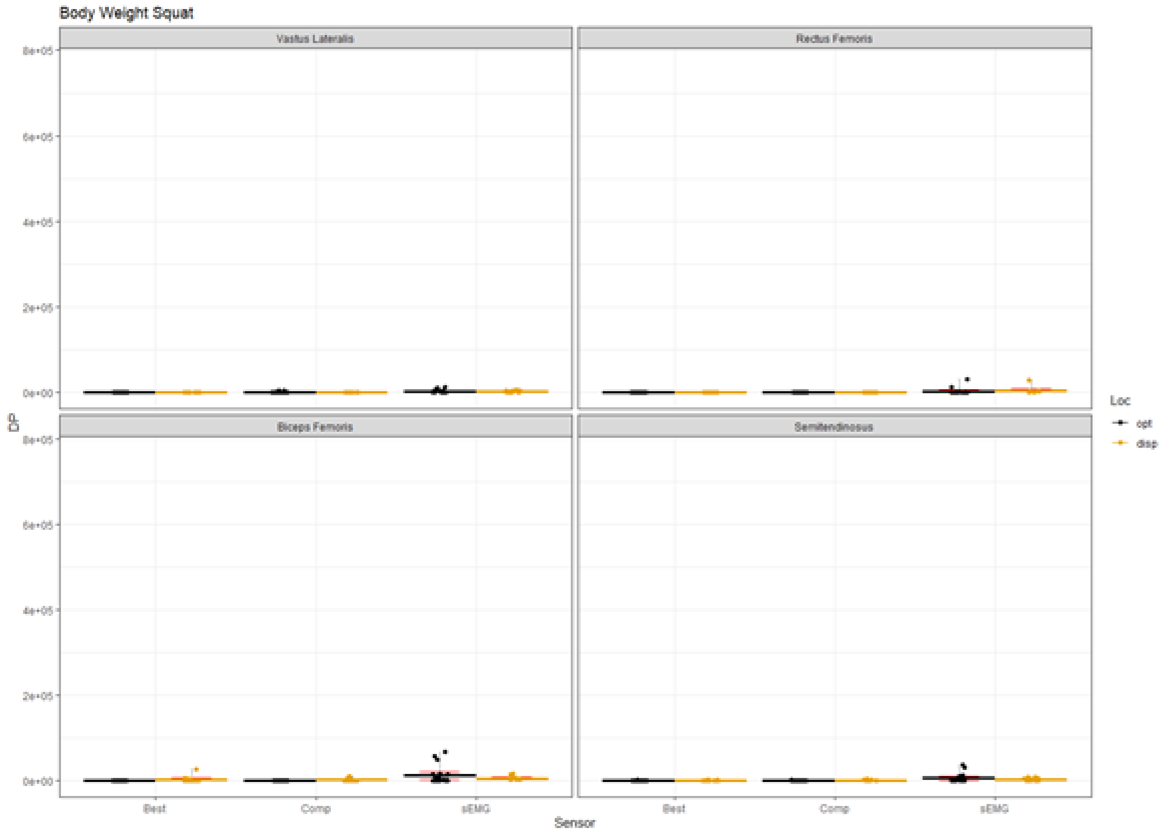

Figure 66: Violin graph of raw DP for Body Weight Squat. Opt is optimal placement, disp is displaced. Best (left) is Best Signal, Comp (middle) is Composite Signal, sEMG (right) is Traditional sEMG. Outliers are not as pronounced for this activity.

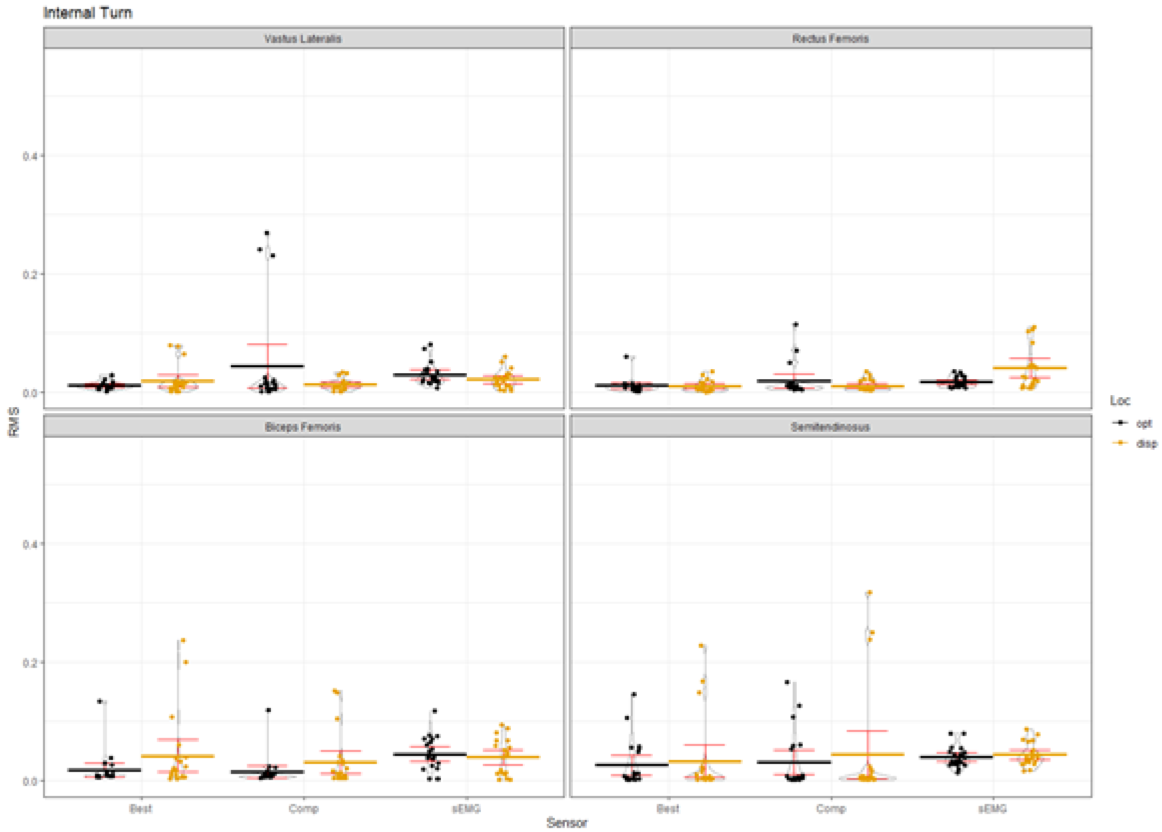

Figure 67: Violin graph of raw RMS (Root Mean Squared) for Body Weight Squats. Opt is optimal placement, disp is displaced. Best (left) is Best Signal, Comp (middle) is Composite Signal, sEMG (right) is Traditional sEMG. Note extra outliers in various conditions.

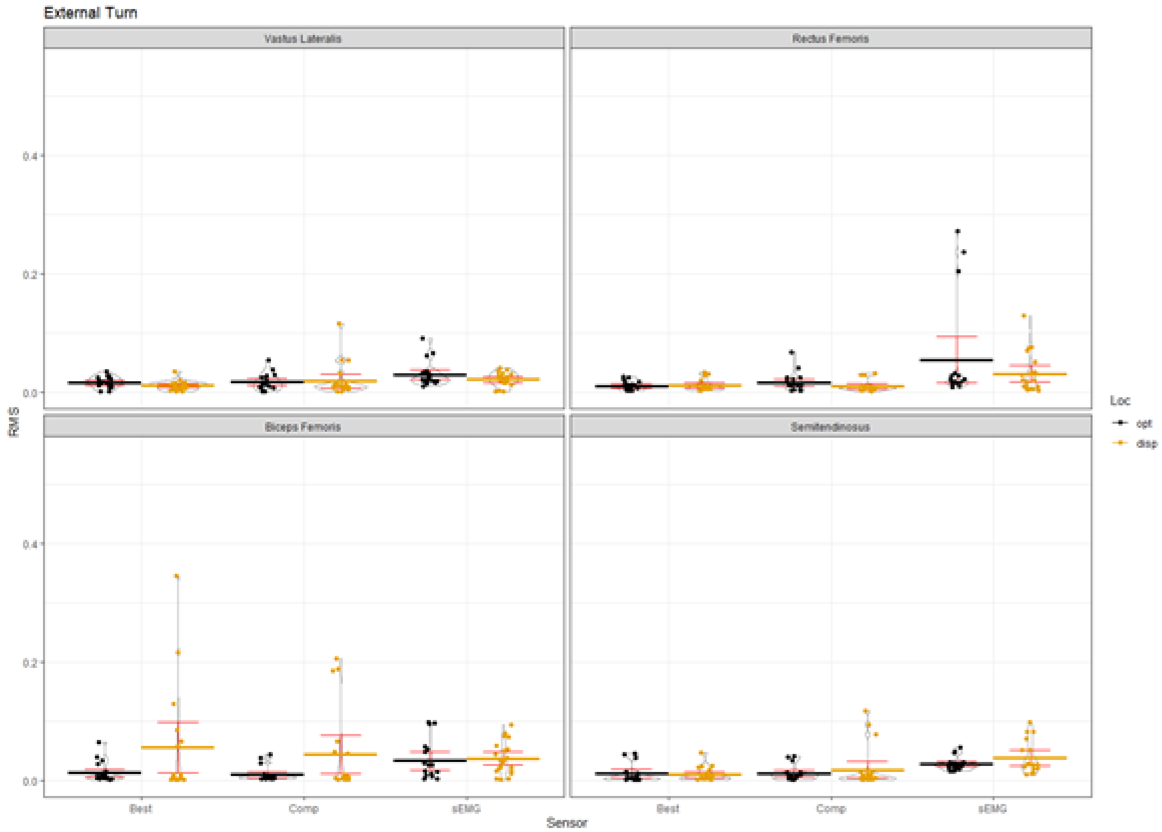

Figure 68: Violin graph of raw RMS (Root Mean Squared) for Body Weight Squats. Opt is optimal placement, disp is displaced. Best (left) is Best Signal, Comp (middle) is Composite Signal, sEMG (right) is Traditional sEMG. Note differences in spread between muscles and sensors, particularly for displaced Best and Comp for Biceps Femoris (bottom left) and Semitendinosus (bottom right).

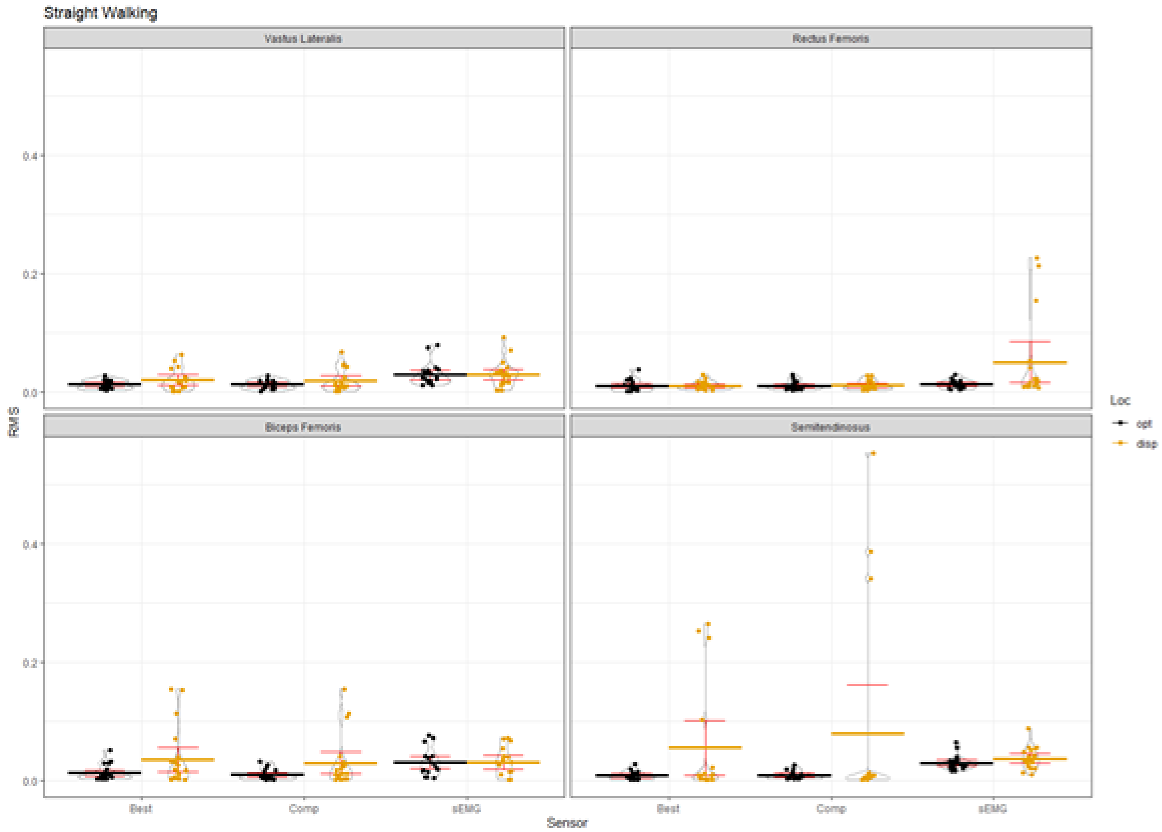

Figure 69: Violin graph of raw RMS (Root Mean Squared) for Body Weight Squats. Opt is optimal placement, disp is displaced. Best (left) is Best Signal, Comp (middle) is Composite Signal, sEMG (right) is Traditional sEMG. Note differences in spread between muscles and sensors, particularly for displaced Best and Comp for Biceps Femoris (bottom left) and Semitendinosus (bottom right).

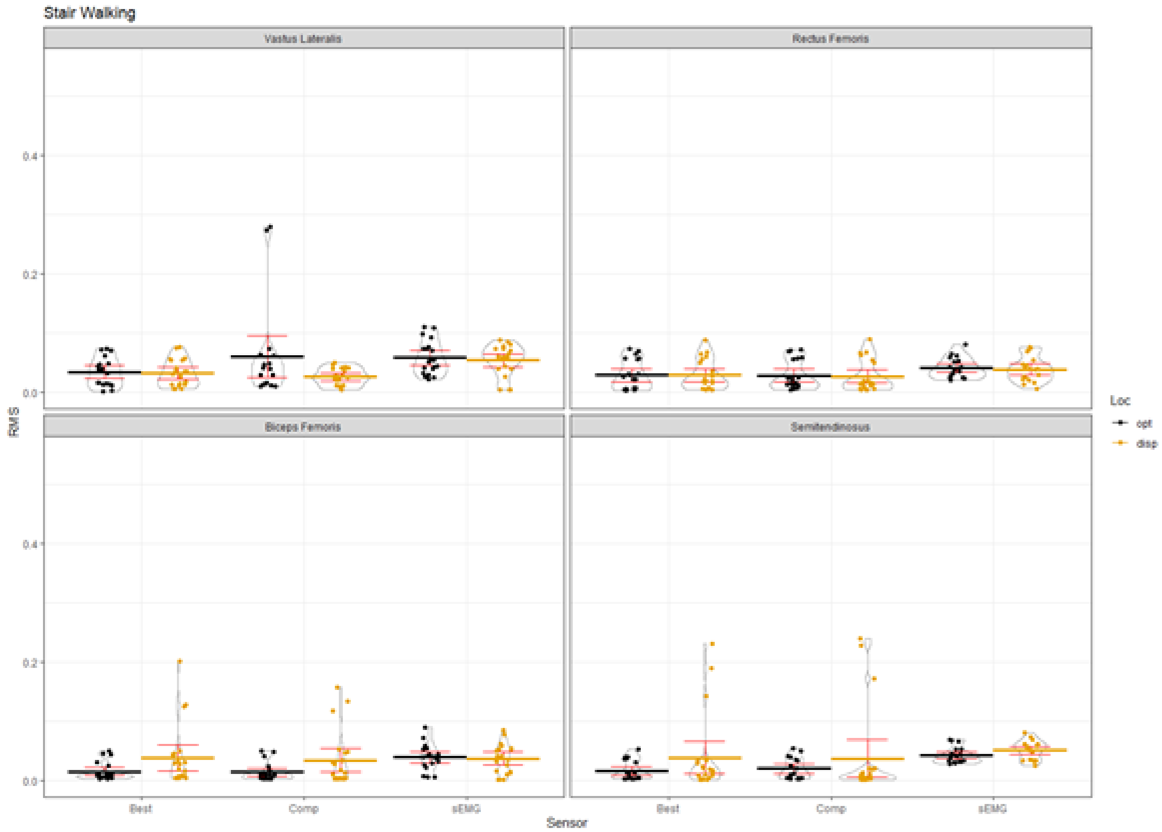

Figure 70: Violin graph of raw RMS (Root Mean Squared) for Body Weight Squats. Opt is optimal placement, disp is displaced. Best (left) is Best Signal, Comp (middle) is Composite Signal, sEMG (right) is Traditional sEMG. Note differences in spread between muscles and sensors, particularly for displaced Best and Comp for Biceps Femoris (bottom left) and Semitendinosus (bottom right).

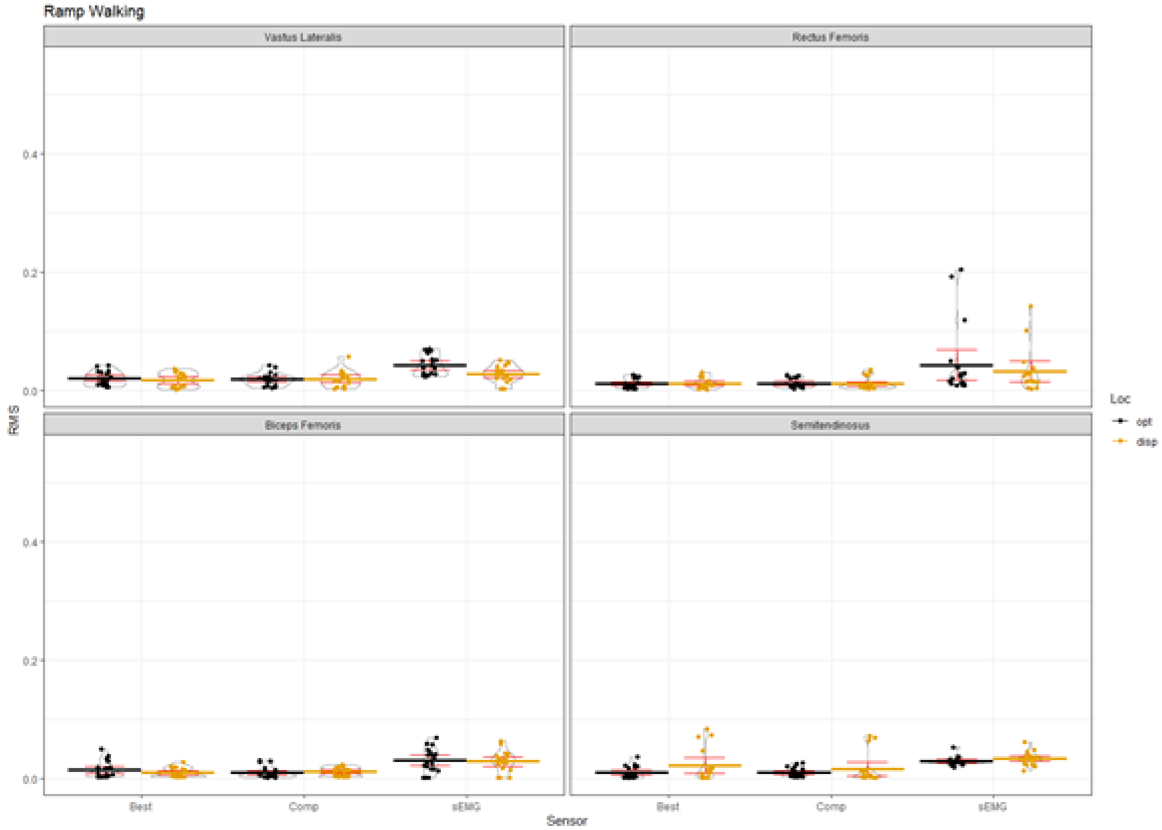

Figure 71: Violin graph of raw RMS (Root Mean Squared) for Body Weight Squats. Opt is optimal placement, disp is displaced. Best (left) is Best Signal, Comp (middle) is Composite Signal, sEMG (right) is Traditional sEMG. Note differences in spread between muscles and sensors, particularly for Rectus Femoris (top right).

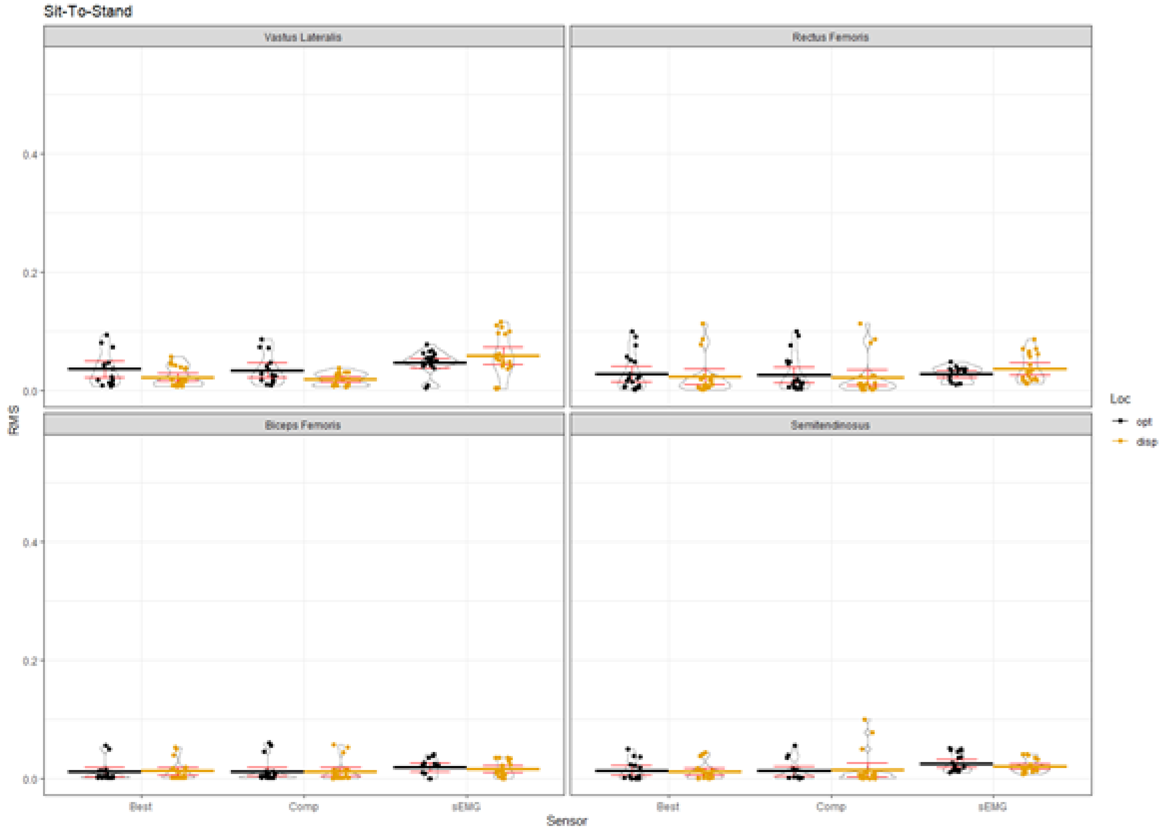

Figure 72: Violin graph of raw RMS (Root Mean Squared) for Body Weight Squats. Opt is optimal placement, disp is displaced. Best (left) is Best Signal, Comp (middle) is Composite Signal, sEMG (right) is Traditional sEMG. Note differences in spread between muscles and sensors.

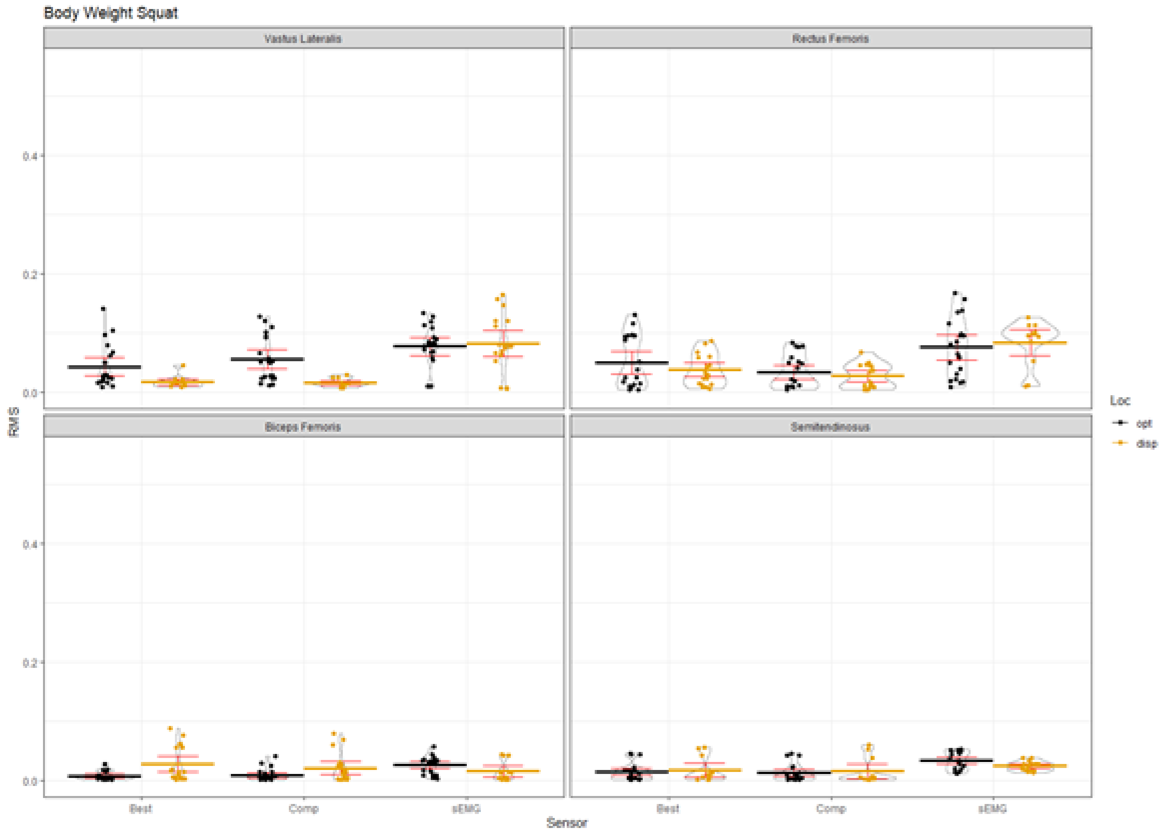

Figure 73: Violin graph of raw RMS (Root Mean Squared) for Body Weight Squats. Opt is optimal placement, disp is displaced. Best (left) is Best Signal, Comp (middle) is Composite Signal, sEMG (right) is Traditional sEMG. Note differences in spread between muscles and sensors.

APPENDIX C

NORMALIZATION PROCEDURES

The best course for normalizing EMG signals is to use maximum voluntary contractions (MVC) for each muscle. In this procedure, the participant is asked to flex the target muscle as hard as possible when provided the correct resistance, either through an experimenter's hand, a physical obstacle, or a resistance machine such as a Biodex. This is guaranteed to give the maximum possible activation value. In some cases, as with this experiment, collecting MVC data is not feasible. For this experiment, battery life of the equipment compared to the time needed to complete an experiment run. Sensor switching makes the collecting of four MVCs necessary. Therefore, an alternate method was determined. Normalization works by comparing magnitudes of signals to the magnitude of a greater, yet relevant, signal. It has been proposed in situations where collecting MVCs is not feasible to normalize to a point in the signals collected. One study compared normalization found through this method to normalization of the same activities through a pre-collected MVC[78]. It was found that the higher number of trials and the more variety of movements included, the closer the in-signal normalized values were to the MVC normalized values. It was decided that all trials and activities would be considered during normalization for this research. Both optimal and displaced sensor conditions would be considered together so that relative RMS and changes in RMS could be determined. It was decided to split each muscle into its own normalization system, to limit interference from different muscle activities. It was also decided to split normalization by sensor type.

REFERENCES CITED

REFERENCES CITED

1. O'Brien, P., Cox, M., & Shortell, C. (2013). Risk Factors for Early Failure of Surgical Amputations: An Analysis of 8,878 Isolated Lower Extremity Amputation Procedures. *Journal of Vascular Surgery*, *58*(3), 844–845. https://doi.org/10.1016/j.jvs.2013.07.034

2. Thompson, S. F., McCall, K. B., Patel, D. V., Schwerdtfeger, W. A., Stoner, J., Hollabaugh, K., & Teague, D. C. (2020). In-Hospital Morbidity and Mortality of Traumatic Lower-Extremity Amputations. *Orthopedics*, *43*(6). https://doi.org/10.3928/01477447-20200721-15

3. Robert, R. S., Ottaviani, G., Huh, W. W., Palla, S., & Jaffe, N. (2010). Psychosocial and functional outcomes in long-term survivors of osteosarcoma: A comparison of limb-salvage surgery and amputation. *Pediatric Blood & Cancer*, *54*(7), 990–999. https://doi.org/10.1002/pbc.22419

4. Furau, R., Popa, A. R., Furau, C., Ionescu, C., Dimitriu, M., Furau, G. O., Romosan, R. S., Socea, B., Gheroghiu, N., Gheorghiu, D. C., & Korodi, A. (2019). Correlations of the Mechanisms Involved in Diabetes Mellitus, Peripheral Arterial Disease and Gangrene Leading to Amputations-a Retrospective Study Over the Non-traumatic Amputations Performed in the Emergency Clinical County Hospital of Arad Between 2014- 2018. *Revista de Chimie*, *70*(9), 3309–3314. https://doi.org/10.37358/rc.19.9.7540

5. Nerlich, A. G., Zink, A., Szeimies, U., & Hagedorn, H. G. (2000). Ancient Egyptian prosthesis of the big toe. *The Lancet*, *356*(9248), 2176–2179. https://doi.org/10.1016/s0140-6736(00)03507-8

6. Binder, M., Eitler, J., Deutschmann, J., Ladstätter, S., Glaser, F., & Fiedler, D. (2016). Prosthetics in antiquity—An early medieval wearer of a foot prosthesis (6th century AD) from Hemmaberg/Austria. *International Journal of Paleopathology*, *12*, 29–40. https://doi.org/10.1016/j.ijpp.2015.11.003

7. Thurston, A. J. (2007). PARÉ AND PROSTHETICS: THE EARLY HISTORY OF ARTIFICIAL LIMBS. *ANZ Journal of Surgery*, *77*(12), 1114–1119. https://doi.org/10.1111/j.1445-2197.2007.04330.x

8. Warne, V. (2008). Artificial Leg. *Victorian Review*, *34*(1), 29–33.

9. Warner, G. (1950, June). *Artificial Limb Development A History of the Northrop Artificial Limb Research Department 96, Project 17, Founded on Prosthesis Development*.

10. *C-Leg 4*. (n.d.). Ottobock. Retrieved August 4, 2022, from https://www.ottobock.com/en-gb/product/3C88-3~23C98-3

11. Sen, E. I., Aydin, T., Bugdayci, D., & Kesiktas, F. N. (2020). Effects of microprocessor-controlled prosthetic knees on self-reported mobility, quality of life, and psychological states in patients with transfemoral amputations. *Acta Orthopaedica et Traumatologica Turcica*, *54*(5), 502–506. https://doi.org/10.5152/j.aott.2020.19269

12. Pew, C., Segal, A. D., Neptune, R. R., & Klute, G. K. (2019). Ideal operating conditions for a variable stiffness transverse plane adapter for individuals with lower-limb amputation. *Journal of Biomechanics*, *96*, 109330. https://doi.org/10.1016/j.jbiomech.2019.109330

13. Ingraham, K. A., Choi, H., Gardinier, E. S., Remy, C. D., & Gates, D. H. (2018). Choosing appropriate prosthetic ankle work to reduce the metabolic cost of individuals with transtibial amputation. *Scientific Reports*, *8*(1). https://doi.org/10.1038/s41598-018-33569-7

14. Martinez-Villalpando, E. C., & Herr, H. (2009). Agonist-antagonist active knee prosthesis: A preliminary study in level-ground walking. *The Journal of Rehabilitation Research and Development*, *46*(3), 361–374. https://doi.org/10.1682/jrrd.2008.09.0131

15. Azocar, A. F., Mooney, L. M., Duval, J. F., Simon, A. M., Hargrove, L. J., & Rouse, E. J. (2020). Design and clinical implementation of an open-source bionic leg. *Nature Biomedical Engineering*, *4*(10), 941–953. https://doi.org/10.1038/s41551-020-00619-3

16. Fougner, A., Stavdahl, Y., Kyberd, P. J., Losier, Y. G., & Parker, P. A. (2012). Control of Upper Limb Prostheses: Terminology and Proportional Myoelectric Control—A Review. *IEEE Transactions on Neural Systems and Rehabilitation Engineering*, *20*(5), 663–677. https://doi.org/10.1109/tnsre.2012.2196711

17. Li, G., Schultz, A. E., & Kuiken, T. A. (2010). Quantifying Pattern Recognition—Based Myoelectric Control of Multifunctional Transradial Prostheses. *IEEE Transactions on Neural Systems and Rehabilitation Engineering*, *18*(2), 185–192. https://doi.org/10.1109/tnsre.2009.2039619

18. Guo, W., Sheng, X., Liu, H., & Zhu, X. (2017). Toward an Enhanced Human–Machine Interface for Upper-Limb Prosthesis Control With Combined EMG and NIRS Signals. *IEEE Transactions on Human-Machine Systems*, *47*(4), 564–575. https://doi.org/10.1109/thms.2016.2641389

19. Daube, J. R., & Rubin, D. I. (2009). Needle electromyography. *Muscle & Nerve*, *39*(2), 244–270. https://doi.org/10.1002/mus.21180

20. Parri, A., Martini, E., Geeroms, J., Flynn, L., Pasquini, G., Crea, S., Molino Lova, R., Lefeber, D., Kamnik, R., Munih, M., & Vitiello, N. (2017). Whole Body Awareness for Controlling a Robotic Transfemoral Prosthesis. *Frontiers in Neurorobotics*, *11*. https://doi.org/10.3389/fnbot.2017.00025

21. Murphy, D. P., Bai, O., Gorgey, A. S., Fox, J., Lovegreen, W. T., Burkhardt, B. W., Atri, R., Marquez, J. S., Li, Q., & Fei, D. Y. (2017). Electroencephalogram-Based Brain–Computer Interface and Lower-Limb Prosthesis Control: A Case Study. *Frontiers in Neurology, 8*. https://doi.org/10.3389/fneur.2017.00696

22. Tschiedel, M., Russold, M. F., & Kaniusas, E. (2020). Relying on more sense for enhancing lower limb prostheses control: a review. *Journal of NeuroEngineering and Rehabilitation*, *17*(1). https://doi.org/10.1186/s12984-020-00726-x

23. Zagrodny, B., Wojnicz, W., Ludwicki, M., & Awrejcewicz, J. (2021). Could Thermal Imaging Supplement Surface Electromyography Measurements for Skeletal Muscles? *IEEE Transactions on Instrumentation and Measurement*, *70*, 1–10. https://doi.org/10.1109/tim.2020.3023216

24. Chowdhury, R., Reaz, M., Ali, M., Bakar, A., Chellappan, K., & Chang, T. (2013). Surface Electromyography Signal Processing and Classification Techniques. *Sensors*, *13*(9), 12431–12466. https://doi.org/10.3390/s130912431

25. Merrill, D. R., Lockhart, J., Troyk, P. R., Weir, R. F., & Hankin, D. L. (2011). Development of an Implantable Myoelectric Sensor for Advanced Prosthesis Control. *Artificial Organs*, *35*(3), 249–252. https://doi.org/10.1111/j.1525-1594.2011.01219.x

26. Memberg, W. D., Stage, T. G., & Kirsch, R. F. (2014). A Fully Implanted Intramuscular Bipolar Myoelectric Signal Recording Electrode. *Neuromodulation: Technology at the Neural Interface*, *17*(8), 794–799. https://doi.org/10.1111/ner.12165

27. Weir, R. F., Troyk, P. R., DeMichele, G. A., Kerns, D. A., Schorsch, J. F., & Maas, H. (2009). Implantable Myoelectric Sensors (IMESs) for Intramuscular Electromyogram Recording. *IEEE Transactions on Biomedical Engineering*, *56*(1), 159–171. https://doi.org/10.1109/tbme.2008.2005942

28. Lowery, M., Weir, R., & Kuiken, T. (2006). Simulation of Intramuscular EMG Signals Detected Using Implantable Myoelectric Sensors (IMES). *IEEE Transactions on Biomedical Engineering*, *53*(10), 1926–1933. https://doi.org/10.1109/tbme.2006.881774

29. Pasquina, P. F., Evangelista, M., Carvalho, A., Lockhart, J., Griffin, S., Nanos, G., McKay, P., Hansen, M., Ipsen, D., Vandersea, J., Butkus, J., Miller, M., Murphy, I., & Hankin, D. (2015). First-in-man demonstration of a fully implanted myoelectric sensors system to control an advanced electromechanical prosthetic hand. *Journal of Neuroscience Methods*, *244*, 85–93. https://doi.org/10.1016/j.jneumeth.2014.07.016

30. Tenore, F. V., Ramos, A., Fahmy, A., Acharya, S., Etienne-Cummings, R., & Thakor, N. V. (2009). Decoding of Individuated Finger Movements Using Surface Electromyography. *IEEE Transactions on Biomedical Engineering*, *56*(5), 1427–1434. https://doi.org/10.1109/tbme.2008.2005485

31. Bolek, J. E. (2009). Electrical Concepts in the Surface Electromyographic Signal. *Applied Psychophysiology and Biofeedback*, *35*(2), 171–175. https://doi.org/10.1007/s10484-009-9118-x

32. Huang, W. (2016, May 7). Wearable Computing for In-home Senior Care A Survey. *ResearchGate*.

33. Fleischer, C., & Hommel, G. (2008). A Human--Exoskeleton Interface Utilizing Electromyography. *IEEE Transactions on Robotics*, *24*(4), 872–882. https://doi.org/10.1109/tro.2008.926860

34. Fleming, A., Stafford, N., Huang, S., Hu, X., Ferris, D. P., & Huang, H. H. (2021). Myoelectric control of robotic lower limb prostheses: a review of electromyography interfaces, control paradigms, challenges and future directions. *Journal of Neural Engineering*, *18*(4), 041004. https://doi.org/10.1088/1741-2552/ac1176

35. Huang, S., & Huang, H. (2019). Voluntary Control of Residual Antagonistic Muscles in Transtibial Amputees: Reciprocal Activation, Coactivation, and Implications for Direct Neural Control of Powered Lower Limb Prostheses. *IEEE Transactions on Neural Systems and Rehabilitation Engineering*, *27*(1), 85–95. https://doi.org/10.1109/tnsre.2018.2885641

36. Young, A. J., Hargrove, L. J., & Kuiken, T. A. (2011). The Effects of Electrode Size and Orientation on the Sensitivity of Myoelectric Pattern Recognition Systems to Electrode Shift. *IEEE Transactions on Biomedical Engineering*, *58*(9), 2537–2544.

37. Gholizadeh, H., Osman, N. A., Kamyab, M., Eshraghi, A., Abas, W. W., & Azam, M. (2012). Transtibial prosthetic socket pistoning: Static evaluation of Seal-In® X5 and Dermo® Liner using motion analysis system. *Clinical Biomechanics*, *27*(1), 34–39. https://doi.org/10.1016/j.clinbiomech.2011.07.004

38. Merletti, R., Holobar, A., & Farina, D. (2008). Analysis of motor units with high-density surface electromyography. *Journal of Electromyography and Kinesiology*, *18*(6), 879–890. https://doi.org/10.1016/j.jelekin.2008.09.002

39. Zhang, C., Dias, N., He, J., Zhou, P., Li, S., & Zhang, Y. (2020). Global Innervation Zone Identification With High-Density Surface Electromyography. *IEEE Transactions on Biomedical Engineering*, *67*(3), 718–725. https://doi.org/10.1109/tbme.2019.2919906

40. Celadon, N., Došen, S., Binder, I., Ariano, P., & Farina, D. (2016). Proportional estimation of finger movements from high-density surface electromyography. *Journal of NeuroEngineering and Rehabilitation*, *13*(1). https://doi.org/10.1186/s12984-016-0172-3

41. Gallina, A., Peters, S., Neva, J. L., Boyd, L. A., & Garland, S. J. (2017). Selectivity of conventional electrodes for recording motor evoked potentials: An investigation with

high-density surface electromyography. *Muscle & Nerve*, *55*(6), 828–834. https://doi.org/10.1002/mus.25412

42. Bracken, D. J., Ornelas, G., Coleman, T. P., & Weissbrod, P. A. (2019). High-density surface electromyography: A visualization method of laryngeal muscle activity. *The Laryngoscope*, *129*(10), 2347–2353. https://doi.org/10.1002/lary.27784

43. Cui, H., Zhong, W., Yang, Z., Cao, X., Dai, S., Huang, X., Hu, L., Lan, K., Li, G., & Yu, H. (2021). Comparison of Facial Muscle Activation Patterns Between Healthy and Bell's Palsy Subjects Using High-Density Surface Electromyography. *Frontiers in Human Neuroscience*, *14*. https://doi.org/10.3389/fnhum.2020.618985

44. Zhu, M., Huang, Z., Wang, X., Wang, X., Wang, C., Zhang, H., Zhao, G., Chen, S., & Li, G. (2021). Automatic Speech Recognition in Different Languages Using High-Density Surface Electromyography Sensors. *IEEE Sensors Journal*, *21*(13), 14155–14167. https://doi.org/10.1109/jsen.2020.3037061

45. Liu, Y., Zhang, C., Dias, N., Chen, Y. T., Li, S., Zhou, P., & Zhang, Y. (2020a). Transcutaneous innervation zone imaging from high-density surface electromyography recordings. *Journal of Neural Engineering*, *17*(1), 016070. https://doi.org/10.1088/1741-2552/ab673e

46. Zverev, Y. P. (2006, March). Special Parameters of Walking Gait and Footedness. *Annals of Human Biology*, 161–176. https://doi.org/10.1080/03014460500500222

47. *International Physical Activity Questionnaire (IPAQ)*. (n.d.). SnapEd. https://snaped.fns.usda.gov/library/materials/international-physical-activity-questionnaire-ipaq

48. Perotto, A. O. (2011). *ANATOMICAL GUIDE FOR THE ELECTROMYOGRAPHER* Charles C. Thomas.

49. Huebner, A., Faenger, B., Schenk, P., Scholle, H. C., & Anders, C. (2015, April). Alteration of Surface EMG amplitude levels of five major trunk muscles by defined electrode location displacement. *Journal of Electromyography and Kinesiology*, *25*(2), 214–223. https://doi.org/10.1016/j.jelekin.2014.11.008

50. *Full body modeling with Plug-in Gait - Nexus 2.13 Documentation - Vicon Documentation*. (n.d.). Retrieved October 11, 2022, from https://docs.vicon.com/display/Nexus213/Full+body+modeling+with+Plug-in+Gait

51. Schreiber, C., & Becker, J. (2020, October 15). Performance on the Single-Legged Step Down and Running Mechanics. *Journal of Athletic Training*, *55*(12), 1277–1284. https://doi.org/10.4085/1062-6050-533-19Wentink, E. C., Prinsen, E. C., Rietman, J. S., & Veltink, P. H. (2013). Comparison of muscle activity patterns of transfemoral

amputees and control subjects during walking. *Journal of Neuroengineering and Rehabilitation*.

52. Saywell, N., Taylor, D., & Boocock, M. (2012). During step descent, older adults exhibit decreased knee range of motion and increased vastus lateralis muscle activity. *Gait & Posture*, 490–494.

53. Iqbal, N., Maqbool, H. F., Khan, M., Awad, M. I., & Dehghani-Sanij, A. A. (2020, July). Intent based recognition of walking and ramp activities for amputee using sEMG based lower limb prostheses. *Biocybernetics and Biomedical Engineering*, *40*(3), 1110–1123. https://doi.org/10.1016/j.bbe.2020.05.010

54. Pew, C., & Klute, G. K. (2017, January). Pilot testing of a variable stiffness transverse plane adapter for lower limb amputees. *Gait &Amp; Posture*, *51*, 104–108. https://doi.org/10.1016/j.gaitpost.2016.10.003

55. Hunt, G., Hood, S., & Lenzi, T. (2021). Stand-Up, Squat, Lunge, and Walk With a Robotic Knee and Ankle Prosthesis Under Shared Neural Control. *IEEE Open Journal of Engineering in Medicine and Biology*, *2*, 267–277. https://doi.org/10.1109/ojemb.2021.3104261

56. Durstberger, S., Cheema, M. S., & Kranzl, A. (2019). Treadmill walking versus ramp walking: What are the differences? *Gait & Posture*, *73*, 600–601. https://doi.org/10.1016/j.gaitpost.2019.07.303

57. Pickle, N. T., Wilken, J. M., Fey, N. P., & Silverman, A. K. (2018). A comparison of stability metrics based on inverted pendulum models for assessment of ramp walking. *PLOS ONE*, *13*(11), e0206875. https://doi.org/10.1371/journal.pone.0206875

58. Waanders, J. B., Murgia, A., DeVita, P., Franz, J. R., & Hortobágyi, T. (2021). Age does not affect the relationship between muscle activation and joint work during incline and decline walking. *Journal of Biomechanics*, 110555. https://doi.org/10.1016/j.jbiomech.2021.110555

59. Rojas-Martínez, M., Serna, L. Y., Jordanic, M., Marateb, H. R., Merletti, R., & Mañanas, M. N. (2020). High-density surface electromyography signals during isometric contractions of elbow muscles of healthy humans. *Scientific Data*, *7*(1). https://doi.org/10.1038/s41597-020-00717-6

60. Fraser, G. D., Chan, A. D. C., Green, J. R., & MacIsaac, D. T. (2014). Automated Biosignal Quality Analysis for Electromyography Using a One-Class Support Vector Machine. *IEEE Transactions on Instrumentation and Measurement*, *63*(12), 2919–2930. https://doi.org/10.1109/tim.2014.2317296

61. Sinderby, C., Lindstrom, L., & Grassino, A. E. (1995). Automatic assessment of electromyogram quality. *Journal of Applied Physiology*, *79*(5), 1803–1815. https://doi.org/10.1152/jappl.1995.79.5.1803

62. *Cross-correlation - MATLAB xcorr*. (n.d.). MathWorks. https://www.mathworks.com/help/matlab/ref/xcorr.html

63. *Cross-covariance - MATLAB xcov*. (n.d.). MathWorks. https://www.mathworks.com/help/matlab/ref/xcov.html

64. *Cross Spectrum and Magnitude-Squared Coherence - MATLAB & Simulink*. (n.d.). MathWorks. https://www.mathworks.com/help/signal/ug/cross-spectrum-and-magnitude-squared-coherence.html

65. Greenwood, M. C. (n.d.). *Chapter 3 One-Way ANOVA | Intermediate Statistics with R*. Retrieved October 11, 2022, from https://greenwood-stat.github.io/GreenwoodBookHTML/chapter3.html

66. *Mixed Models with R*. (n.d.). Retrieved October 11, 2022, from https://m-clark.github.io/mixed-models-with-R/

67. Ghislieri, M. (2021, October 21). *Long short-term memory (LSTM) recurrent neural network for muscle activity detection - Journal of NeuroEngineering and Rehabilitation*. BioMed Central. Retrieved October 11, 2022, from https://jneuroengrehab.biomedcentral.com/articles/10.1186/s12984-021-00945-w

68. Di Nardo, F., Morano, M., Strazza, A., & Fioretti, S. (2022, June 28). Muscle Co-Contraction Detection in the Time–Frequency Domain. *Sensors*, *22*(13), 4886. https://doi.org/10.3390/s22134886

69. St-Amant, Y., Rancourt, D., & Clancy, E. A. (1998, June). Influence of Smoothing Window Length on Electromyogram Amplitude Estimates. *IEEE Transactions on Biomedical Engineering*, *45*(6).

70. Vonsevych, K., Goethel, M. F., Mrozowski, J., Awrejcewicz, J., & Bezuglyi, M. (2018). Fingers Movements Control System Based on Artificial Neural Network Model. *Radioelectronics and Communications Systems*, *62*(1), 23–33.

71. Malešević, N., Marković, D., Kanitz, G., Controzzi, M., Cipriani, C., & Antfolk, C. (2018). Vector Autoregressive Hierarchical Hidden Markov Models for Extracting Finger Movements Using Multichannel Surface EMG Signals. *Complexity*, *2018*, 1–12. https://doi.org/10.1155/2018/9728264

72. Holobar, A., & Farina, D. (2014). Blind source identification from the multichannel surface electromyogram. *Physiological Measurement*, *35*(7), R143–R165. https://doi.org/10.1088/0967-3334/35/7/r143

73. Hardoon, D. R., Szedmak, S., & Shawe-Taylor, J. (2004). Canonical Correlation Analysis: An Overview with Application to Learning Methods. *Neural Computation*, *16*(12), 2639–2664. https://doi.org/10.1162/0899766042321814

74. Liu, Q., Liu, A., Zhang, X., Chen, X., Qian, R., & Chen, X. (2019). Removal of EMG Artifacts from Multichannel EEG Signals Using Combined Singular Spectrum Analysis and Canonical Correlation Analysis. *Journal of Healthcare Engineering*, *2019*, 1–13. https://doi.org/10.1155/2019/4159676

75. Matrone, G., Savoia, A. S., Caliano, G., & Magenes, G. (2015). The Delay Multiply and Sum Beamforming Algorithm in Ultrasound B-Mode Medical Imaging. *IEEE Transactions on Medical Imaging*, *34*(4), 940–949. https://doi.org/10.1109/tmi.2014.2371235

76. *Wavelet coherence and cross-spectrum - MATLAB wcoherence*. (n.d.). MathWorks. https://www.mathworks.com/help/wavelet/ref/wcoherence.html

77. Ghazwan, A., Forrest, S. M., Holt, C. A., & Whatling, G. M. (2017). Can activities of daily living contribute to EMG normalization for gait analysis? *PLOS ONE*, *12*(4), e0174670. https://doi.org/10.1371/journal.pone.0174670